



The University of
Nottingham

UNITED KINGDOM • CHINA • MALAYSIA

George, Dickson Dungau (2008) Effects of 4-lobe swirl-inducing pipe on pressure drop. MSc(Res) thesis, University of Nottingham.

Access from the University of Nottingham repository:

<http://eprints.nottingham.ac.uk/10509/1/Thesis.pdf>

Copyright and reuse:

The Nottingham ePrints service makes this work by researchers of the University of Nottingham available open access under the following conditions.

This article is made available under the University of Nottingham End User licence and may be reused according to the conditions of the licence. For more details see:
http://eprints.nottingham.ac.uk/end_user_agreement.pdf

A note on versions:

The version presented here may differ from the published version or from the version of record. If you wish to cite this item you are advised to consult the publisher's version. Please see the repository url above for details on accessing the published version and note that access may require a subscription.

For more information, please contact eprints@nottingham.ac.uk

School of Chemical and Environmental Engineering



The University of
Nottingham

**EFFECTS OF 4-LOBE SWIRL-INDUCING PIPE ON
PRESSURE DROP**

Dickson Dunggau George, BEng (Hons)

**Thesis submitted to the University of Nottingham for the
degree of Master in Science (by Research) in
Petroleum and Environmental Process Engineering**

September 2007

ABSTRACTS

This thesis describes the effects of the 4-lobe swirl-inducing pipe on pressure drops for water, sand-water slurry and carboxymethyl cellulose fluids. The pressure drops were measured for two 4-lobe swirl-inducing pipe combined, one 4-lobe swirl-inducing pipe and without swirl-inducing pipe. The swirling pipe applications were installed before a bend on radius-to-diameter (R/D) ratio of 4. The pressure drops were measured on three different locations, before and after the 4-lobe swirl-inducing pipe, and after the bend.

Swirling flow behaviours were observed for sand-water slurry at different concentrations. Reynolds number indicated water and sand-water slurries in turbulent regimes. The sand particles were evenly distributed when induced with swirling flow, which caused less wear effect on a pipe-cross section. Results indicated that the swirl-inducing pipe increased the pressure drop for higher concentrations.

The 4-lobe swirl-inducing pipe caused an increased in pressure drop over horizontal pipe and a reduction in pressure drop over the bend. Results showed that the overall pressure drops across pipe (after swirl and bend) were increased with swirl-inducing pipe.

ACKNOWLEDGEMENTS

This thesis would not have been possible without everyone's interest in the project. I particularly want to thank Professor Nicholas Miles (Head of School of Chemical and Environmental Engineering, The University of Nottingham) for helping and supervising throughout this research.

I acknowledge help received from Professor Azzopardi B.J., Professor Nidal Hilal, and Dr. Ian S. Lowndes.

I greatly extend my gratitude to Dr. Doug Brown, Tony Gospel, Bryce Marion, Heaper Mark and Hall Philip for technical help and advice.

I particularly appreciate colleagues who spent considerable effort and time for responding to some difficult issues.

I am also indebted to the support of my family and friends.

CONTENTS

ABSTRACT	i
ACKNOWLEDGEMENTS	ii
CONTENTS	iii
LIST OF FIGURES	vi
LIST OF TABLES	viii
NOMENCLATURE	ix
Chapter 1 INTRODUCTION	
1.1 Background	1
1.2 Aim and Objectives	3
1.3 Thesis Structure	4
Chapter 2 LITERATURE REVIEW	
2.1 Theoretical Pipe Flow	5
2.1.1 Slurry Transport Processes	5
2.1.2 Non-Newtonian Transport Processes	8
2.2 Flow in Bends	11
2.3 Problems Encountered in Pipeline System	12
2.4 Swirling Pipe Flow	13
2.5 Carboxymethyl Cellulose Sodium Salt	18
2.5.1 Applications	21
2.6 Summary	22

Chapter 3 TEST MATERIALS

3.1	Introduction	24
3.2	Sand-water Slurry	24
3.3	Carboxymethyl Cellulose	26
3.3.1	Procedures using Brookfield Viscometer	26
3.3.2	Methodology	27
3.3.3	Apparent Viscosity of Carboxymethyl Cellulose	27
3.3.4	Shear Stress – Viscosity Gradient for Carboxymethyl Cellulose	28
3.4	Flow – Pressure Relationship (Model)	29
3.5	Summary	32

Chapter 4 STEEL PIPE LOOP

4.1	Brown Mixer Tank	34
4.2	Steel Rig Pipe Layout	34
4.2.1	Pipe Network	36
4.2.2	4-Lobe Swirl Inducing Pipe	37
4.2.3	Inverter and Mono Pump	38
4.2.4	De-aerator	39
4.2.5	Conical Tank, Weigh Tank and Settling Tank	40
4.2.6	Splitter Box	41
4.2.7	Measuring Parameters	41
4.3	General Procedures on Steel Pipe Rig	45
4.4	Dissolution for Carboxymethyl Cellulose Fluid	46
4.5	Summary	47

Chapter 5 EFFECTS of 4-LOBE SWIRL-INDUCING PIPE

5.1	Introduction	48
5.2	Methodology Specifics	48
5.3	Effects of Swirl-Inducing Flow over Horizontal Pipe	50
5.4	Effects of Swirl-Inducing Flow over a Bend (R/D of 4)	57
5.5	Effects of Swirl-Inducing Flow across a Pipe	61
5.6	Summary	67

Chapter 6	CONCLUSIONS AND RECOMMENDATIONS	
6.1	Effects of 4-Lobe Swirl-Inducing Pipe on Settling Slurries	69
6.2	Effects of 4-Lobe Swirl-Inducing Pipe on Non-Newtonian Fluid	69
6.3	Contribution of Thesis	70
6.4	Recommendations	70
	REFERENCES	71
	APPENDIX A	
	STEEL RIG PIPE COMPONENTS	78
	APPENDIX B	
	TEST MATERIALS AND VISCOSITY	89
	APPENDIX C	
	EXPERIMENTAL DATA	93

LIST OF FIGURES

Figure 1.1	Pipeline system (adopted from www.ens-newswire.com)	1
Figure 1.2	Construction on pipeline (adopted from www.ncl.ac.uk)	2
Figure 1.3	Erosion inside a steel pipe (adopted from www.aludra.nl)	2
Figure 2.1	Illustration of slurry flow regimes in a pipeline system	6
Figure 2.2	Rate of deformation of a fluid	9
Figure 2.3	The rate of deformation of fluids against shear stress, τ (a); and against apparent viscosity, η (b)	10
Figure 2.4	4-lobe swirl pipe used by Tonkin (2004)	17
Figure 2.5	Apparent viscosity with shear rate for 2.5% w/w CMC (Tonkin, 2004)	20
Figure 3.1	Temperature dependence of apparent viscosity for CMC fluids	27
Figure 3.2	Shear stress – velocity gradient (shear rate)	28
Figure 3.3	Shear stress of CMC solutions on day 2 and day 5	29
Figure 3.4	Flow in a pipeline	29
Figure 4.1	View inside the mixer tank with an anchor impeller	34
Figure 4.2	Illustration of steel pipe rig and its components	35
Figure 4.3	220mm radii pipe (R/D of 4)	36
Figure 4.4	4-Lobe swirl pipe	37
Figure 4.5	Illustration of one 4-lobe swirl pipe	38
Figure 4.6	Illustration of two 4-lobe swirl pipes when connected together	38
Figure 4.7	Mono Pump	39
Figure 4.8	De-aerator	39
Figure 4.9	Weigh tank, conical tank and settling tank	40
Figure 4.10	Illustration of splitter box and its components	41
Figure 4.11	The location of pressure measurements of P1, P2 and P3	42
Figure 4.12	Simple manometer tube (ID of 9mm and OD of 12mm)	43
Figure 4.13	A liquid pressure gauge (up to 4 bars)	43
Figure 4.14	A schematic diagram of Bourdon-tube gauge (adapted from www.britannica.com)	44
Figure 4.15	1 swirl 4-lobe swirl-inducing pipe flow	44
Figure 4.16	2 swirl 4-lobe swirl-inducing pipes flow when connected together	45

Figure 5.1	Illustration of pressure locations	48
Figure 5.2	Pressure drop, ΔP_{12} (Pa) for water over horizontal pipe	50
Figure 5.3	Pressure drop, ΔP_{12} (Pa) for sand-water slurry at different concentrations over horizontal pipe (a) 1.4% v/v slurry; (b) 2.1% v/v slurry; and (c) 2.7% v/v slurry	51
Figure 5.4 –	Flow behaviour of sand-particles at 1.5m/s and 1.4% v/v	
Figure 5.6	with and without swirl-inducing pipe	53
Figure 5.7	Pressure drop, ΔP_{12} (Pa) for carboxymethyl cellulose at different concentration over horizontal pipe (a) 0.5% w/w CMC; and (b) 1.0% w/w CMC	55
Figure 5.8	Pressure drop, ΔP_{23} (Pa) for water over the bend ($R/D = 4$)	57
Figure 5.9	Pressure drop, ΔP_{23} (Pa) for sand-water slurry at different concentrations over the bend with and without swirl inducing pipe	58
Figure 5.10	Pressure drop, ΔP_{23} (Pa) for CMC at (a) 0.5% w/w CMC, and (b) 1.0% w/w CMC, concentrations over the bend	60
Figure 5.11	Pressure drop, ΔP_{13} (Pa) for water across a pipe	61
Figure 5.12	Pressure drop, ΔP_{13} (Pa) for slurries at different concentrations across pipe (a) 1.4% v/v; (b) 2.1% v/v; and (c) 2.7% v/v	62
Figure 5.13	Pressure drop, ΔP (Pa) over horizontal pipes for coarse sand slurries (2000 μ m) (taken from Tonkin, 2004)	63
Figure 5.14	Pressure drop, ΔP_{13} (Pa) against velocity, v (m/s) CMC at different concentrations (a) 0.5% w/w; (b) 1.0% w/w; and (c) 1.5% w/w	64

LIST OF TABLES

Table 2.1	Flow parameter used in CFD simulations by Ganeshalingam (2002) and Ariyaratne (2005)	18
Table 3.1	Test fluid and concentration	24
Table 4.1	Flow rate and velocity for fluid tests	46

NOMENCLATURE

Symbol	Description	Unit
C_m	Slurry mixture concentration (weight)	% w/w
C_s	Mass fraction of sand-water slurry	% w/w
C_v	Slurry mixture concentration (volume)	% v/v
D	Diameter	m
g	Gravity	m/s^2
H_n	Height of fluid travel (manometer tube)	m
K	Empirical erosion constant (2×10^9 for carbon steel)	
K	Fluid consistency coefficient	
k^*	Fluid consistency index	
L	Length	m
M_p	Mass of particle	kg
n	Characteristic velocity exponent (2.6 for carbon steel)	
n	Fluid ability index	
P_f	Pressure head loss	
P_h	Pressure by vertical elevation	
U_p	Particle impact velocity	m/s
V	Fluid velocity	m/s
V_s	Volume of sand	m^3
V_l	Volume of water	m^3
W_t	Total eroded volume per impact	m^3/kg
Re	Reynolds number	
Re_{MR}	Metzner and Reed Reynolds number	

Abbreviations

CMC	Carboxymethyl cellulose
R/D	Ratio of radius to diameter

Subscripts

l	Liquid
w	Water
s	Solid

Greek Letters

α_s	Volumetric concentration of sand-water slurry	% v/v
f	Friction head	
$f(\alpha)$	Angle dependency constant	
η_e	Swirl effectiveness	
Ω	Swirl intensity	
ρ	Density	kg/m ³
ρ_s	Density of sand	kg/m ³
ρ_l	Density of water	kg/m ³
ρ_m	Density of sand-water slurry	kg/m ³
ΔP	Pressure drop	Pa
ΔP_{12}	Pressure drop over horizontal pipe	Pa
ΔP_{23}	Pressure drop over bend	Pa
ΔP_{13}	Pressure drop across horizontal pipe	
τ	Shear stress	Pa.s
u	Velocity of fluid	m/s
μ	Viscosity	Pa.s
γ	Viscosity index	

Chapter 1

INTRODUCTION

1.1 Background

Fluid flow both single and multiphases encountered in many of day-to-day activities are transported by pipelines (Figure 1.1). Many pipeline systems are built to deliver fluids (water, crude oil, petroleum products etc.) as shown in Figure 1.2. Crude oil can be transported in pipelines sometimes for thousands of miles before it reaches its destination. Crude oil can be transported in tankers but pipeline systems are preferred because they are cost effective, safe and an environmentally acceptable method for transporting fluids.



Figure 1.1: Pipeline system (adopted from www.ens-newswire.com)

In a pipeline design, it is important to understand types of flow that are occurring in the pipe as it is essential to maintain the flow for long durations and to ensure it does not change with time. Types of flow can be categorised as steady or unsteady, laminar or turbulent, Newtonian and non-Newtonian, uniform or non-uniform, and isothermal or adiabatic flows. Although fluid will not flow like a laminar flow along the pipe, to achieve steady flow, fluids are pumped at optimum energy of flow rate through long straight pipes to ensure it flows uniformly. Not all the uniform flows in pipelines occurred due to fluid properties. Flow behaviours and pipes geometry also contribute to the effect.



Figure 1.2: Construction on pipeline (adopted from www.ncl.ac.uk)

The transport of viscous fluids (Non-Newtonian fluids) particularly in slurry (solid-liquid) form by pipelines is widely used in petroleum, food, sewage, pharmaceutical and other industries. It is an essential element in handling transportation of solid particulates in liquid to ensure the pipeline transportation and processing systems are safe and it is a cost effective design and operation. Research showed that when pumping Newtonian, non-Newtonian and slurries, problems have occurred. Failure to address the problems when transporting slurry liquid in pipeline systems can lead to erosive wear (Figure 1.3), reduction in pumping performance, high maintenances cost, and increase in energy usage.



Figure 1.3: Erosion inside a steel pipe (adopted from www.aludra.nl)

Extensive work has been carried out to improve fluids delivery along pipeline systems. Large amounts of money have been invested into analysis, modelling and experimental methods to enhance and improve the pipeline system and pipeline flow. The University of Nottingham has carried out research to develop the swirl inducing flow in pipeline system. The application of swirling flow when transporting slurries increased particle distribution and reduced localised wear (Raylor, 1999; Wood, 2001; Ganeshalingam, 2002; Tonkin, 2004 and Ariyaratne, 2005). A considerable amount of effort has been undertaken to optimise the transportation of slurries. Ariyaratne (2005) produced a 4-lobe prototype swirl pipe and investigated swirling pipe flow involved non-Newtonian fluids and solid particles using CFD model.

Tonkin (2004) continued work by Ganeshalingam (2004) and Raylor (2004) on swirl inducing flow with different types of particle and a selected non-Newtonian fluid. Ariyaratne (2005) performed a CFD optimisation to optimise and design the 4-lobe swirl pipe. The current project was carried out to expand the potential of 4-lobe swirl inducing pipe on pressure drops. The research was experimented on steel pipe rig, which were previously used by Tonkin (2004). The pressure drops measurements were performed on mixture of coarse sand particle (approximately 2000 μm size particle) with water as a carrier liquid. The experiment was also tested with a selected non-Newtonian fluid at different nominal velocity profiles.

1.2 Aim and Objectives

The aims of this investigation was to analyse the energy consumption in terms of pressure drop when applying the swirl inducing pipe (4-lobe swirl pipe) in the pipeline and also to test the viability of swirl inducing pipe for slurry Newtonian and viscous fluid transportation of non-Newtonian fluids.

The objectives of this research were to:

1. Investigate the effect of swirl-inducing pipe on pressure drop.
2. Observe the slurry flows when preceded with swirl inducing pipe flow.
3. Analyse the pressure difference when using non-Newtonian and slurries fluids

1.3 Thesis Structure

This thesis is divided into 6 chapters including this chapter which provides a brief introduction and understanding to the subject area and outlines the aims of the research and description of each chapter. Three experimental procedures are outlined including the preparation of solutions, operation of pipe flow loops and viscosity measurement. In this current thesis, the experiment was carried out on coarse slurries and cellulose-based polymer of non-Newtonian fluid at different concentrations.

Chapter 1 (INTRODUCTION) introduces a brief overview on the importance of the pipe flow and problems encountered during delivery. The current chapter also covers the aim and objectives of the research.

Chapter 2 (LITERATURE REVIEW) is a literature review covering some theories on fluids flow and relevant issues in pipeline system utilised in this research. It also covers literature relevant to the current research, an overview of swirling flow and carboxymethyl cellulose (CMC).

Chapter 3 (TEST MATERIALS) specify the selected test materials used. The viscosity of CMC was presented. The pressure drop relationship (model) is presented for Newtonian, settling slurry and non-Newtonian fluids

Chapter 4 (STEEL PIPE LOOP) details the components of instruments used in this research such as viscometer, mixer tank, pump, steel rig pipe loop, pressure measuring device, 4-lobe swirl-inducing pipe etc. The general methodology used in operating the steel rig pipe loop is also described.

Chapter 5 (EFFECTS of 4-LOBE SWIRL-INDUCING PIPE) presents the statistical data obtained when the test fluids were preceded with and without the application of 4-lobe swirl-inducing pipe in terms of pressure drops.

Chapter 6 (CONCLUSIONS AND RECOMMENDATIONS) presents the conclusion and recommendation for future research.

Chapter 2

LITERATURE REVIEW

2.1 Theoretical Pipe Flow

A fluid (single or multiple phase) is defined as a substance, which deforms continuously by shear stress (shear force) (Clayton, 2006). An understanding of the flow and fluid properties are essential to analyse the system parameters and scope of this research. The flow of fluids through the pipe is an important field of interest in many industries such as in oilrigs, evaporators, water pipeline systems etc. (Richardson et al., 2004). The transport of fluids from one destination to another through pipe requires the determination of pressure drops, pumping power and flow rates (Mukhtar, 1995). Fluid properties, flow pattern, and energy and momentum of a fluid at various positions and pipeline geometry also have a profound effect in a pipeline system (Heywood, 2002).

In many cases, the fluids of higher viscosity (non-Newtonian) containing solid particles in suspension (slurries) are also important in coal, food, water and other industries. The flow velocity of slurries is normally higher than in some single-phase liquid (water) to maintain solid particles in suspension. Charles and Charles (1971) reported a reduction of power requirement approximately by 6% when transporting sand particles in water-clay mixture of 30-50% by weight. An understanding of slurries and non-Newtonian behaviour for this project is important, which dominated the research idea.

2.1.1 Slurry Transport Processes

Slurry flow is a mixture of solid particles and a carrier liquid commonly water, which may be transported through circular pipelines (Clayton, 2006). Hydraulic transport of slurries occurs in many applications such as in the mining industry where coal slurries and other minerals are conveyed through pipelines. The slurry transport may be invariably horizontal or vertical over long distance. It is also important to identify types of solid particle on slurry transport processes either fine slurry or coarse slurry. The mixture of fine solid particles (below 40 μm) in liquid is called fine slurry and the mixture of larger solid particles (40 μm to 2 mm) in liquid is called coarse slurry (Richardson et al., 2004). The suspended of solid particles in slurries is depends on the settling velocity and density of the solid particles. A solid particle which has higher

density than carrier liquid tends to settle on the bottom of pipe when occurs at low slurry superficial velocity (Turian et al., 1997; Fangary et al., 1997). Pressure drop is an important parameter in hydraulic transport of slurries (Konrad and Harrison, 1980; Heywood, 2000).

The slurry flow regimes are dependent on solid particles and carrier liquid properties (Stack and Abd El-Badia, 2007). Pressure drops and the flow rate also contribute to the slurry flow regimes (Doron and Barnea, 1995). There are four common classifications of slurry flow in a pipeline, which are homogeneous, heterogeneous, heterogeneous with a moving bed (also referred to as flow with a moving bed) and heterogeneous with a stationary bed (also referred to as flow with a stationary bed) (Newitt et al., 1955; Charles and Charles, 1971; Brown and Heywood, 1991). Figure 2.1 shows the schematic views of slurry flow regimes at different solid concentrations and velocity profiles.

The flow patterns are mainly dependent on velocity. The solid-liquid flow reached its homogeneity solid particles distributed thoroughly throughout a carrier fluid in a pipe-cross section, when transported under turbulent flow. This is because the solid particles movement are disrupted due to the motion of the fluid surrounding the particles and arise from the fluctuations by fluid turbulence. In some cases, homogeneous slurry flow can be seen in a slurry mixture of fine solid particles with high concentration and low density (Fangary et al., 1997). In this regime, the homogeneous slurry resembles a single-phase flow.

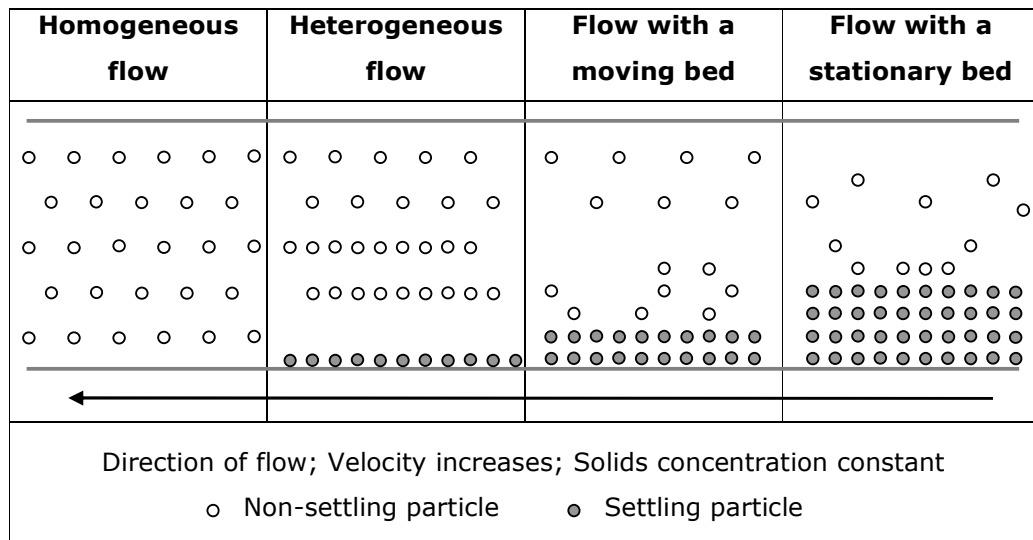


Figure 2.1: Illustration of slurry flow regimes in a pipeline system

Heterogeneous slurry flow is characterised by sufficiently higher and denser solid particles (40 μm – 2 mm) than in homogeneous slurry flow. The solid particle in heterogeneous slurry flow tends to settle to various levels on the bottom of pipe. The solid particles in this category are no longer in a uniform distribution although most of the particles are fully suspended (Clayton, 2006).

In some cases, heterogeneous with moving bed can occur when the flow rate of solid-liquid mixture is slow. Part of the solid particles in this regime tends to move or slide along the bottom of pipe. Doron and Barnea (1995) investigated the pressure drop and observed the flow pattern of solid-liquid mixture in a pipe flow. They stated that

"... as the flow rate is increased, the stationary deposit does not diminish until its height approaches zero. Rather, it starts moving as a bulk when its height is several particle diameters."

Under certain conditions, when the solid-liquid mixture flow rate is relative too low to enable all solid particles suspended, a stationary bed deposit is formed. The stationary bed deposit may transport to various separated layers. This behaviour appears in the heterogeneous flow with a stationary bed as illustrated in Figure 2.1. In practical situation, heterogeneous flow with a stationary bed is avoided whenever possible because they tend to result in plugging or create unsteady flow behaviour. Therefore, the design of the pumping system in a pipeline is based on the understanding of type of slurry flows, which may occur, associated with the solid concentration, size distribution, flow rate requirements etc.

Fangary et al. (1997) investigated the effect of fine particles in a polydisperse phosphate slurry on pressure drop. At the same flow rates, flow of fine particles gave higher pressure drop than coarse particles because the coarse particles tend to damp turbulent eddies, which lead to a lower pressure drop. A correct fine particle concentration in powdered transports could lead to reduction in pressure drop, which contributed to the implication of designing and operating conveying systems. Matousek (2005) suggested that a prediction of pipeline hydraulic performance is required in designing slurry pipelines. The solid particles have a high potential to cause pipe-wall friction. In addition, fine slurries exhibited higher-pressure gradient compared to coarse slurries when flows at same concentration and velocity.

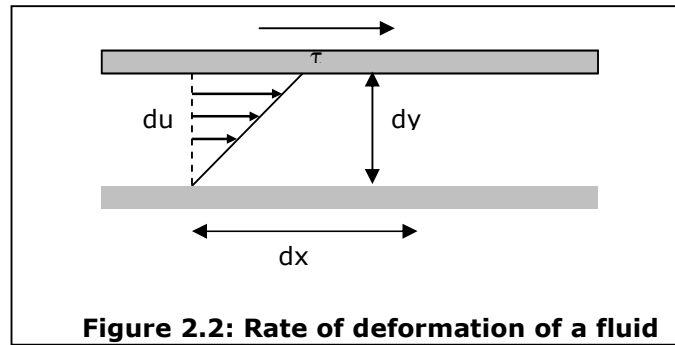
In some cases, hydraulic transport of slurries is associated with erosion damage, which is caused by solid particle impingement. Millions of pounds are spent every year to repair erosion damage in slurries transport and other particle-liquid mixtures in pipes. Wood et al. (2004) performed a computational modelling to predict erosion damage levels in slurry ducts when particles are in contact with the duct. The sand-water slurries showed wear distribution on a straight pipe (top and bottom) and bend. Stack and Abd El-Badia (2007) identified the effects of slurry concentration (sea water) on the mechanisms of erosion and corrosion. The experiments were tested at various impact velocities. They discovered that the slurry concentration and the impact velocity of sand particles have a significant erosion and corrosion on test materials such as mild steel.

Kaushal et al. (2002) studied the deposition velocity of solid particles on the bottom of pipe at different concentrations and velocities. They discovered that the solid concentrations at the bottom of pipe are three times higher than the output product concentration (effluent and static settled products). These studies as mention above shows that the slurry transport processes are very complex and may require a better transport mechanism such as by inducing a swirling flow before a bend.

2.1.2 Non-Newtonian Transport Processes

In processing industries, fluids are pumped over long distance. There will be a great magnitude in pressure drop along the pipeline. Some fluids are incompressible because their densities are independent on the pressure. A simple molecular structure of fluid exhibits Newtonian behaviour, where its viscosity is independent on temperature changes and forces on it. A fluid of complex molecular structure, such as cellulose-base polymer exhibits non-Newtonian behaviour. Some non-Newtonian fluids used in the industry are liquid detergents, oils, paints, printing inks, etc.

Figure 2.2 Illustrates fluid behaviour with a shear stress, τ , applied at constant velocity, du . The upper plate moves at certain length, dx . For a Newtonian fluid, the shear rate, du/dy (velocity gradient) will increase proportionally (linearly) with shear stress, τ under constant temperature and pressure.



The relationship of Newtonian viscosity can be expressed as follows (Reynolds, 1881-1901) (cited in Richardson et al., 2004):

$$\tau_{yx} = \mu \frac{du}{dy} \quad \text{Eq. 1}$$

Where, τ_{yx} is the shear stress, μ is the viscosity (Pa.s) and du/dy is the shear rate (s^{-1}).

The consistency of viscosity (under constant static pressure and temperature) is constant for Newtonian liquids and known as absolute viscosity. The consistency of non-Newtonian fluids (toothpaste, paint, cellulose polymer, etc.) varies even though the static pressure and temperature are constant. It shows that the viscosity of non-Newtonian fluid depends on the applied shear stress. This explains that a non-Newtonian fluid does not obey Newton's law of viscosity and its shear stress is not directly proportional to the deformation rate. The consistency of non-Newtonian fluids is expressed as apparent viscosity.

Tanner (1985) (cited in Clayton, 2006) divided the non-Newtonian fluids into three categories consisting of time-dependent (thixotropic and rheopectic), time-independent and viscoelastic. A time-dependent non-Newtonian fluid has an apparent viscosity, which is a function of shearing duration. The shear rate of a time-independent non-Newtonian fluid is a function of shear stress and not the time fluid sheared, which either exhibits shear thinning or shear thickening. The apparent viscosity of a shear thinning fluid (such as paint) is decreased with shear rate, while on the other hand, shear thickening of fluid increases with shear rate. Figure 2.3 illustrates the time-independent behaviour of non-Newtonian fluids.

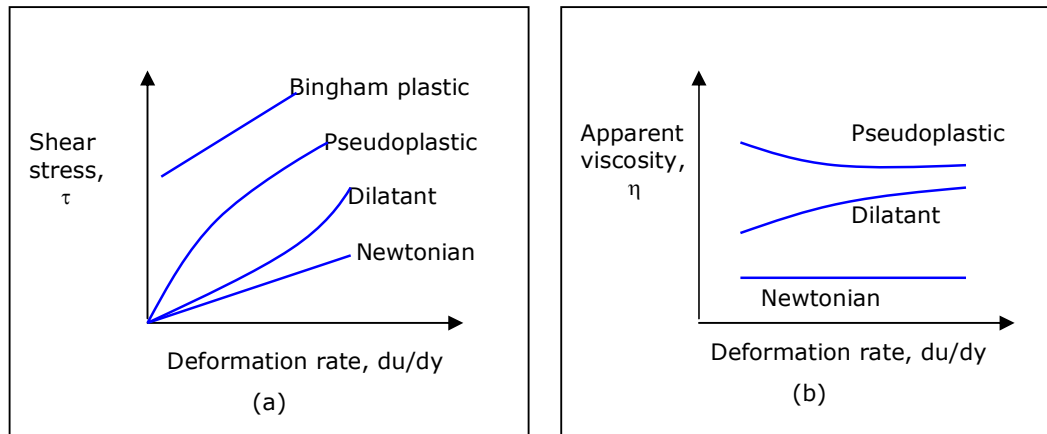


Figure 2.3: The rate of deformation of fluids against shear stress, τ (a); and against apparent viscosity, η (b)

The pressure drop measurement is important in some practical problems involving non-Newtonian fluids to flow in pipelines. It is because a non-Newtonian fluid has higher apparent viscosity, η (Ns/m^2). Here, restriction is made to explain power-law non-Newtonian fluids behaviour, as it covers part of the research objectives.

The relation between shear stress and shear rate for power-law non-Newtonian fluid (Ostwald-de Waele law):

$$\tau_y = k \left(\frac{du}{dy} \right)^n \quad \text{Eq. 2}$$

Where, n is the fluid ability (behaviour) index and k is the consistency coefficient.

For power-law (shear-thinning) non-Newtonian fluid, n value is less than 1 because the apparent viscosity of fluid tends to decrease with increasing shear rate. Agarwal and Chhabra (2007) embraced a new data for Newtonian and power law liquids and concluded that a power law liquid has a fluid ability index between 0.61 to 1.0 and consistency coefficient between 0.0078 – 15.31 Pa.s.

Geldard et al. (2002) conducted an experiment in the selection of suitable non-Newtonian (pseudoplastic and time-independent) fluid for swirling pipe flow, which included hydroxypropyl-cellulose (HPC), methylcellulose or hydroxypropyl methylcellulose (MC or HPMC), polyvinylpyrrolidone (PVP), carboxymethyl cellulose sodium (CMC), guar gum (GG) and xanthan gum (XG). The objective was to choose an

applicable non-Newtonian material that has a shear thinning characteristic which has widespread use in the industry. Through the thixotropy and rheology tests, they selected a CMC fluid for its non-thixotropic and shear thinning properties, showed minimal frothing and do not degrade with bacteria and age. The CMC fluid also showed a temperature dependent characteristic.

2.2 Flow in Bends

Another issue to be considered in a pipeline system is flow behaviour in bends. In many cases, a fluid regardless of flow type travels through several configurations in a pipeline system before reaching its destination and this includes a flow in bends. Bend applications are important in many types of industrial equipments such as ventilators, heat exchangers, evaporators, condensers, transport pipelines, etc. The pressure drops, ΔP over a bend are affected by radius to diameter ratio (R/D), phase flow of fluids (single phase or multiphase), fluid properties (with or without solid particles), boundary layer at the wall, pipe diameter, friction factor, bend angle and flow velocity (Mukhtar et al., 1995; Azzi et al., 2000; Tonkin, 2004; Spedding et. al., 2007).

Ayukawa (1969) and Toda et al. (1972) investigated the pressure drop at different radius of curvatures, fluid concentrations and velocities both on vertical and horizontal bends. They discovered the existence of secondary generations (flows) in a horizontal bend, which suspended the settling particles along the inside wall. The larger radius of curvature performed better results compared to small radius of curvature. It was because the pressure drops when tested with larger particles in small radius of curvature showed no increase with concentration.

Mukhtar et al. (1995) conducted heterogeneous slurries (iron ore slimes and zinc tailings with a specific gravity of 4.2 and 2.6 respectively) transport on 90° horizontal bend. The iron ore slimes particles were coarser and approximately 96% finer than 75 μ m zinc tailing. Mukhtar et al. (1995) found that for radius 90° horizontal bend, the loss coefficient was less than water, which showed the pressure drop is largely independent of solids concentration and specific gravity. The results obtained were due to secondary generation flows created by the centrifugal forces and boundary layer at the wall (Cha et al. 2003).

Azzi et al. (2000) investigated the two-phase flow behaviour with Newtonian liquid phase in the horizontal 90° bend. These two-phase flow behaviours were correlated with Chisholm models type B and C, and Lockhart-Martinelli parameter. The pressure loss was higher when the total mass flow rate increased. The steam-water phases showed larger pressure losses compared to air-water phases due to density ratio of steam-water was half than the air-water mixture.

Spedding et al. (2006) investigated a pressure drop for two phase (gas-liquid) flow through a vertical to horizontal 90° elbow bend in 0.026m internal diameter pipe. They discovered a significant pressure drop in vertical inlet tangent compared to the straight vertical pipe due to elbow bend, which build-up the pressure drop.

Flows in bend are more complex compared to a straight horizontal or vertical pipe. Marn and Ternik (2006) conducted a numerical study of a non-Newtonian (shear thickening fluid) laminar flow in a 90° pipe bend. The data obtained shows the power law correlation with the predicted pressure loss and pressure drop coefficient when applied within a range of tested Reynolds number.

2.3 Problems Encountered in Pipeline System

The most common problems encountered in a pipeline system are wears and erosions. This has prompted designers and engineers to look for better solutions. This necessity has emerged researchers to review the importance of various fundamental considerations relating to the motion of fluid flow and its properties.

Due to particle abrasive nature, slurry flow has a high potential to cause wear in pipelines (Raylor, 1998). Engineers tend to predict a sufficient flow velocity to achieve a state of suspension or partial settling into the flow to transport the slurry as to minimise the wear along the pipe. Wood et al. (2003) measured the erosion penetration on AISI 304 stainless steel pipe when transported the 10% solids slurry fluid, which has a particle size approximately 1mm and density of 2670 kg/m³.

Wood et al. (2001) who collaborated with The University of Nottingham, predicted a reduction of erosion damage when transported slurries in pipeline bend (carbon steel, AISI 1020) based on the impact of characteristic velocity of particle. The prediction was determined using a model suggested by Haugen et al (1995):

$$W_t = M_p K f(\alpha) U_p^n \quad \text{Eq. 3}$$

Where:

- W_t = Total eroded volume per impact
- M_p = Mass of particle
- K = Empirical erosion constant (2×10^9 for carbon steel)
- $f(\alpha)$ = Angle dependency constant
- U_p = Particle impact velocity
- n = Characteristic velocity exponent (2.6 for carbon steel)

Wood et al. (2001) found that the erosion rate is less sensitive when the impact angle is doubling compared to doubling the velocity. For example, when impact angle moved from 10° to 20° , the erosion rate was $2.8 \times 10^{-8} \text{ m}^3/\text{kg}$ while when velocity increased from 5 m/s to 10 m/s, the erosion rate was $6.0 \times 10^{-8} \text{ m}^3/\text{kg}$.

Researchers have experienced severe problems when fluids flow in bends. Peakall et al. (2007) conducted a series of physical experiments for flow processes and sedimentation in submarine channel bends. The data obtained suggested that the reversal cross-stream flow direction is an important factor to determine the bend effect, and the behaviour of reversal in secondary generation cell direction, which influenced the grain size deposits.

To address these problems, Jones (1997) and Raylor (1998) proposed the use of swirl-inducing flow to transport slurries. Transporting Newtonian, non-Newtonian and more complex fluids could be an advantage when preceded with swirl-inducing flow applications.

2.4 Swirling Pipe Flow

Transportation of either single or multiphase fluid through a pipe consumes a lot of pumping power or energy requirements. Erosive wears and corrosion in pipeline and pressure losses have also been experienced. Interest in finding the possibility of reducing energy requirements and subsequently improve a pipeline flow in a horizontal or vertical pipe and bend have been growing especially on a flow to enhance the suspension of solid particles in fluids. A swirl-inducing flow inside the pipeline is one of the methods to overcome these issues. Swirling flow in the pipe is considered as the

combination of vortex motion with axial motion in the pipe axis (Baker and Sayre, 1974).

During the past decades, researchers have experienced the disadvantages and difficulties in creating a mechanical swirling flow in a pipeline. Some experiments have taken many forms of non-circular cross-sections pipe geometry to optimise the potential of creating swirl flows.

Robinson (1921) (cited in Tonkin, 2004) patented rifling ribs in a spiral arrangement to create a homogeneous mixture. The application of ribs caused the water to follow a spirally (swirl) through the pipe. Then, Yuille (1927) suggested different types of finned sections to be installed in a pipeline. The finned section has larger outside diameter than any regular sections with a spiral fin within. Yuille assumed this would be more economical than creating a continuous series of spiral fins.

For transporting solid-liquid mixtures (Howard, 1938 and 1939) (cited in Ganeshalingam, 2004) added rifles inside a pipeline to increase the capacity used for transporting solid-liquid mixture such as sand and gravel. The combination of rifles and swirling flow caused a uniform solid distribution and increased the efficiency of settling in acceptable quantities. Wolf (1967), created the helically-rib pipe to induce swirling flow. The purpose of invention was to reduce wear effect, maintain particulate solid in suspension at lower velocity and saved the energy.

Wang (1973) (cited in Ganeshalingam, 2002) investigated several different non-circular cross-sectional geometries (square, triangle, rectangle etc.) of pipe for transporting slurries to create a transverse flows by constantly lifting (sweeping) deposits and carried through the pipe. It was discovered invention caused more damages (wear) in a pipe-cross section.

Heywood et al. (1998) recommended few methods to minimise a frictional pressure loss when transporting slurry fluids, as mentioned below:

1. Use a material which has high molecular weight polymer,
2. Use spiral ribs to reduce the limit of settling velocity, and
3. Vibrate the pipeline without disturbing its slurry flow rate.

Following this invention, The University of Nottingham has taken intensive measures and effort to begin a research on swirl-inducing flow.

Raylor (1998) investigated the advantages of using swirl-inducing flow to reduce wear and create a sustainable particle distribution throughout a bend. The experiments were determined using a Computational Fluid Dynamic (CFD) programme. Raylor (1998) discovered that the swirling flow causes a reduction in pressure drop before a bend compared to a non-swirl inducing flow. This pressure changes resulted from a spontaneous change of fluid into the entry and exit cross-section of the swirl pipe. Another discovery is that swirling flow of particles before the bend tends to create better distributions, which ensure the potential to reduce or minimise wear characteristic in the pipe.

A circular pipe has a great potential to promote settling behaviour of particles (more dense than carrier fluid) at low velocity compared to use of internal helical ribs (Wang, 1973) (cited in Ganeshalingam, 2002). This accompanied with a turbulent flow to transport solid-liquid mixtures and keep the particles in suspension. It was reported that (Fangary et al., 1997; Wood et al., 2001; Hussain and Robinson, 2006) the turbulent flow with high velocity profile of solid particles leads to wear, erosion or corrosive (depending on solid particle and carrier fluid properties).

To address these problems and improve suspension flow of solid particles in pipeline, a swirl-inducing flow was suggested (Jones, 1997; Raylor, 1998). In addition, Wood et al. (2001) suggested the potential of swirl-inducing flow in commercial slurry pipelines could be achieved in terms of reducing local wall penetration (erosion) by optimised the impingement angles for bend.

Following this, Ganeshalingam (2002) intensively investigated the effect of swirling flow for transporting solid-liquid mixture using the Computational Fluid Dynamics (CFD) modelling. The CFD was also used as a design tool to validate and optimise the available 3-lobed swirl-inducing pipe design. The findings were based on interest attributed to Howard (1939, 1941), who performed studies on methods to generate swirl flow using a non-circular pipes. The solid concentration, flow visualisation and particle distribution of slurry transports were observed using Electrical Resistance Tomography (ERT) and Particle Image Velocity (PIV) techniques. Ganeshalingam (2002) found that the 4-lobed (length = 0.4 m; pitch-to-diameter ratio = 8) swirl-inducing pipe was more effective than 3-lobed (length = 0.4 m; P/D = 4) pipe design. The pressure loss contributed from swirl-inducing flow was higher than circular pipe. The effectiveness (optimum performance) of swirl-inducing pipe was determined using a parameter below:

$$\eta_e = \frac{\Omega}{\left(\frac{\Delta P}{0.5\rho u^2}\right)} \quad \text{Eq. 4}$$

Where, η_e is the swirl effectiveness, Ω is the swirl intensity, and $\left(\frac{\Delta P}{0.5\rho u^2}\right)$ is the normalised pressure drop. The η_e for different pitch-to-diameter ratio (P/D) of 3-lobe swirl pipe and 4-lobe swirl pipe were 6 and 8 respectively.

To validate Ganeshalingam's (2002) work, Tonkin (2004) investigated the application of swirl inducing pipe at different pipe configuration (incline pipe, different R/D of bends, etc.) when pumping a range of fluids such as non-Newtonian and solid-liquid mixtures. The investigations include the observation of a flow pattern using flow visualisation technique with PIV. The effect of swirl on pressure drop when pumping slurries of different particle sizes and densities also investigated. Tonkin (2004) found that a swirling flow has more advantages for slurries with higher concentrations (2.7% v/v) and the pressure drop increased for horizontal and inclined pipe flow. The 4-lobe swirl-inducing pipe (Figure 2.4) showed higher pressure drop than 3-lobe swirl pipe when pumping sand-water slurries as claimed by Ganeshalingam (2002).

Stevenson et al. (2006) analysed the advantage of swirling flow for slurries transports (swirling flow of quartzite and plastic beads) using electrical resistance tomography (ERT) system. The ERT system was selected for the investigation of a swirling flow because the technique is widely accepted in process engineering application (Cillears et al., 2001). The 3D image model shows clear visualisation for solid-liquid mixtures across pipe cross-sections, which guides better improvement and understanding of swirling flow pattern.

Geldard et al. (2002) investigated a suitable non-Newtonian fluid to be tested for swirl-inducing pipe rig. The sodium carboxymethyl cellulose (CMC) containing 100ppm Nalco 2593 biocide was chosen as a non-Newtonian fluid test material because it behaves as a pseudoplastic fluid (thixotropic), time-dependence and temperature dependent. Geldard et al (2002) claimed that the CMC solutions were ideal for used in swirl pipe test up to 11 days without any bacterial degradation (Tonkin, 2004).



(a) Length = 20cm; diameter = 0.05m (b) View inside 4-lobe swirl pipe

Figure 2.4: 4-lobe swirl pipe used by Tonkin (2004)

Based on Ganeshalingam (2002) findings of swirl-inducing pipe using CFD, Ariyaratne (2005) explored and validated the method to expand and optimise the swirl pipe geometry using a CFD model. A swirl-inducing behaviour also tested with carboxymethyl cellulose (CMC) as a non-Newtonian and high viscous fluid. Tonkin (2004) found that the swirl-inducing flow for CMC does not sufficiently swirl as compared to water. Three swirl pipes (length = 0.4m and diameter = 0.05m) with different pitch to diameter ratio ($P:D = 3, 6$ and 10) were created using the Gambit software. The smallest $P:D$ ratio ($P:D = 3$) have the closer twist and the $P:D$ of 5 found as the most optimum geometry for a non-Newtonian fluid. Table 2.1 shows the flow parameters used by Ganeshalingam (2002) and Ariyaratne (2005) for the CFD simulations of high viscous fluid (CMC).

The viscosity of a non-Newtonian fluid changes with shear rate (or velocity gradient). A CMC fluid when pumped through a swirl-inducing pipe is subjected to three direction of velocity gradient, which were axial, tangential and radial (Ariyaratne, 2005; Tonkin, 2004). Correspond to this statement, Ariyaratne (2005) found the CFD simulation shows a high viscosity, which appeared on the core of swirl pipe with low transmission of tangential velocities when used CMC as a carrier fluid (Tonkin, 2004).

Table 2.1: Flow parameter used in CFD simulations by Ganeshalingam (2002) and Ariyaratne (2005)

Description		Unit	Value	
			Ganeshalingam	Ariyaratne
Total length of swirl-inducing pipe (transitional / swirl / combination)		m	0.4	0.55 (CMC)
				0.1 - 0.6 (water)
Inlet velocity				
	Axial (u)	m/s	1.0 - 3.0	1.5
	Radial (v)	m/s	0.0	0.0
	Tangential (w)	m/s	0.0	0.0
Reynolds number (water)				
			50,000 - 150,000	75,000
Outlet pressure		Pa	0.0	
Inlet turbulent intensity		%	10	4
Hydraulic diameter		m		0.05
Fluid properties				
Water				
	Density	kg/m ³	998.2	
	Viscosity	kg/ms	0.001	
Carboxymethyl cellulose (CMC)				
	Density	kg/m ³		1002.8
	Consistency index, n			0.6 or 1.2
	Power law index, k			0.6

2.5 Carboxymethyl Cellulose Sodium Salt

Synonyms of CMC can be recognised as carboxymethyl ether cellulose sodium salt, sodium carboxymethyl cellulose, sodium cellulose glycolate, and cellulose glycolic acid sodium salt. Carboxymethyl cellulose sodium salt (CMC) appeared as a white to off white powder and easily soluble in aqueous solution such as water. During mixing, a small portion of CMC is added carefully to the water to avoid clumps of solid, which may result in difficulty to dissolve.

Many published authors have investigated the chemical and physical properties of sodium carboxymethyl cellulose (CMC) into wider applications (Kaistner et al., 1997; Geldard et al., 2002; Yasar et al. 2007). Geldard et al. (2002), Ganeshalingam (2002)

and Tonkin (2004) have selected CMC solutions among other six pseudoplastic fluids as a non-Newtonian fluid at different concentrations to be used in swirling flow investigation.

Kastner et al. (1997) examined the macroscopic structure and solution properties of eight commercial samples of sodium carboxymethyl cellulose. They discovered that the ionic strength of CMC solutions at different concentrations are able to decrease the relaxation times, viscosity and Kerr constants.

Mitsumata et al. (2003) investigated the pH-response and swelling properties of complex hydrogels, which consisted of carboxymethyl cellulose sodium salt (NaCMC), chitosan and κ -carrageenan in pure water and alkaline solutions. They discovered that the combination composition and salt concentration of NaCMC and κ -carrageenan have a significant influence on the swelling properties of complex gels. This showed that the CMC properties play an important role in swelling behaviour of polyelectrolyte complex hydrogel.

The viscosity of CMC solutions are both concentration and temperature dependent (non-Newtonian behaviour, Tanner 1985). If the temperature increases, the viscosity would decrease and if the concentration increases, the viscosity would increase. Yasar et al. (2007) etherificated CMC using sugar beet pulp cellulose and optimised the solution through carboxymethylation with sodium chloroacetate and isobutyl alcohol (solvent medium). The viscosity CMC solutions were measured using a rotational viscometer at different temperatures and concentrations.

Yaseen et al. (2004) studied the rheological properties of gum including the CMC at different concentrations. The CMC showed an exponential relationship described by power-law relationship. Tonkin (2004) examined that the CMC fluids apparent viscosity, η is time-dependent. The thixotropic of CMC fluids (Figure 2.5) showed a decrease in η under a constant applied shear stress.

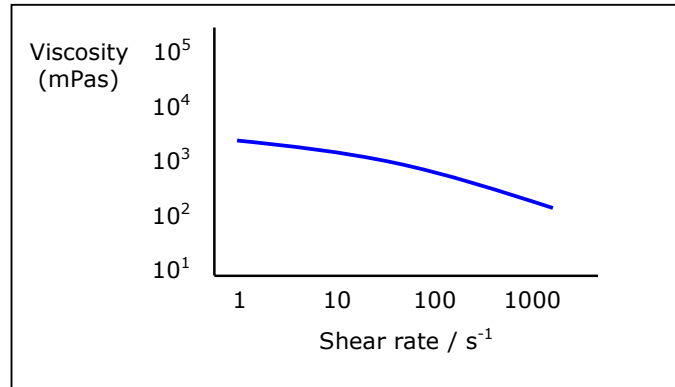


Figure 2.5: Apparent viscosity with shear rate for 2.5% w/w CMC (Tonkin, 2004)

Yasar et al (2006) investigated the rheological properties of CMC from orange peel cellulose using a rotational viscometer at different temperature and concentrations. The viscosity of CMC as a function of temperature was determined using the Arrhenius and Andrade equation.

$$\eta = \eta_o \exp\left(\frac{E_a}{RT}\right) \quad \text{Eq. 5}$$

Where

- η = Viscosity of CMC solution (mPa.s)
- η_o = Pre-exponential factor (mPa.s)
- E_a = Flow activation energy (kJ/mol)
- R = Universal gas constant (8.314×10^3 kJ/mol K)
- T = Absolute temperature (K)

The published articles described above, proved that CMC solutions behaved as a pseudoplastic and seem to be adequately described using the power law model. The viscosity of CMC solutions was found to be the function of temperature and concentration (Yasar et al. 2006).

2.5.1 Applications

Gomez-Diaz and Navaza (2003) have studied the rheological properties of CMC by determining its molecular weight (polymers) using Huggins and Kramer equations. They found that at different polymers concentration, the apparent viscosity and shear rate of CMC exhibited shear thinning and non-Newtonian fluid behaviour. This shows that CMC is suitable to use as thickening agent in food products.

CMC has the ability to improve the material consistency and flow properties. The availability of CMC to be produced in different viscosity and rheological grades allowed the application of CMC to be used in many food systems. In cake mixes, CMC is used to improve the moisture retention or binding because it can control viscosity of batter, improves cake volume, can be used in frosting and icing, prevent the film from sticking to the package, reduce the sugar graininess (sugar crystal growth), and stabilise the emulsion. In pet foods, CMC at low viscosity has a tendency to hold the product (pellet) together and prevent any accumulation in its package during delivery. In pharmaceuticals CMC is used as a suspending and viscosity-increasing agent.

Because of its thixotropic behaviour, CMC is also commonly used in detergents (soil-suspending agent), resin emulsion paints, adhesives, printing inks, textile sizes and in mud-drilling. Kästner et. al (1997) has investigated a wide range of CMC solutions to be commercialised. The monografted and bigrafted of modified CMC (hydrophobically modified carboxymethylcellulose, HMCMC) is used in cosmetic and paint industries because HMCMC performed better as a stabiliser, binder and viscosifying or gelling agents.

2.6 Summary

The flow of fluids through pipes is a very important process for many industries and areas of interest. The particle distributions profiles in a pipe for different slurry flow regimes have been briefly presented. It shows that the slurry flow regime varies with the solid particles properties, which is relative to its carrier fluids. The slurry flow regimes is broadly categorise into four regimes, which are homogeneous, heterogeneous, heterogeneous with moving beds, and heterogeneous with stationary beds.

Non-Newtonian fluids vary even though the static pressure and temperature are fixed, which shows that a non-Newtonian fluid does not obey the Newton's law of viscosity. Tanner (1985) divided the non-Newtonian fluids into three categories consisting of time-dependent (thixotropic and rheopectic), time-independent and viscoelastic based on its apparent viscosity.

The transportation of slurry fluids through a pipe consumes a lot of pumping power and can cause erosive wears and pressure losses. To address these issues, a swirl-inducing pipe flow was invented and analysed to show that the application of swirl induction has the possibility of reducing energy requirements and improve the slurries pipeline system. Swirling flow in the pipe is considered as the combination of vortex motion with axial motion in the pipe axis (Baker and Sayre, 1974). Raylor (1998), Ganeshalingam (2002), Tonkin (2004) and Ariyaratne (2005) have designed and investigated the applications of swirl inducing pipe flows at different fluids conditions. The swirl-inducing pipe also optimised using a Computational Fluid Dynamics (CFD) modelling. They concluded that the swirl-inducing flows have advantages in increasing the homogeneity of solid particle distribution at lower velocity and hence reducing the wear effect and power consumption.

Mukhtar et al. (1995), Azzi et al. (2000), Tonkin (2004) and several sources in the literature highlights that when transporting slurry, the pressure drop, ΔP in horizontal or bend pipe flow is affected by radius to diameter ratio (R/D), carrier fluid, solid particles, boundary layer at the wall, pipe diameter, bend angle and flow velocity. Ayukawa (1969) and Toda et al. (1972) discovered the existence of secondary generations (flows) in a horizontal bend, which suspended the settling particles along the inside wall. Mukhtar et al. (1995) conducted a heterogeneous slurry transport on 90° horizontal

bend and the experimental data showed that the pressure drop relatively independent of solids concentration and specific gravity.

Carboxymethyl cellulose (CMC) is a cellulose-based polymer consists of two co-polymer units (β -D-glucose and β -D-glucopyranose-2-O-carboxymethyl-monosodium salt). The viscosity showed that CMC solutions are both concentration and temperature dependent (non-Newtonian behaviour, Tanner 1985). Yaseen et al. (2004) found that CMC showed an exponential relationship described by power-law relationship, while Tonkin (2004) determined that the apparent viscosity, η , for CMC fluids is a time-dependent. The rheological properties of CMC exhibits shear thinning and non-Newtonian fluid behaviour, which shows that the CMC is suitable to use as a thickening agent in food products. CMC has the ability to improve the material consistency and flow properties, useful in improving moisture retention in the food industry and as a suspending and viscosity-increasing agent in the pharmaceutical industry. CMC also used in resin emulsion paints, printing inks, textile sizes etc.

The pipeline analysis includes a driving force (pressure drop), flow rates, fluid properties and pipeline dimensions. The pressure drop, ΔP (Pa) correlations and relationship has been highlight to be applied under different flow conditions. This includes a determination of Reynolds number using a modification (non-Newtonian and time-independent) of Rabonowitsch-Mooney equation, pipe friction coefficient using Hagen-Poiseuille (laminar flow) and Colebrook (turbulent flow) equations and pressure head loss.

Chapter 3

TEST MATERIALS

3.1 Introduction

Geldard et al. (2002), Ganeshalingam (2002) and Tonkin (2004) have investigated different kinds of cellulose-based polymers for swirling pipe flow tests. They found that CMC complied with the required viscosity, shear-thinning, non-thixotropic properties and showed minimal frothing compared to other cellulose-based polymer fluids. The CMC concentrations used were 0.5, 1.0 and 1.5% v/v. Table 3.1 summarises the test fluid and concentration required.

Table 3.1: Test fluid and concentration

Fluid	Water	Slurry (% v/v)			CMC (% w/w)		
Concentration	N/A	1.4	2.1	2.7	0.5	1.0	1.5

Tap water was used as the standard or base and carrier fluid to transport sand particles.

3.2 Sand-water Slurry

The sand particles used in sand-water slurry has average diameter particles of 1000-2000 μm and density of 2640 kg/m^3 . The sand-water slurry concentration is expressed as volume fraction α_s or mass fraction C_s (Shenggen Hu, 2006) (cited in Clayton, 2006). The volumetric fraction of sand is:

$$\alpha_s = \frac{V_s}{(V_s + V_l)} \quad \text{Eq. 7}$$

and the mass fraction, C_s is:

$$C_s = \frac{\rho_s V_s}{(\rho_s V_s + \rho_l V_l)} \quad \text{Eq. 8}$$

Where the V_s and V_l represent the volume of sand and water (m^3) respectively.

In terms of percentage volume per volume (% v/v), the solid concentration can be calculated as follows (Appendix C.5) (Tonkin, 2004):

To obtain the volume of sand or solid particles (V_s) and liquid (V_l):

$$V_s(m^3) = \frac{m_s(kg)}{\rho_s(kg/m^3)} \quad \text{Eq. 9}$$

Therefore, the concentration of sand used in % v/v:

$$C_v = \frac{V_s}{V_l} \quad \text{Eq. 10}$$

The sand-water slurry density mixture, ρ_m (Shenggen Hu, 2006) (cited in Clayton, 2006):

$$\rho_m = \alpha_s \rho_s + (1 - \alpha_s) \rho_l \quad \text{Eq. 11}$$

Density of sand-water slurry equation below (Nesbitt, 2000):

$$\rho_m = \rho_l + \frac{C_v(\rho_s - \rho_l)}{100} \quad \text{Eq. 12}$$

$$\rho_m = \frac{1}{\left(\frac{C_m}{100\rho_s} + \frac{1}{\rho_l} - \frac{C_m}{100\rho_l} \right)} \quad \text{Eq. 13}$$

Where the ρ_L and ρ_s represent the density of liquid and solid respectively and the C_v and C_m represent the concentration of slurry mixture in percentage volume per volume (% v/v) and percentage weight per weight (% w/w) respectively. Appendix (table) C.6 shows the amount of sand required for each concentration.

3.3 Carboxymethyl Cellulose (CMC)

The CMC solutions were prepared to examine the effect of swirl-inducing flow on non-Newtonian fluids. Tonkin (2004) used deionised water when making the CMC solutions to avoid any changes in CMC rheological behaviour. The apparent viscosity of some fluids tend to change with time when in storage under no shear or very low shear.

The temperature is dependent on apparent viscosity and tends to increase with time, which means that the behaviour of the fluid would change over the course of a run. The apparent viscosity range is dictated by the concentration in solution and therefore a suitable concentration needed to be determined. Escudier et al. (2001) discovered a rheology that CMC is insensitive with water. Therefore it is suitable to be used as a solvent to dissolve CMC powder and ensure the fluids concentrations were fairly reproducible.

3.3.1 Procedures using Brookfield Viscometer

The Brookfield Viscometer model LV (Appendix B.1) is a rotational type of viscometer (concentric cylinder viscometer), which is commonly used to measure the viscosity of plastisols and thixotropic liquid (Clayton, 2006). The principle behind the rotational viscometer is based on the shearing stress created from a spindle when rotating at a constant speed while immersed in the sample. The degree of spindle lag is displayed on a rotating dial bar (Appendix B.2). LV viscometer has different types of spindle (Appendix B.3). Each spindle is differentiated by its disk. The display reading was taken between 10% and 100% torque to obtain accurate and repeatable results. For known viscosity of fluid, the maximum viscosity range produced from a spindle (at given speed) and reading from rotating dial (bar) was equal to the spindle speed multiplied by a corresponding factor. For unknown viscosity of a fluid and rotating dial below 10% or above 100%, a different speed was adjusted to obtain a reading in the recommended range.

The viscosity of viscous fluid (non-Newtonian) has an inverse relationship with temperature, where as temperature increases, viscosity decreases. Therefore, it is compulsory to measure and to control the temperature of a sample during measurements. The accuracy of a viscometer reading was determined as 1% of the full scale range (FSR) of the viscometer. The FSR is defined as the highest achievable viscosity reading with a given spindle and speed.

3.3.2 Methodology

The Brookfield viscometer was placed on a flat surface and an appropriate spindle was chosen by trial and error. 500ml of CMC solution was prepared inside a 600ml beaker as the minimum requirement to measure the viscosity when using the selected viscometer. Spindle was lowered and centred into the test fluid until the meniscus of the fluid was at the centre of the immersion groove on the spindle's shaft. Extra care was taken to avoid any air bubble from being trapped around the disk spindle. The motor was switched 'ON' to drive the viscometer and the viscosity was measured. 20 – 25 seconds was allowed for the indicator reading to stabilise before the red pointer is raised to obtain the viscometer reading. The time required for stabilisation depends on the speed at which the viscometer is running and the characteristics of the fluid.

The viscosities of CMC were recorded at different temperatures ranging from 14°C to 22°C. To ensure that the viscosity of fluid is obtained accurately, each test was performed at least three times at different speeds.

3.3.3 Apparent Viscosity of Carboxymethyl Cellulose

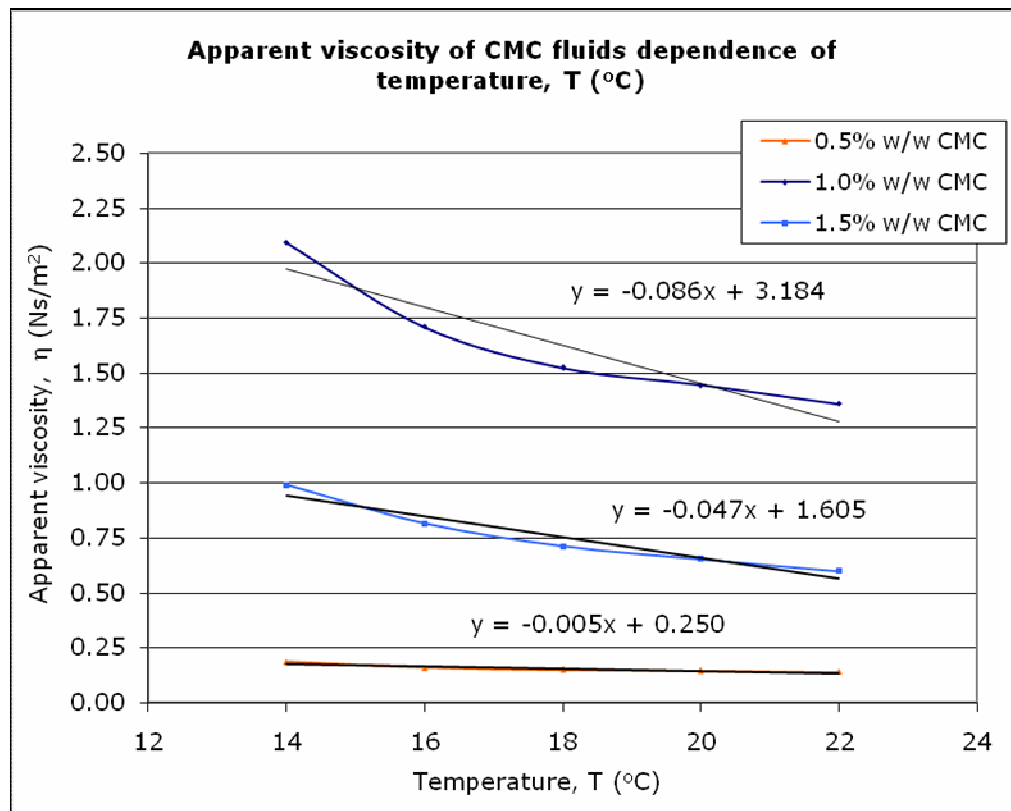


Figure 3.1: Temperature dependence of apparent viscosity for CMC fluids

Figure 3.1 shows that the apparent viscosity of CMC solutions was decreased with increasing temperature. The viscosity of CMC solutions was found to be a function of temperature and concentration (Yasar et al. 2006). Here, restriction was made to the viscosity measurement only. The CMC flow behaviour, shear-dependent, time-dependent or time-independent characteristics (rheology tests) were not determined due to limitation of instrument used. The swirl-induced pipe for CMC at different concentrations was performed averagely at 18°C. At this temperature, the effect of swirl-induced flow on pressure drops did not change with changes in temperature and viscosity since the concentrations of CMC were maintained at 0.5, 1.0 and 1.5% w/w (refer Chapter 5).

3.3.4 Shear Stress – Velocity Gradient of Carboxymethyl Cellulose

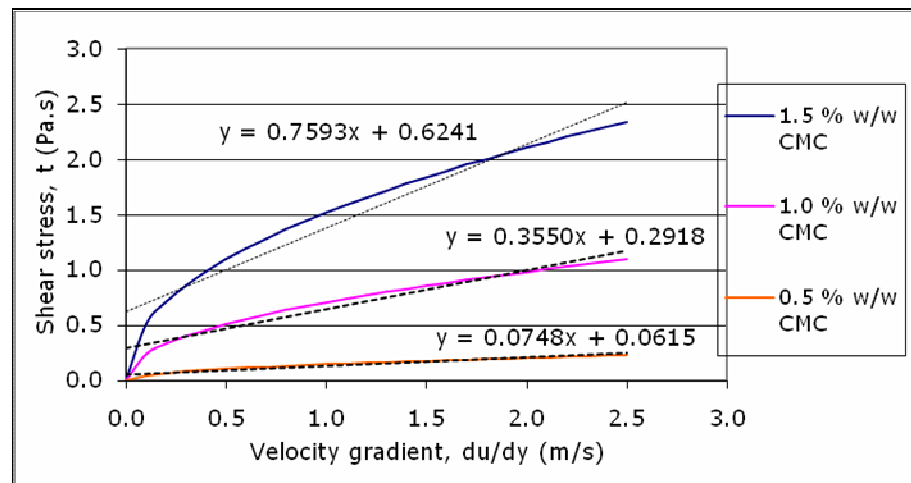
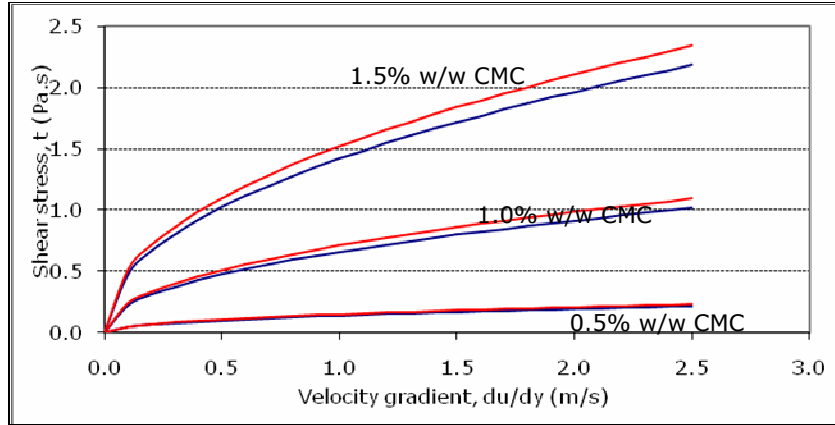


Figure 3.2: Shear stress-velocity gradient (shear rate)

Figure 3.2 shows the CMC fluids behaved as a shear thinning (power-law) and have high shear stress. 0.5% w/w CMC exhibits lower shear stress compared to 1.0 and 1.5% w/w CMC.



- Before storage (Day 2)
- After storage (Day 5)

Figure 3.3: Shear stress of CMC solutions on day 2 and day 5

The CMC solutions were prepared on day 1 before use in steel rig pipe loop from day 2 to day 5 and the viscosity was measured on day 2 and day 5. Figure 3.3 shows that the CMC solutions degraded after a long run (approximately 20 hours in total for 4 days operation). Tonkin (2004) also found that the viscosity of CMC solutions changed whilst stored in the pipe from day 2 to day 15 and traces of bacterial presence was detected. Tonkin (2004) concluded that CMC solution containing biocide was suitable to be tested in steel pipe rig (with swirl pipe test) for up to 11 days.

3.4 Flow– Pressure Relations (Model)

The pipeline analysis includes a driving force (pressure drop), flow rates, fluid properties and pipeline dimensions. The driving force, ΔP (Pa) is the difference between the pressures at two points along the pipeline. The pipe dimensions are the diameter (D) and length (L) and the fluid properties are the density (ρ) and viscosity (μ). These variables are illustrated in Figure 3.4.

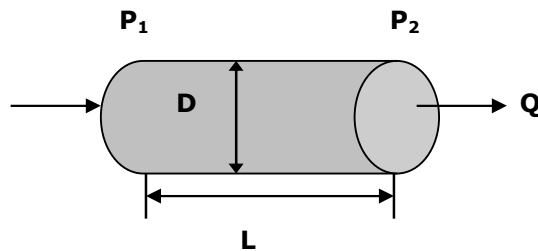


Figure 3.4: Flow in a pipeline

The flow regimes in this research when using water, slurry and CMC solutions were assumed to be steady and isothermal single-phase flow. In a fully developed flow, the pressure drop in a pipe loop caused by frictional losses is proportional to the pipe length and can be denoted as the (positive) quantity:

$$\Delta P = P_1 - P_2 \quad \text{Eq. 14}$$

It was assumed that the pressure at P_1 is higher than P_2 . For a Newtonian fluid in a smooth pipe, the Fanning friction factor, f and Reynolds number, Re are related by the frictional pressure drop per unit length ($\Delta P/L$) to the pipe diameter, D (m), density, ρ (kg/m^3) and average velocity profile, v (m/s). The pressure drop along a pipeline system can be calculated in the following order:

1. Determine the Reynolds number (Newtonian fluid)

$$Re = \frac{u \times D}{\nu} = \frac{\rho \times u \times D}{\mu} \quad \text{Eq. 15}$$

If $Re < 2000$, the flow is laminar, Re 2000-4000 the flow is transition and if $Re > 4000$, the flow is turbulent. The Reynolds number is a ratio of the inertia momentum flux in the flow direction to the viscous momentum flux in the transverse direction. Stable (laminar) flow occurs at low Reynolds numbers where viscous forces dominate, whereas unstable (turbulent) flow occurs at high Reynolds numbers where inertial forces dominate (Darby, 2001).

For power law fluid (non-Newtonian and time-independent), Metzner and Reed (1955) developed the Rabonowitsch-Mooney equation to:

$$Re_{MR} = \frac{\rho D^n V^{2-n}}{\gamma} \quad \text{Eq. 16}$$

and

$$\gamma = k^* \cdot 8^{n-1} \quad \text{Eq. 17}$$

$$k^* = k \left(\frac{1+3n}{4n} \right)^n \quad \text{Eq. 18}$$

Where,

k^* = Non-Newtonian fluid consistency index

n = Non-Newtonian flow behaviour index

Equation 16 is reduced to:

$$\text{Re} = \frac{\rho DV^n}{\eta} \quad \text{Eq. 19}$$

Where, η is the apparent viscosity of non-Newtonian power law fluids (Ns/m^2).

2. Pipe friction coefficient

For laminar flow, the pipe friction coefficient, f (Hagen-Poiseuille equation):

$$f = \frac{64}{\text{Re}} \quad \text{Re} \leq 2000 \quad \text{Eq. 20}$$

For turbulent flow, the pipe friction coefficient, f (Colebrook equation, 1939):

$$\frac{1}{\sqrt{f}} = -4 \log \left[\frac{1.256}{\text{Re} \sqrt{f}} + \frac{\varepsilon}{3.7D} \right] \quad \text{Re} \geq 5000 \quad \text{Eq. 21}$$

The friction factor f is the function of Reynolds numbers (Re) and the non-dimensionless surface roughness $\frac{\varepsilon}{D}$. The friction factor can be obtained from the Moody Diagram (Appendix A, Figure A.1).

3. Head loss

The pressure head loss (friction head), P_f is required to overcome the resistance of fluid to flow in pipe and fittings. From equation 11 and 12, the friction head loss, f in a length of pipe is given by:

$$P_f = f \times \frac{L}{D} \times \frac{u^2}{2g} \quad \text{Eq. 23}$$

4. Pressure by vertical elevation (pressure-height relation)

$$P = P_f + P_h \quad \text{Eq. 24}$$

$$\text{Where, } P_h = \rho \cdot g \cdot H_n \quad \text{Eq. 25}$$

H_n is the height of fluid travel along the manometer tube, which was determined by measuring the highest elevation fluid travelled. Therefore, the pressure drop, ΔP (Pa) across the pipeline was from equation 14

$$\Delta P_{n,n+1} = P_n - P_{n+1} \quad \text{Eq. 26}$$

Assumption made for the pressure drop model:

1. The fluid flows is an isothermal and adiabatic flow
2. The pressure, P (Pa) increases with increasing flow rate, Q (m^3/hr)

3.5 Summary

Water, sand-water slurries and carboxymethyl cellulose (CMC) were selected for the test materials. The concentrations of sand-water slurries used were 1.4, 2.1 and 2.7% v/v and 0.5, 1.0 and 1.5 % w/w for CMC.

The viscosity of CMC fluid was measured using the Brookfield Viscometer model LV at different concentrations and temperatures. The apparent viscosity of CMC solution was decreased with increasing temperature and found to be a function of temperature and concentration. Shear stress-velocity gradient graph showed that CMC behaved as a pseudoplastic (shear thinning, power law) fluid. The viscosity of CMC was measured on day 2 (after preparations) and day 5 (end of experimental tests). The CMC solutions were degraded after a long run (Tonkin, 2004). Biocide solutions were added to prevent any bacterial growth.

The pipeline analysis was determined by a driving force (pressure drop), flow rates, fluid properties and pipeline dimensions. If the flow is fully developed, the pressure drop in a pipe loop would be affected by frictional losses, which is proportional to pipe length. A Newtonian fluid flows in a smooth pipe has a Fanning friction factor, f and Reynolds number, Re , which are related by the frictional pressure drop per unit length ($\Delta P/L$) to the pipe diameter, D (m), density, ρ (kg/m^3) and average velocity profile, v (m/s).

The pressure drop model used based on Bernoulli's equation and the fluids flowing inside the steel pipe rig were assumed to be in an isothermal and adiabatic flow; and the pressure, P would be increased with increasing the flow rate, Q .

The pressure drop in this experiment was calculated in the following order: Reynolds number (Newtonian fluid) → Pipe friction coefficient → Head loss → Pressure by vertical elevation (pressure-height relation)

Chapter 4

STEEL PIPE LOOP

4.1 Brown Mixer Tank

The carboxymethyl cellulose sodium salt (CMC) appeared as a white powder. CMC solutions at different concentrations were prepared using a mixer tank – Brown Mixer Tank (Figure 4.1), which has the capacity and speed to mix solutions up to 2.0 m³ and 400 rpm respectively. The mixer tank has anchor impellers (close-clearance impellers), which operated near the tank wall. These types of impellers are effective in mixing a pseudoplastic fluid such as CMC (Perry et al., 1997). Each CMC solutions were mixed for several hours (up to 4 hours) depending on the concentrations before left overnight to fully hydrate (Geldard, 2000). The tank was sealed with polyester laser sheets to prevent heat conduction through the tank to the outside atmosphere.

The mixer tank was not connected to the steel pipe rig. Therefore, the CMC solutions inside the mixer tank need to be transferred into the conical tank using a submersible pump (Sub 2001 Mk2, SIP Industrial Products Ltd) as shown in Appendix A.1.



Figure 4.1: View inside the mixer tank with an anchor impeller

4.2 Steel Rig Pipe Layout

A pipeline is a system which consists of pipes, fittings (valves and joints), pumps, storage facilities, connectors, flow meter and other parameter devices. The steel pipe used in this experiment was designed by Tonkin (2004), which consisted of two

platforms. The steel rig was designed based on the Perspex pipe loop used by Raylor (1998) and Ganeshalingam (2002). The design was carried after several considerations were made, such as a selection of the route traversed by the pipe, amount of fluid transported, operational velocity, pressure gradient, types of pump, pipe thickness and material (whether to use steel, cast iron, or PVC pipe), and the facility to add or remove solid particles. In each design, careful consideration was also focused on safety, leak and damage prevention. Figure 4.2 illustrates the steel pipe loop.

Tonkin (2004) investigated three options of layout on steel pipe rig at different total length of pipe, which were 33.4 m (option 1), 37.7m (option 2) and 35.8m (option 3). The option 3 was selected for this research because it did not require any inclined sections or short horizontal straight pipe before the bend. Tonkin (2004) discovered that the fluid flows in option 1 and 2 took longer time to stabilise than option 3. Therefore, option 3 was selected in this research to investigate the effect of swirl inducing pipe flow on pressure drop prior before and after the swirl pipe and bend.

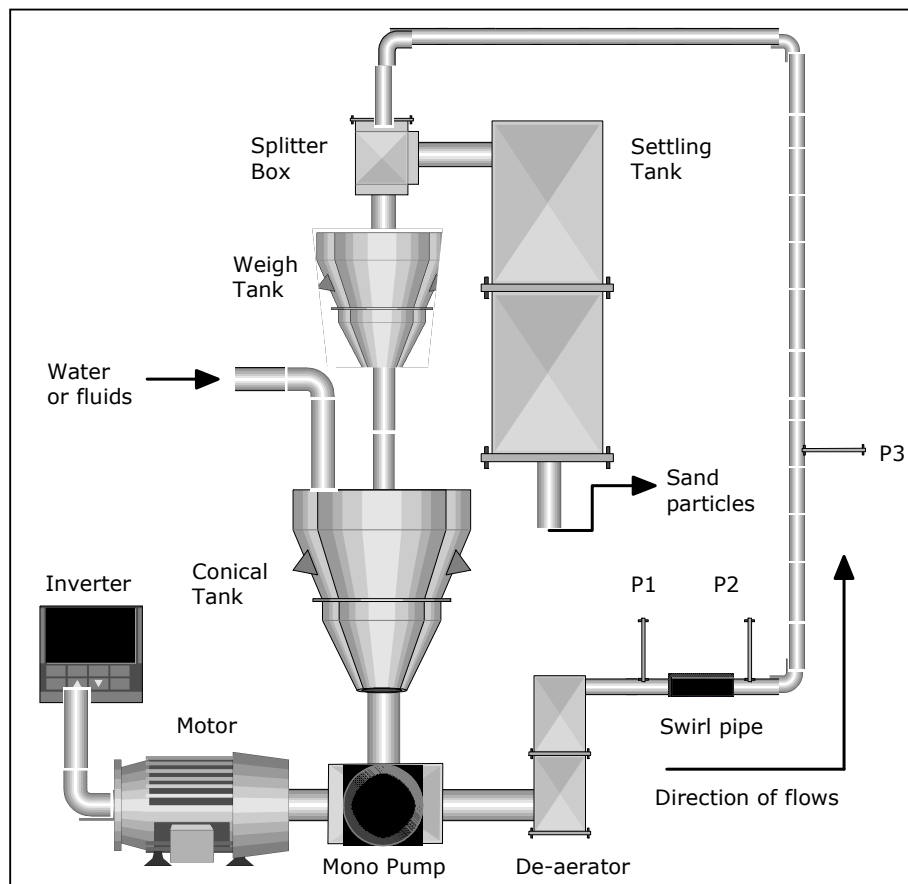


Figure 4.2: Illustration of steel pipe rig and its components

4.2.1 Pipe Network

A smooth steel pipe and a flexible perspex pipe were used in steel pipe rig, which consisted of several sections between 0.1m and 2m in length with a diameter of between 0.050m and 0.075m. These pipes were connected by flange sealed with O-ring. The pipe material chosen in this experiment was steel because of its wide availability and usage in the industry and high resistance to corrosion.

The lower horizontal pipe and vertical pipe were connected by a bend pipe (Figure 4.3), which has a 220mm radius of radius to diameter ratio (R/D) 4. This bend pipe was also used by Tonkin (2002).



Figure 4.3: 220mm radii pipe ($R/D=4$)

The pipe loop was arranged horizontally (downstream) straight from the de-aerator to the vertical bend (Appendix A.5) and horizontally (upstream) back to the weigh tank through the splitter box (Appendix A.6). Three flexible pipes were positioned from mono pump to inlet de-aerator, outlet of de-aerator to the entry of horizontal (downstream) pipe loop and outlet of horizontal (upstream) pipe loop to splitter box. These flexible pipes were installed to incorporate the pipe loop configuration and transfer settling particles into the settling tank (through splitter box).

4.2.2 4-Lobe Swirl Pipe

Ganeshalingam (2002) successfully optimised the swirl-inducing pipe flow with single-phase flow using the Computational Fluid Dynamics (CFD) and concluded that the 4-lobed pipe cross-section had significant advantages over other geometries of swirl-pipe such as 3-lobed swirl pipe design. There were two main factors which determined the mechanical advantages of swirl pipe, namely the cross-section twisted and pitch-to-diameter (P/D) ratio. Ganeshalingam (2002) found that the optimum P/D ratio for 4-lobe swirl pipe is 8 and 0.4m in length compared to P/D of 6 and 0.8m for 3-lobe swirl pipe. In this research, the 4-lobe swirl pipe was selected to determine the pressure drop on the steel pipe rig. The 4-lobe swirl pipe shown in Figure 4.4 has a cylindrical-end and swirl-end (4-lobe).

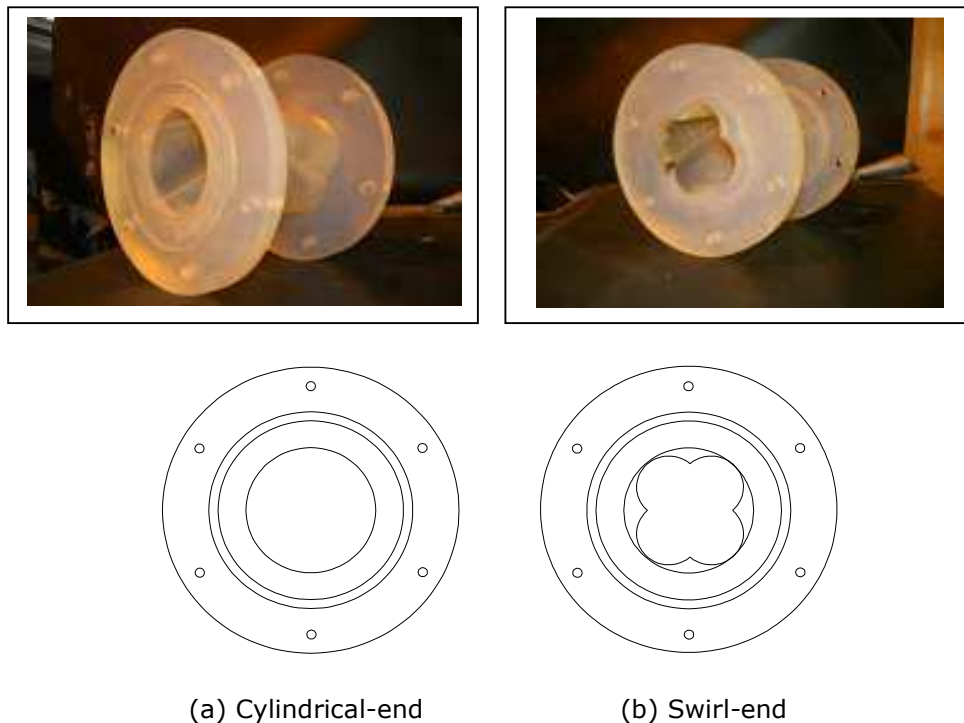


Figure 4.4: 4-lobe swirl pipe

The cylindrical-end was used as the entry to reduce any resistance when flowing from straight pipe. The cylinder-end had the same diameter as the steel straight pipe used. For one 4-lobe swirl pipe effect, the swirl-end was the outlet (Figure 4.5). For two 4-lobe swirl pipes effect, the cylindrical-end was the inlet and outlet. This was because the swirl-end of first 4-lobe swirl pipe connected with the swirl-end of second swirl pipe left the

cylindrical-end as the outlet (illustrated in Figure 4.6). Experiments were performed at velocities between 0.2 m/s and 2.5 m/s depending on the fluid characteristics (viscosity and concentration).

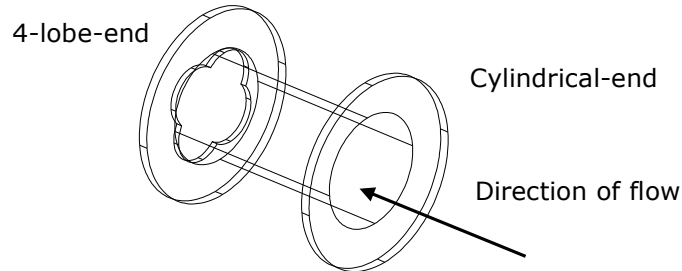


Figure 4.5: Illustration of one 4-lobe swirl pipe

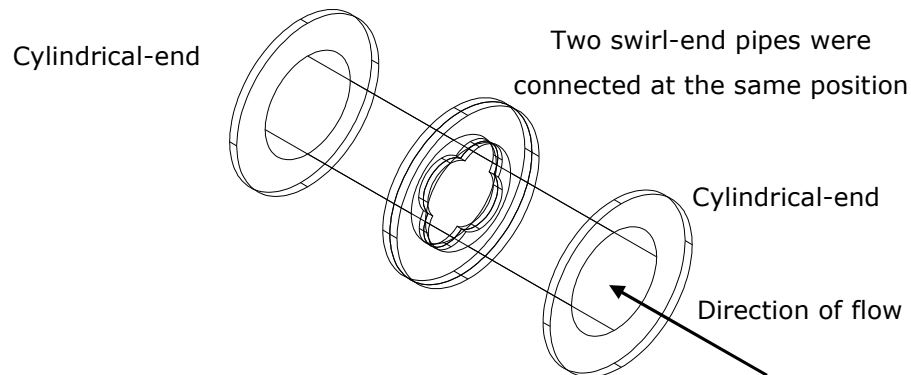


Figure 4.6: Illustration of two 4-lobe swirl pipes connected together

4.2.3 Inverter and Mono Pump

Many types of pumps are available to transport slurry and power-law fluids and pumping at constant capacity against varying heads. A progressive cavity pump (Mono Pump, Figure 4.7) was used, as it is suitable to pump water, high viscous fluid such as CMC (non-Newtonian fluid) and a mixture of sand and water at various concentrations. During the slurry experimental work, the coarse sand particles (2000 μm in diameter) used have high settling velocity, which tend to settle down in the pump and caused the pump to stop pumping. The pump motor (Appendix A.7) has a 15kW and was equipped with constant torque inverter drive (Appendix A.8). The flow control was achieved by the inverter (connected to the mono pump), which was manually adjusted (increased or

decreased) to achieve a desire flow rate. The frequency from the inverter was adjusted accordingly to the output signal from a digital flow meter.



Figure 4.7: Mono Pump

4.2.4 De-aerator

The de-aerator (Figure 4.8) is made of steel with Perspex on the top for the observation and consisted of a cylinder within an inlet at the top and outlet at the bottom. When the fluid travels into the de-aerator, a vortex would produce on a stand, which allowed any trapped bubbles to escape via a tube atmosphere. At the base of the de-aerator, a valve was installed to assist in draining the fluids or to empty the de-aerator end of the experiment.

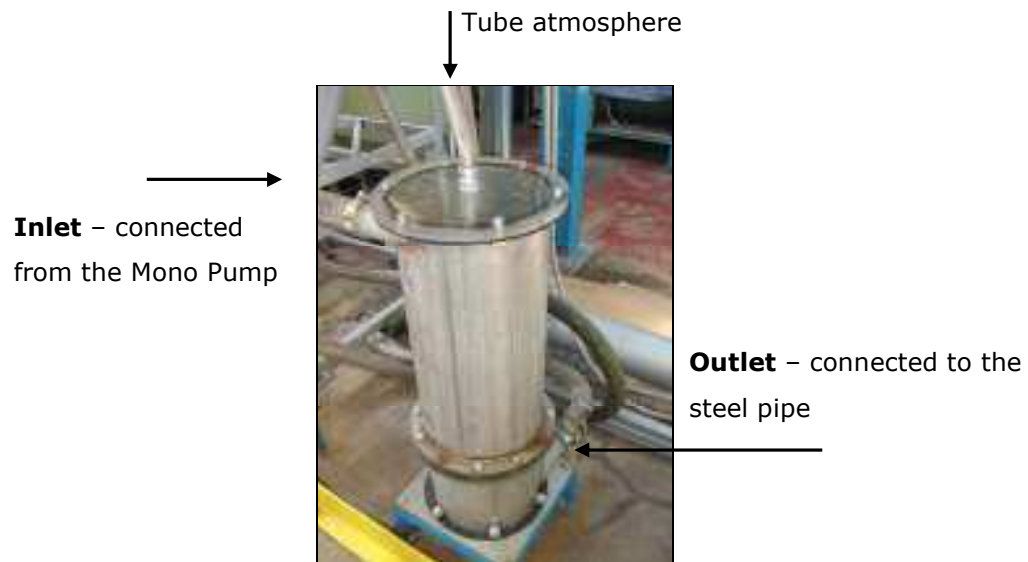


Figure 4.8: De-aerator

The inlet and outlet of the de-aerator were constructed at different levels. The flexible pipe was used to connect the outlet of Mono Pump to the inlet of de-aerator. The connection on both end of flexible pipe was tightened using worm drive hose clips and clamps. These flexible pipes were not suitable to withstand vibration of flow at high velocity. For example, at velocities above 3.2 m/s for water and 2.2 m/s for CMC, the flexible pipe became disconnected. This restricted the velocity for CMC operated up to 2.0 m/s. Due to this consideration, a maximum velocity allowed in the experiments were below 3.0 m/s (Tonkin, 2004) or at flow rates up to 21.2 m³/hr.

4.2.5 Conical Tank, Weigh Tank and Settling Tank

Figure 4.9 shows three types of tank used in this experiment – conical tank, weigh tank and settling tank at different sizes to fit the volume of the flow loop and pipeline configuration (Appendix A). The total volume of flow loop (volume of pipe loop plus volume of de-aerator) was 0.15m³. The conical tank has a capacity to occupy a volume of fluid up to 1.0m³ with an extra of 0.25m height installed on the top tank to prevent any overflow.

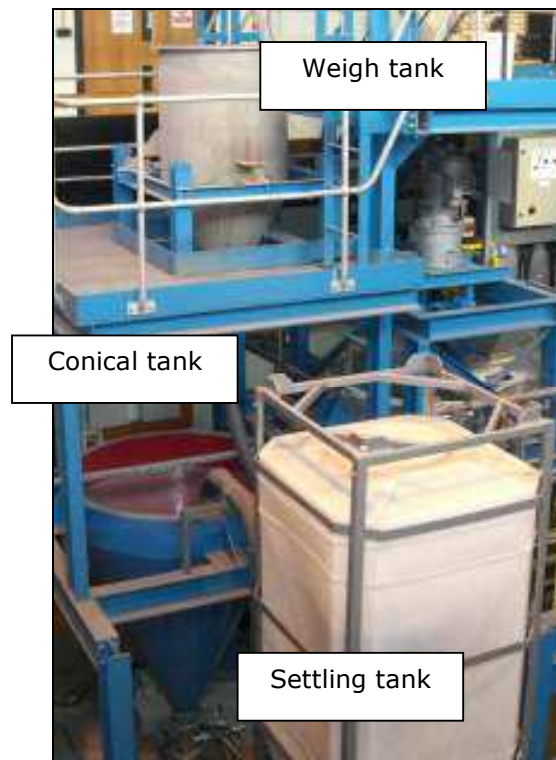


Figure 4.9: Weigh tank, conical tank and settling tank

4.2.6 Splitter Box

A flexible pipe was installed to connect the end steel pipe with a splitter box (Appendix A.9). Then this splitter box was attached on the top of weigh tank. The splitter box consisted of three parts namely, the flexible pipe with an adjuster, settling compartment and weigh compartment as illustrated in Figure 4.10. The flexible pipe positioned on the top of splitter box can be adjusted from weigh compartment to the settling compartment, which transferred or diverted the flow to weigh tank or settling tank respectively.

The use of splitter box was to enable the flow to be diverted from the conical tank to the settling tank. This method is useful to collect the sand particles when it settling at the bottom of the settling tank and prevent any blockage inside the pipe loop and Mono pump at the end of experiment.

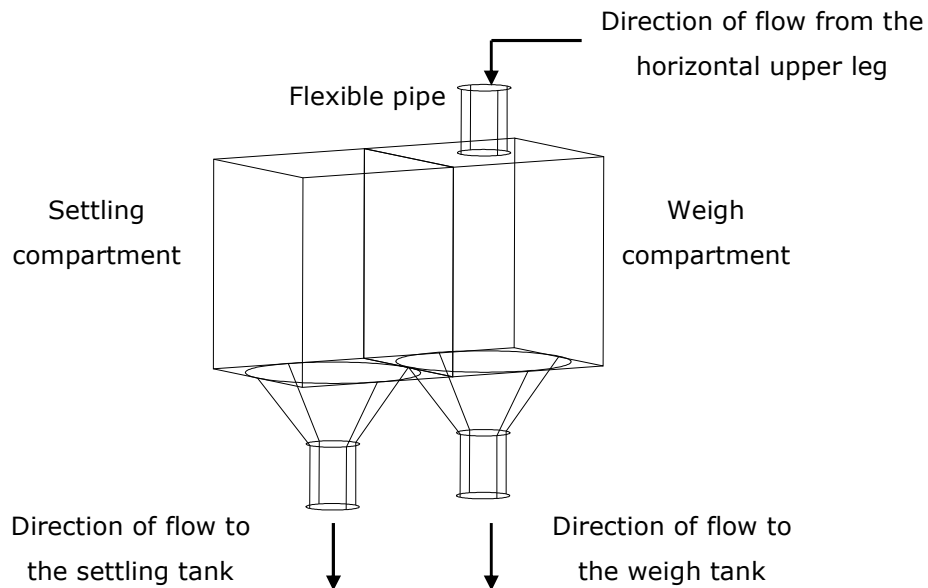


Figure 4.10: Illustration of splitter box and its parts

4.2.7 Measuring Parameters

Three types of parameters measured in this experiment were the temperature, flow rate, and pressure. The apparatus used to measure temperature was a K-type thermocouple (Appendix A.7) and the value was obtained from the controller box (Appendix A.9). The flow rate was measured using a digital flow meter (Appendix A.8).

The objective of this research was to measure the pressure drop when the fluid flows inside the pipe loop. There were two types of pressure measuring devices had been used prior before and after the swirl and bend – simple manometer tube and liquid pressure gauge. Three measuring points were placed as shown in Figure 4.11 to measure the pressure (1) before the swirl, P1; (2) after the swirl, P2 and; (3) after the bend (and swirl), P3.

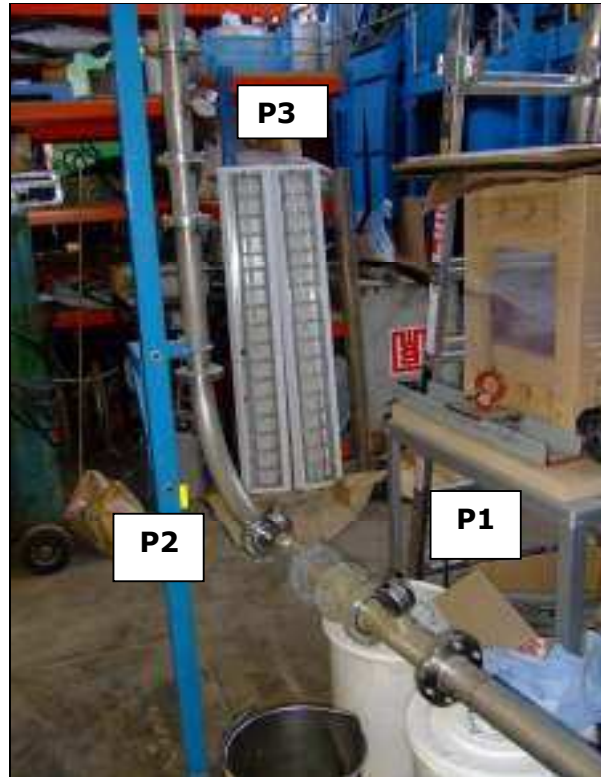


Figure 4.11: The location of pressure measurement – P1, P2 and P3

Initially, the simple manometer tube was used to calculate the pressure when using water and sand-water slurry fluid based on the elevation of fluids travel along the vertical tube. The vertical tube was installed vertically up to 9m from the horizontal lower leg pipe. Due to high concentration and viscosity when using the CMC solutions, the length of simple manometer tube was not long enough to determine the total length of CMC solutions travelled along the manometer tube. Therefore, the liquid pressure gauge (up to 4 bars) was used to replace the simple manometer tube. The simple manometer tube as shown in Figure 4.12 is a transparent straight tube with 9mm inner diameter and 12mm outer diameter.

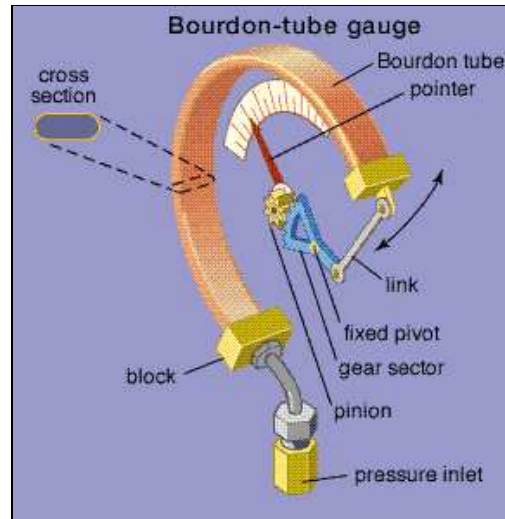


Figure 4.12: Simple manometer tube (ID = 9mm and OD = 12mm)

The pressure gauge (also known as Bourdon gauge), shown in Figure 4.13 invented around 1850, was widely used for measuring the pressure of steam, water, and air up to 100,000 pounds per square inch (psi). The device consists of a flattened circular tube coiled into a circular arc (Figure 4.14). One end is soldered to a central block and opened to the fluid, which its pressure to be measured; and the other end is sealed and coupled to the pointer spindle. When the pressure inside the tube is higher than the outside pressure, the Bourdon tube will straighten and caused the pointer to turn, which indicate the pressure reading on a circular scale.



Figure 4.13: A liquid pressure gauge (up to 4 bars)



**Figure 4.14: A schematic diagram of Bourdon-tube gauge
(adapted from www.britannica.com)**

For pressure measurements, the terms of no swirl, 1 swirl and 2 swirls applied as follows:

1. No swirl represents the conditions of fluids flow when not preceded with 4-lobe swirl-inducing pipe flow.
2. 1 swirl represents the conditions of fluids flow when one 4-lobe swirl-inducing pipe flow (10cm in length) was installed between P1 and P2 as shown in Figure 4.15.
3. 2 swirls represents the conditions of fluids flow when two 4-lobe swirl-inducing pipes were connected together and installed between P1 and P2 as shown in Figure 4.16.

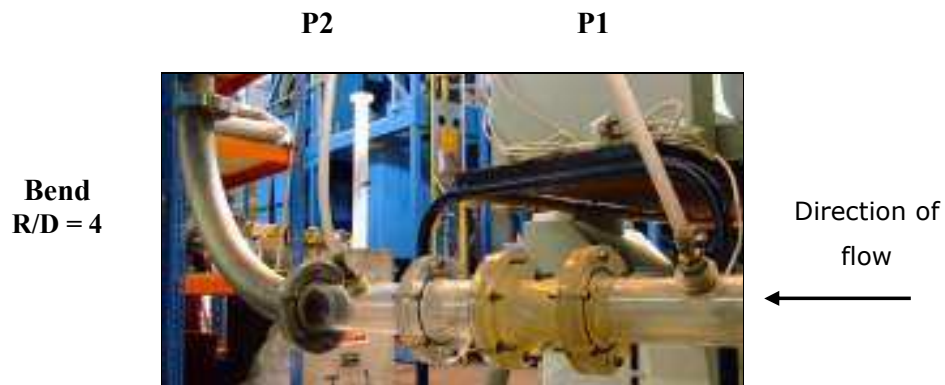


Figure 4.15: 1 swirl 4-lobe swirl-inducing pipe flow



Figure 4.16: 2 swirl 4-lobe swirl-inducing pipes flow connected together

4.3 General Procedures on Steel Pipe Rig

The conical tank was filled with 1.0 m³ of water from the main water. The initial experiment involved a short circuit flow, which utilised a conical tank and 0.25 m pipe diameter. The Mono Pump pumped the fluid on short circuit flow at low frequency (5.0 Hz to 6.0 Hz depends on fluid viscosity) before delivery to a long circuit flow (consisted of a de-aerator, horizontal lower leg, vertical leg, horizontal upper leg and conical tank) with a frequency between 8.0 to 35.0 Hz. Water circulated in the pipeline for 10 minutes to stabilise the flow and ensure tested fluids distributed throughout the flow loop before taking any readings. The measurements for temperature and pressure were taken in correspondence to the flow rate. Table 4.1 shows the flow rates and velocities required in each test.

The above procedures were repeated when using one or two 4-lobe swirl pipe (length = 10cm; internal diameter = 5cm), which was installed at the end of horizontal lower leg, before the bend as shows in Figure 4.16. Then the same procedure, except for the application of short circuit, was applied when using sand-water slurry and CMC solution at different concentrations. To examine sand-water slurries, the conical tank was initially filled with water depending on the solid concentration requirements. Then sand particles were added from the top balcony into the conical tank through a weigh tank, as there was no direct route accessed to conical tank.

4.4 Dissolution for Carboxymethyl Cellulose fluid

Before the CMC solutions were mixed constantly at high speed inside a mixer tank, a biocide solution was added (100 – 130ml) to avoid microbial growth, although it does give little effect on the rheology of the CMC (Tonkin, 2004). However, it was assumed (Tonkin, 2004) that the biocide solution will cause give differences to the viscosity and concentration of CMC. Geldard (2002) claimed that the viscosity of CMC would increase over the first 24 hours while being hydrated. The CMC solutions appeared as clear fluid and were tested in the pipe loop for up to five days. When the CMC solution was not in use, it was stored in the pipe loop.

Table 4.1: Flow rate and velocity for fluid tests

Flow rate Q (m ³ /hr)	Velocity, v (m/s)						
	Water	Slurries (% v/v)			CMC (% w/w)		
		1.4	2.1	2.7	0.5	1.0	1.5
1.414	No measurement taken					0.2	
2.828						0.4	
3.535	0.5					No measurement taken	
4.242	No measurement taken					0.6	
5.656						0.8	
7.070	1.0					No measurement taken	
8.483	No measurement taken					1.2	
9.897						1.4	
10.604	1.5					No measurement taken	
11.311	No measurement taken					1.6	
12.725						1.8	
14.139	2.0					No measurement taken	
17.674	2.5			No measurement taken	2.5	No measurement taken	

For shutting down procedure, when tested with water alone, the pump was stopped (frequency was lowered to 10Hz before stopped the pump) and the drain valves opened. There were two main drain valves each located at the bottom of Mono Pump (Appendix A.10) and de-aerator (Appendix A.11). In the presence of sand particles (slurries), the splitter box was switched to pump the solid particles to the settling tank. The water inlet valve (Appendix A.10) was open to fill the pipe loop with water until some of the sand particles were pumped to the settling tank. Then the pump was stopped and the slurry

remains drained through the two drain valves. Inside the settling tank, the sand was deposited at the bottom, while water was drained off. The shutting down procedure of the pump when tested with CMC solution was, the water inlet and drained valves were opened while pumping to clean the pipe loop.

4.5 Summary

This chapter details the components used in the operation of steel pipe rig. Brown Mixer Tank was used to prepare the requirements of CMC solutions at high volume to be tested in steel pipe rig and viscosity measurement of CMC. A submersible pump was used to deliver the CMC solutions inside the mixer tank into the conical tank because the pipe loop connection between the tanks was not available.

The steel pipe rig used consisted of:

1. Mono pump, which is a progressive cavity type of pumps driven by a motor. The pumping rate of Mono pump was controlled automatically by adjusting the frequency of inverter manually.
2. De-aerator to allow any trapped bubbles escape via a tube atmosphere.
3. Conical tank, weigh tank and settling tank at different sizes to fit the volume of the flow loop and pipeline configuration (Appendix A). The conical tank could occupy a volume of fluid up to 1.0m^3 . Settling tank was used to trap sand particles.
4. Splitter box which transferred or diverted fluids with solid particles from weigh tank to settling tank respectively.
5. Pressure devices – simple manometer tube or Bourdon gauge (liquid).
6. A pipe loop which consisted of several sections of smooth steel and flexible perspex pipes, 220mm radii pipe (R/D of 4) and valves.
7. Parameters apparatus – flow rate transducer and digital flow meter, temperature transducer (K-type).

Three types of fluids were used in the experimental procedures – water, sand-water slurry and carboxymethyl cellulose (CMC) fluids. The concentrations used for sand-water slurries were 1.4, 2.1 and 2.7 % v/v. For CMC, the concentrations used were 0.5, 1.0 and 1.5% w/w. The experimental procedure for the steel pipe loop experiments and viscosity measurements has been described, covering the start up and shut down of the pipe flow loop for different types of fluids.

Chapter 5

EFFECTS OF 4-LOBE SWIRL INDUCING PIPE

5.1 Introduction

In order to assess the performance of pipeline application, pressure measurements were assessed. A fluid flow in a pipeline causes pressure changes due to fluctuations in elevation, friction or flow rates. The Bernoulli equation was applied in this experiment. This section evaluates the pressure drops of the incompressible flow in straight horizontal pipe before and after the bend, when preceded with and without swirl-inducing pipes.

In this experiment, the investigation made with slurries was restricted to sand particle size with a specific gravity of 2.64. The R/D of 4 was used to measure the pressure drop with and without swirl-inducing pipe effects. The investigation also determined the similarity of the pressure drop effect obtained from Tonkin (2004) with different concentration of sand-water slurry.

5.2 Methodology Specifics

Refer to Chapter 4 for viscosity testing of the CMC, fluids preparation and dissolution, and the operation of the steel pipe loop. For each test fluid and velocity, the pressure drop was measured at three pressure points, P1, P2 and P3 as illustrated in Figure 5.1:

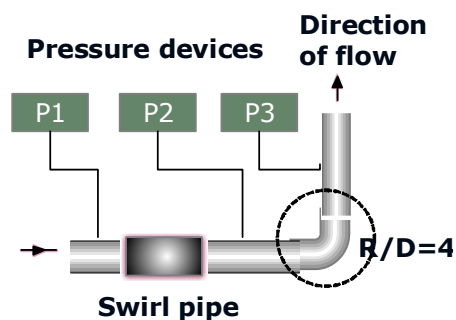


Figure 5.1: Illustration of pressure locations

The description of pressure measurement for P1, P2 and P3 are as follows:

1. Pressure point 1 (P1) measured the inlet pressure of fluids when preceded either by a straight cylindrical or 4-lobe swirl-inducing pipe (lower horizontal leg) before the bend.
2. Pressure point 2 (P2) measured the outlet pressure of fluids when preceded either by a straight cylindrical or 4-lobe swirl-inducing pipe (lower horizontal leg) before the bend.
3. Pressure point 3 (P3) measured the pressure of fluids after preceded with the effect of bend ($R/D = 4$) and with or without swirl-inducing pipe.

P2 was installed approximately 40cm from P1 just before the bend (R/D of 4). The swirl-inducing pipe was installed in between P1 and P2. The pressure drop, ΔP (Pa) against velocity, v (m/s) was plotted to establish data for comparison at different fluid conditions. Three conditions of pressure drops, ΔP (Pa) measured included:

1. Pressure drop, ΔP (Pa) on horizontal pipe (lower leg)

$$\Delta P_{12} = P_1 - P_2$$

2. Pressure drop, ΔP (Pa) over the bend (R/D of 4)

$$\Delta P_{23} = P_2 - P_3$$

3. Overall pressure drop across the horizontal pipe and bend (R/D of 4)

$$\Delta P_{13} = \Delta P_{12} + \Delta P_{23} = P_1 - P_3$$

It was predicted that the $\Delta P_{13} \geq \Delta P_{23} \geq \Delta P_{12}$ when the fluids flow velocity (or flow rate) increased. ΔP_{12} represents the pressure loss by swirl application.

5.3 Effects of Swirl Inducing Flow over Horizontal Pipe

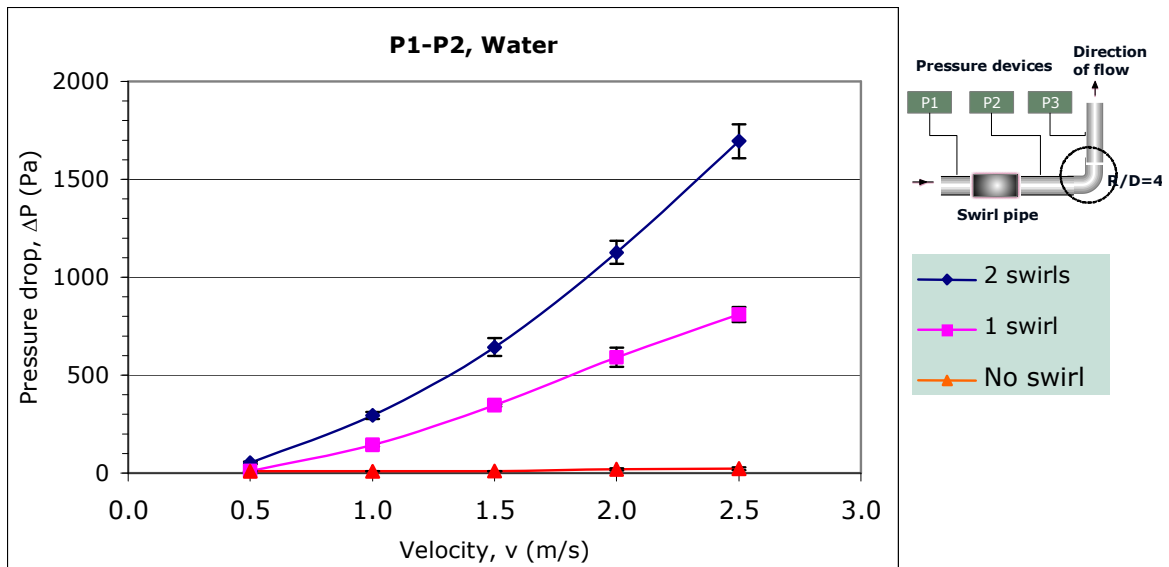


Figure 5.2: Pressure drop, ΔP_{12} (Pa) for water over horizontal pipe

Figure 5.2 shows increase in pressure drops, ΔP_{12} (Pa) when water preceded by swirl-inducing pipes. As expected, there was no significant pressure drops for ΔP_{12} (P1-P2) when the lower leg of horizontal pipe was preceded without swirl inducing pipe. Different results were discovered when one or two swirl-inducing pipes were installed between pressure measurements P1 and P2. It was also found that the application of two swirl-inducing pipes created twice the pressure drops as compared to one swirl-inducing pipe.

The effect of pressure drops, ΔP (Pa) were proportional with velocity, v (m/s) of fluids flowing inside the pipe. If the velocity, v increase, the pressure drop, ΔP would increase. At lower velocity of 0.5m/s, the pressure drops for 2 swirls, 1 swirl and no swirl were almost the similar. However, when the velocity increased to 1.5 m/s, the pressure drops for 2 swirls, 1 swirl and no swirl were approximately 650Pa, 350Pa and 10Pa respectively. As the velocity increased up to 2.5 m/s, the 2 swirls and 1 swirl pressure drops were 1700Pa and 800Pa respectively. The figure shows that the pressure drop obtained from 2 swirls was almost two times higher than the pressure drop from 1 swirl.

If the water flowing inside the horizontal pipe was not subjected to or preceded with swirl-inducing pipe, the direction of flows would not be changed. However, when swirl-inducing pipes were installed, the flow of water changed slightly in its axial horizontal position. This behaviour can be seen clearly in Figure 5.4 – 5.6 when using slurry.

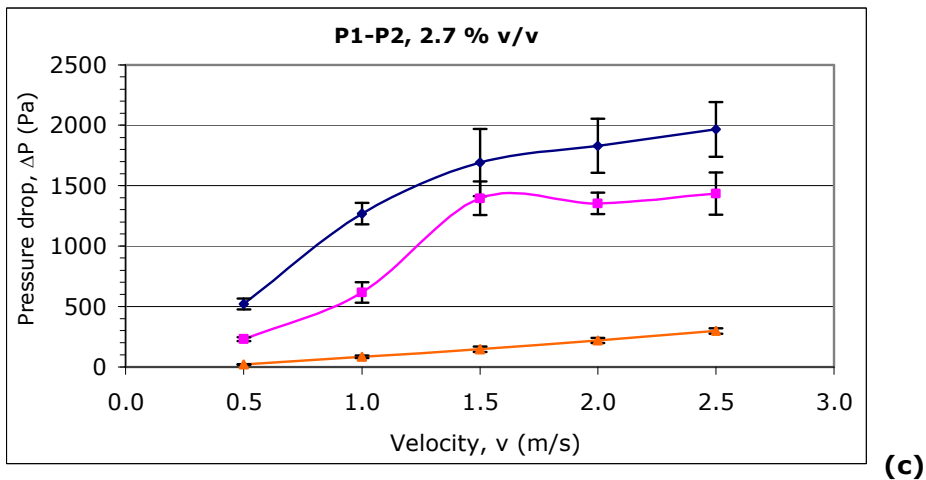
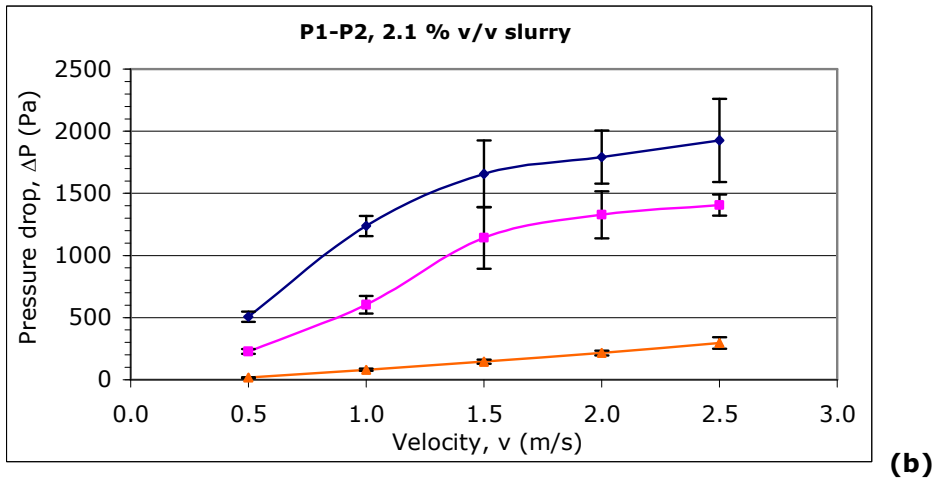
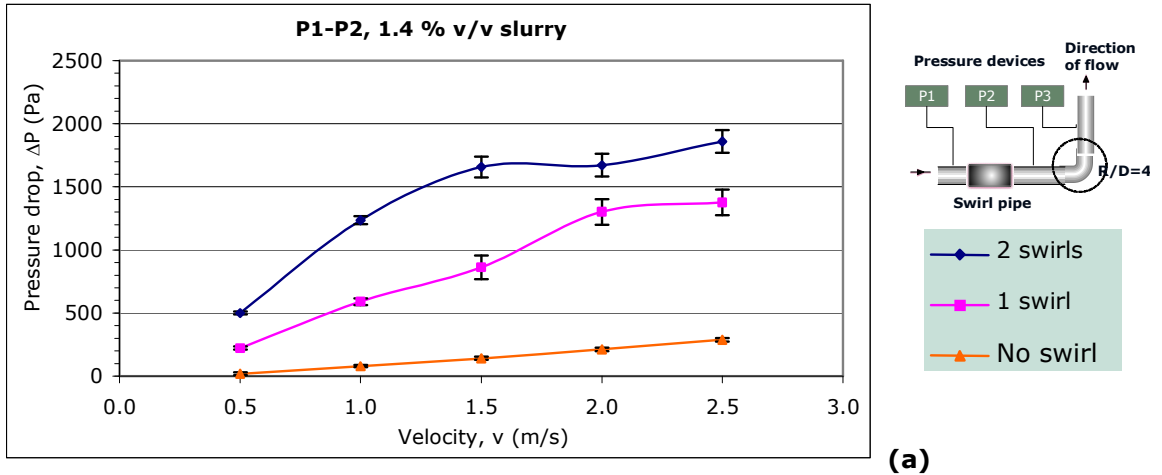


Figure 5.3: Pressure drop, ΔP_{12} (Pa) for sand-water slurry at different concentrations over horizontal pipe (a) 1.4% v/v slurry; (b) 2.1% v/v slurry; and (c) 2.7% v/v slurry

The effect of 4-lobe swirl-inducing pipe on horizontal pipe was further experimented using solid-liquid flow (slurry). When using slurries, similar curves were found as shown in Figure 5.3. The pressure drops, ΔP_{12} for sand-water slurries on horizontal pipe increased with slurries concentrations. The swirling flow application also increased the ΔP_{12} for slurries (depending on a length of swirl flow induced) compared to no swirl-inducing pipe application on the horizontal pipe.

At lower velocity of 0.5 m/s, the pressure drops at 1.4% v/v slurry concentration for 2 swirls, 1 swirl and no swirl were approximately 500Pa, 200Pa and 20Pa respectively. The pressure drop changes were not significant at lower velocity. However, at 1.5 m/s, the pressure drops at 1.4% v/v, 2.1% v/v and 2.7% v/v slurry concentrations for 2 swirls were approximately 1650 - 1700Pa. The pressure drops for 1 swirl were approximately 870Pa, 1150Pa and 1400Pa. The pressure drops for no swirl application at 1.4% v/v, 2.1% v/v and 2.7% v/v slurry concentrations were approximately 140 - 150Pa.

It was predicted that the pressure drops for no swirl-inducing pipe performed were not significant even though the slurries flowed at different concentrations on the horizontal pipe. It was because there were no changes on flow direction along horizontal pipe. However, the application of 1 and 2 swirl-inducing pipes increased the pressure drops as the velocity of the slurry increased. 1 swirl gave distinctive values of pressure drops compared to 2 swirls application.

Figures 5.4 – 5.6 shows the visualisation of flow behaviour for 1.4% v/v sand particles slurries when travelled at 1.5m/s. As shown in figure 5.4, the sand particles behaved as a flow with moving bed. After preceded with swirl-inducing pipe flow, the sand particles tend to distribute evenly as shown in Figure 5.5. From this visualisation, the swirl-inducing pipe worked as a *lifter* (as shown in Figure 5.6) for solid-liquid mixture. This increased the sand particles homogeneity and subsequently reduced the solid particles friction across the pipe wall.



Figure 5.4



Figure 5.5



Figure 5.6

Figure 5.4 – 5.6: Flow behaviour of sand-particles at 1.5m/s and 1.4% v/v with and without swirl-inducing pipe

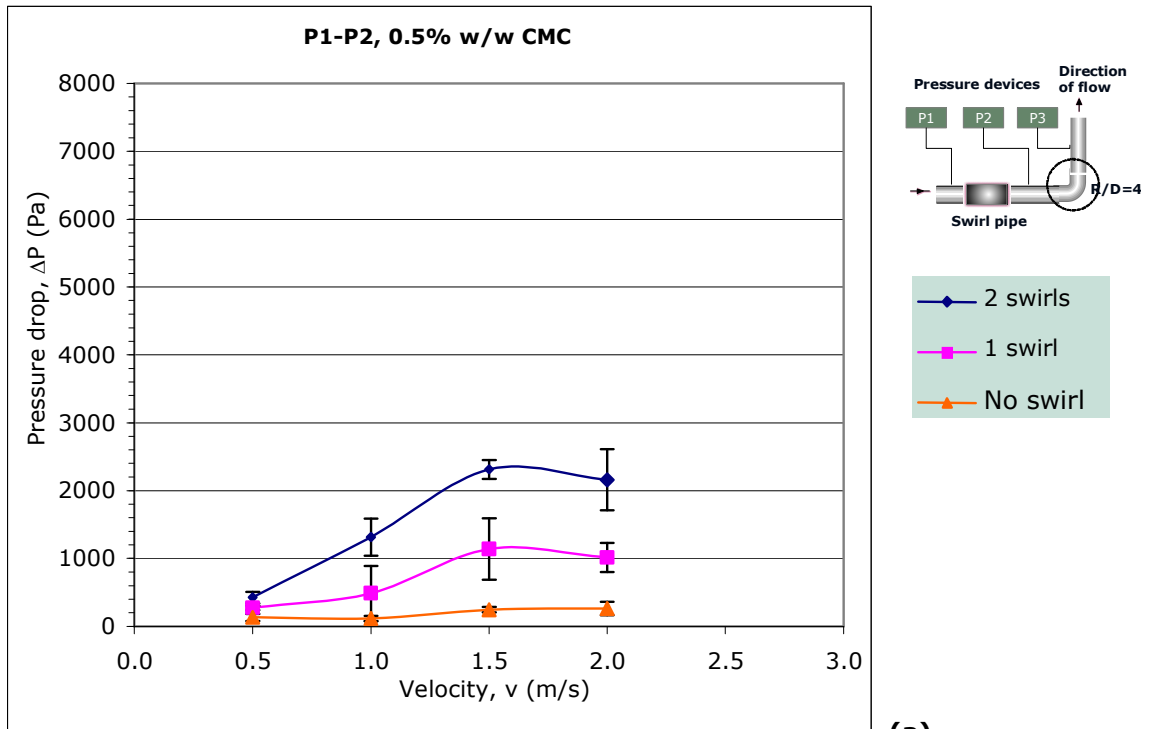
The slurries behaviour in Figure 5.4 shows that sand particles tend to settle in the water due to the action of gravitational force. The sand particle has high density, therefore it tends to settle to the bottom of the pipe. This flow behaviour shows that the sand-water slurry is a heterogeneous slurry. The sand particles were not uniformly distributed although most of the particles were fully suspended. At 1.5m/s, the sand particles behaved as a heterogeneous with moving bed due to the flow rate of slurry, which was considered slow. Parts of the sand particles tend to slide along the bottom of the horizontal pipe.

Tonkin (2004) discovered that fine ($118\mu\text{m}$) or medium ($500\text{-}1000\mu\text{m}$) sand particle exhibited the same characteristics as slurry flow and tends to settle. In a horizontal pipe, the sand particles settled at the bottom of the pipe cross-section. This phenomenon formed heterogeneous flow behaviour. When the settling slurry proceeded from horizontal to vertical pipe, the particles behaved as homogeneous flow and distributed well in the pipe-cross section. This similar effect can be visualised when the sand-water mixtures were preceded with swirl-inducing pipe as shown in Figures 5.5 and 5.6.

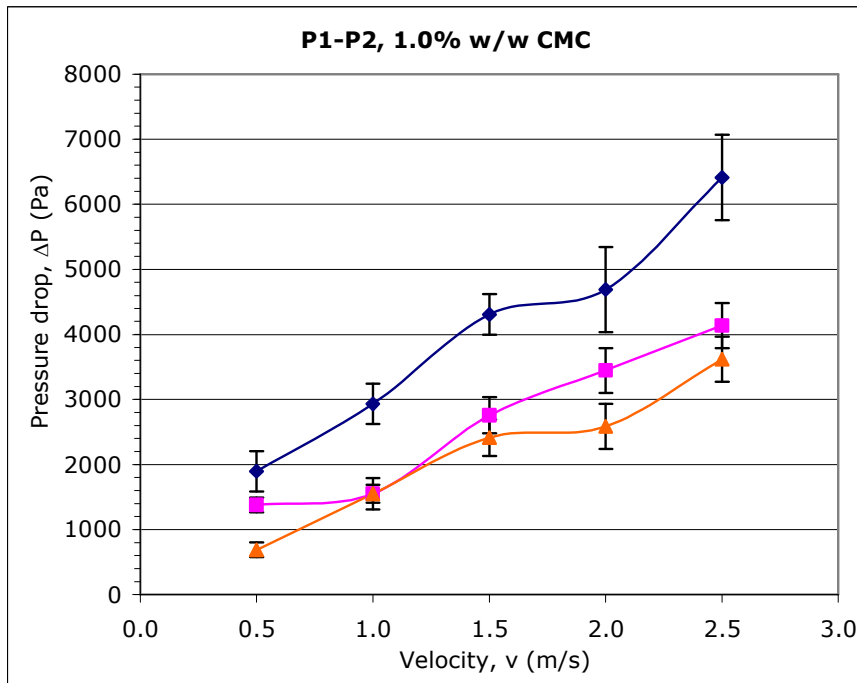
The experimental data showed that there was a lift force produced by flow from the bend effect to repel the sand particles from the wall when travelled across vertical pipe. This phenomenon contributed to a pressure drop. When swirl-inducing pipe flow was applied, the same characteristics was observed, where coarse particles were homogeneously distributed.

It was predicted that the sand particles travelled at higher velocity compared to without swirling flow as shown in Figure 5.6. The swirl-inducing pipe created a *lift force* (or acted as a lifter) between the sand particle and carrier fluid flow across the swirl-inducing pipe. This behaviour was responsible for the reduction of pressure drop over the bend (ΔP_{23}) and low secondary flow generation as shown in Figure 5.9.

As mentioned in Chapter 3 (Test Materials), the CMC fluid exhibited non-Newtonian characteristics (shear thinning, power-law). When experimented at nominal velocities ranging from 0.2 to 2.5 m/s, the CMC fluids travelled within a laminar regime (Appendix B; Table B.4) compared to water and sand-water slurries which travelled in a turbulent regime. The pressure drops, ΔP_{12} (Pa) for CMC exhibited similar curves with water (figure 5.2) and slurries (figure 5.3) as shown in Figure 5.6. At a higher concentration (1.5% w/w) the ΔP_{12} for CMC was not significant when preceded either by one or two applications of swirl-inducing pipe (Appendix C.14). The application of one 4-lobe swirl-inducing pipe and straight cylinder pipe showed no significant pressure drop behaviour for CMC at concentrations 0.5 and 1.0 % w/w.



(a)



(b)

Figure 5.7: Pressure drop, ΔP_{12} (Pa) for carboxymethyl cellulose at different concentration over horizontal pipe (a) 0.5% w/w CMC; and (b) 1.0% w/w CMC

The effect of 4-lobe swirl inducing pipe was further investigated using carboxymethyl cellulose (CMC) as a non-Newtonian fluid. As shown in Figure 5.7, the pressure drops for both concentrations at 0.5 and 1.0% w/w CMC were increased with increasing velocity, v (m/s). The 2 swirls gave higher pressure drops compared to 1 swirl and no swirl applications along the horizontal pipe. The 0.5% w/w CMC was experimented up to 2.0m/s and the pressure drops were calculated and measured using a simple manometer tube (Figure 4.15). The pressure drops, ΔP_{12} for CMC at 1.0 and 1.5% w/w were determined using Bourdon gauge (a liquid pressure gauge).

The pressure drops, ΔP_{12} at concentration of 0.5% w/w CMC and 0.5 m/s velocity for 2 swirls, 1 swirl and no swirl were approximately 430Pa, 270Pa and 130Pa respectively as shown in figure 5.7(a). When the velocity increased up to 2.0m/s, the pressure drops for 2 swirls, 1 swirl and no swirl application were approximately 2200Pa, 1000Pa and 260Pa respectively. At approximately 18°C, CMC had a high apparent viscosity of 0.15 Ns/m². Due to this characteristic, when flow rates or velocity were increased, the pressure drops along horizontal pipe increased up to 500% depending on the application of swirl-inducing pipes.

Figure 5.7(b) shows the effect of swirl-inducing flow for the CMC at 1.0 w/w and 0.5m/s velocity with pressure drops, ΔP_{12} of approximately 1900Pa, 1400Pa and 700Pa for 2 swirls, 1 swirl and no swirl respectively. At velocity of 2.0m/s, the pressure drops were approximately 4700Pa, 3400Pa and 2600Pa respectively. The CMC fluid which travelled at 0.5m/s had 670Re. The apparent viscosity for CMC at 1.0% w/w and 18°C was 0.712 Ns/m², which when pumped at 2.0m/s had 140Re. The CMC fluids at these two concentrations were flowing under a laminar regime (Appendix B: Table B.4). Its high viscosity and low Reynolds number contributed to an increase in pressure drops when the CMC fluids were preceded with a swirl-induced flow.

5.4 Effects of Swirl Inducing Flow over the Bend (R/D of 4)

In pipework, valves, fittings, or bends can cause impact to the pressure drop and the distribution of flow (Azzi, Friedel and Belaadi; 2000). The following results show the changes which occurred when swirl-inducing pipe was used in straight horizontal pipeline.

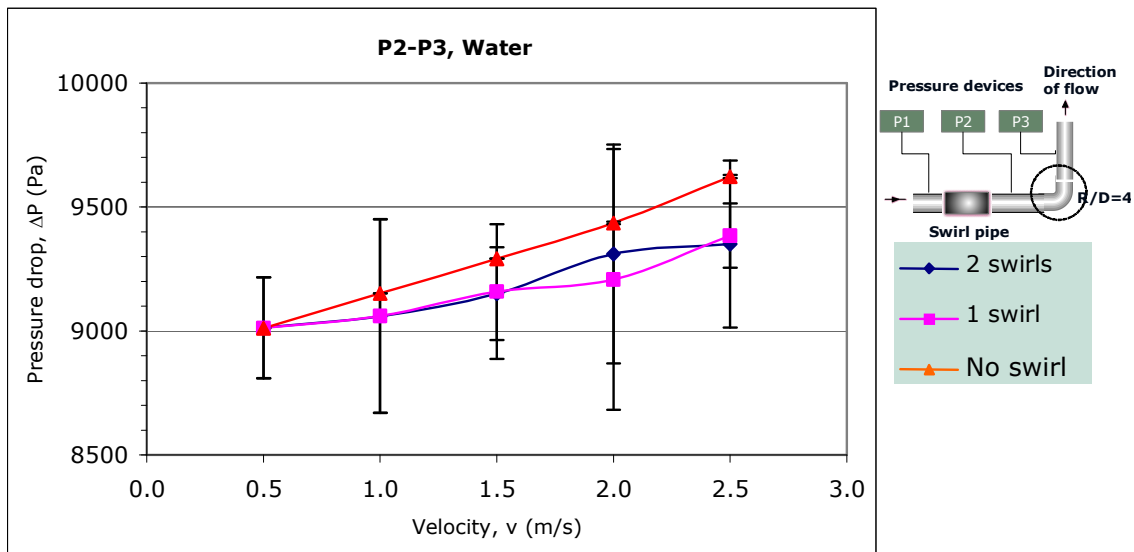
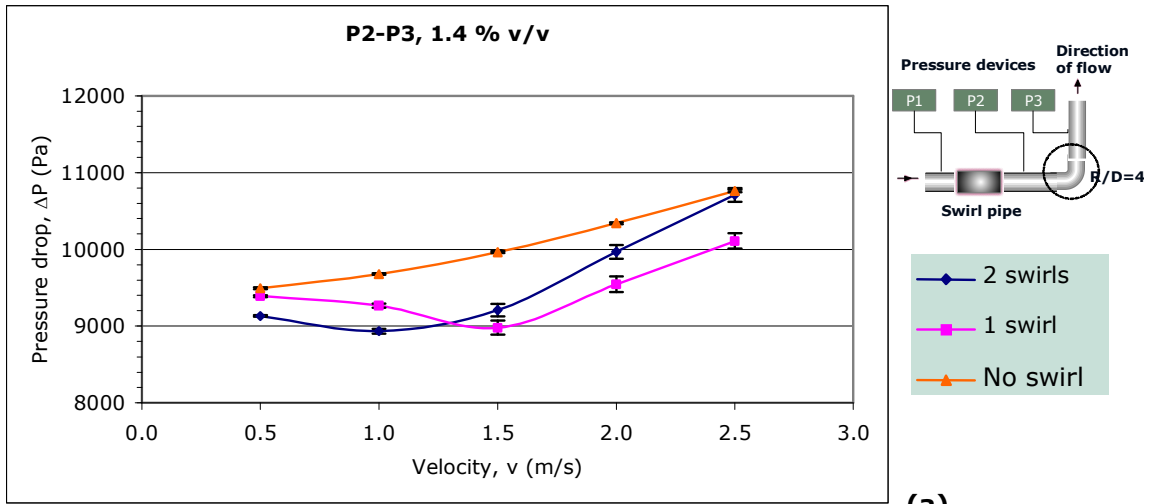
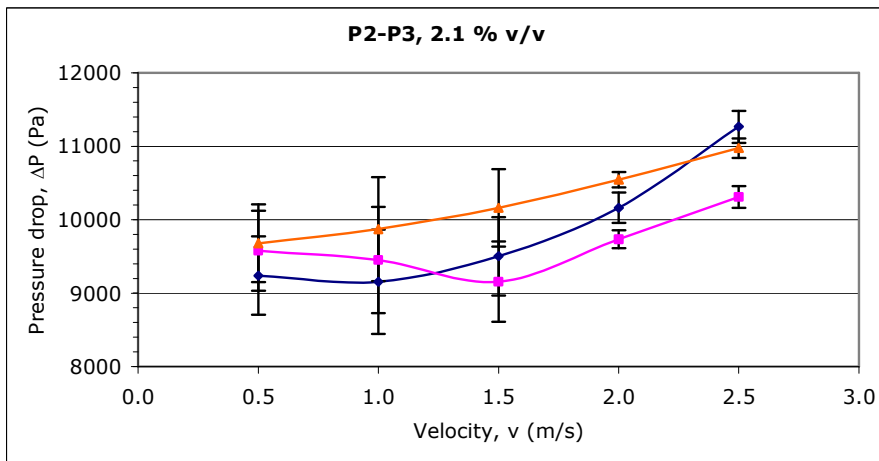


Figure 5.8: Pressure drop, ΔP_{23} (Pa) for water over the bend (R/D = 4)

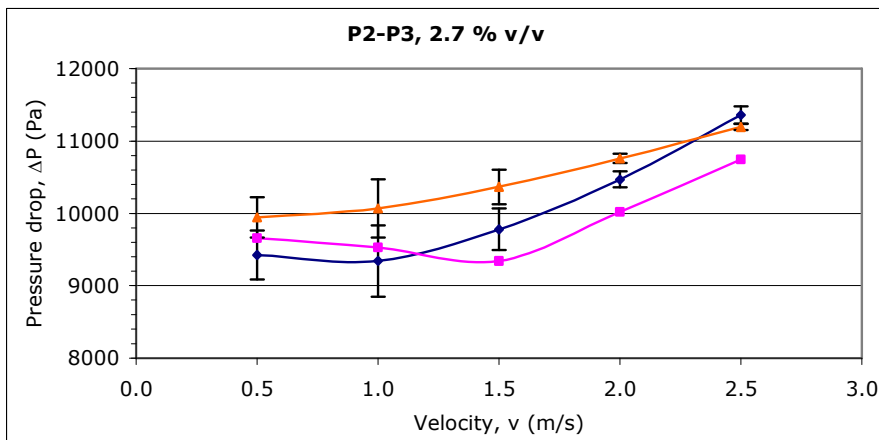
Figure 5.8 shows a graph of pressure drop, ΔP_{23} (Pa) against velocity, v (m/s) ranging at 0.5 – 2.5m/s. The pressure drops at 0.5m/s were not significant (approximately 9000Pa) among 2 swirls, 1 swirl and no swirl application. As the velocity of water increased, the pressure drops for no swirl application were higher compared to swirl-induced pipe flow. At 1.5m/s, the pressure drops for 2 swirls, 1 swirl and no swirl were approximately 9200Pa, 9200Pa and 9300Pa respectively and at 2.5m/s, were approximately 9350Pa, 9400Pa and 9600Pa. The overall pressure drops over the bend when the velocity increased for water was approximately 50 – 300Pa higher compared to swirl-induced flow.



(a)



(b)



(c)

Figure 5.9: Pressure drop, ΔP_{23} (Pa) for sand-water slurry at different concentrations over the bend with and without swirl inducing pipe

Figure 5.9 shows that the pressure drop of 1.4, 2.1 and 2.7% v/v slurry without swirl-inducing pipe increases against velocity. The ΔP_{23} (Pa) over the bend was reduced after the slurries passed through the swirl inducing pipe flow. Pressure drop in the bend was reduced due to the reacceleration of fluids during transit. It is assumed that the pressure dropped due to bend effects, which consisted of wall friction and momentum exchange between the liquid and pipe wall. Secondary flow generation and the bend arrangement in either upstream or downstream also affected the pressure drop.

The 10cm length of the 4-lobe swirl pipe (1 swirl pipe) showed a lower pressure drop than the 20cm length of 4-lobe swirl pipe (2 swirl pipes). This was true for an approximate velocity of 1.5 m/s onwards. Both swirl applications showed lower pressure drops compared to not having a swirl-inducing pipe. At velocity of 0.5m/s, the ΔP_{23} for 2 swirls, 1 swirl and no swirl were approximately 9200 Pa, 9000 Pa and 10,000 Pa respectively. The ΔP_{23} without swirl-inducing pipe showed increase in pressure drop compared to 2 swirls and 1 swirl approximately 9 and 11%. For 2.1 and 2.7% w/w slurry, the ΔP_{23} without swirl-inducing pipe increased approximately 9-11% and 6-% respectively.

Normally, when fluid travels over a bend, there will be a significant pressure drop created by the existence of secondary generation flows. This phenomenon (secondary generation flows) is produced by a combination of centrifugal force, which depended on the movement of a fluid directed from the momentaneous centre of curvature to the outer wall, and the effect from the boundary layer at the wall of the bend (Azzi et al., 2000).

The swirl-induce pipe tend to create a swirling flow, which caused less centrifugal forces and shear stress on the boundary layer over a bend. The mechanical behaviour of the swirl inducing pipe as a lifter (creating homogeneous distribution over a pipe cross section) also contributed to a reduction of pressure drop over the bend.

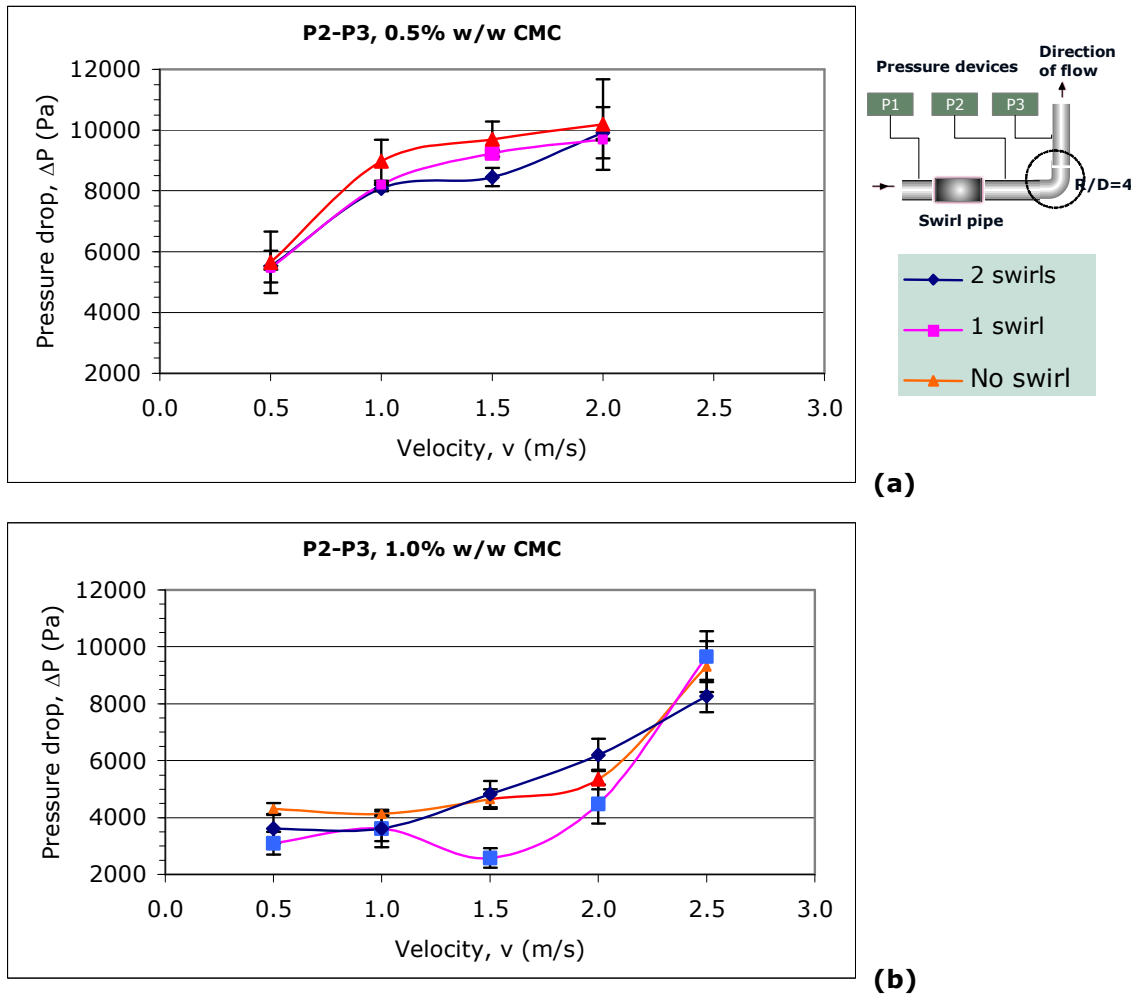


Figure 5.10: Pressure drop, ΔP_{23} (Pa) for CMC at (a) 0.5% w/w CMC, and (b) 1.0% w/w CMC, concentrations over the bend

When 0.5% w/w CMC was preceded without swirl-induced flow, it had a similar trend of graph with water and slurries. The pressure drops for no swirl application were higher than swirl-inducing flow as shown in figure 5.10 (a). At 0.5m/s, the pressure drops for 2 swirls, 1 swirl and no swirl were approximately 5500Pa, 5470Pa and 5600Pa respectively. When the velocity increased up to 2.0m/s, the pressure drops were approximately 10000Pa, 9700Pa and 10200Pa respectively.

When the concentration of CMC was increased to 1.0% w/w, the CMC fluids travelled under a laminar regime (140Re). Due to this flow behaviour, the pressure drops obtained in Figure 5.10(b) at 0.5m/s for 2 swirls, 1 swirl and no swirl were approximately 3600Pa, 3100Pa and 4300Pa respectively. At 2.0m/s, the pressure drops obtained were approximately 6200Pa, 4500Pa and 5300Pa respectively.

The pressure drops for a non-Newtonian fluid at different concentrations and viscosity produced different trends of curves. The CMC fluids which proceeded without swirl-inducing flow had higher pressure drops compared to swirl-inducing pipe flow as shown in Figure 5.10(a). However, when the concentration of non-Newtonian fluid was increased and had lower Reynolds number, the pressure drops for swirl-induced pipe would be higher compared to flow without swirl-inducing pipe. The same results were obtained for CMC fluid 1.5% w/w (Appendix C:17). At 2.0m/s, the pressure drops for 2 swirls, 1 swirl and no swirl were approximately 12400Pa, 11200Pa and 8300Pa respectively.

5.5 Effects of Swirl Inducing Pipe Across Pipe

Based on theoretical assumption (Clayton, 2006) that under the same operating conditions (such as velocity, pipe diameter and length, etc.), increases in the slurries concentrations will increase the overall pressure drop (ΔP_{13}) across the horizontal pipe and bend with and without swirl-inducing pipe. To test this hypothesis, measurements were made for various flow velocities ranging 0.5 – 2.5 m/s.

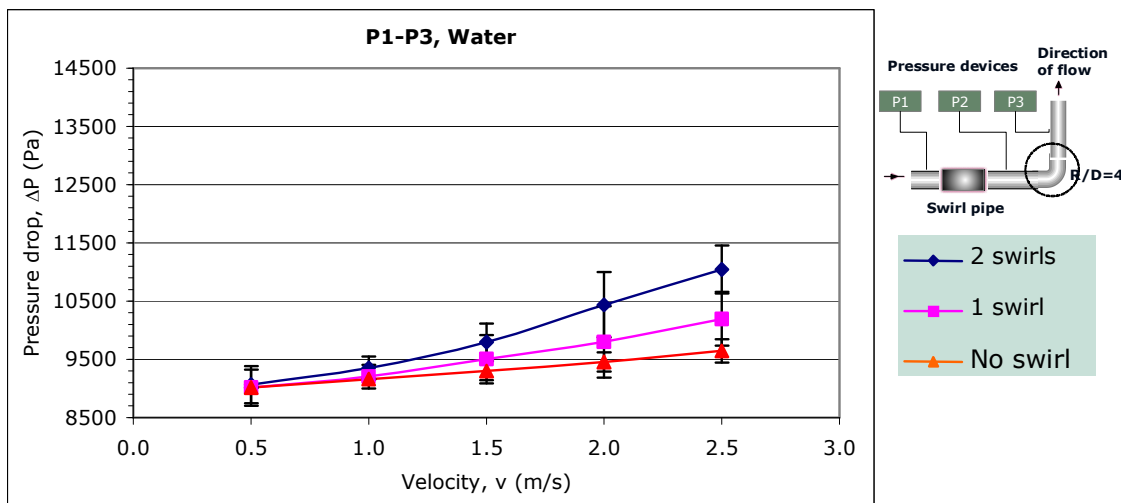
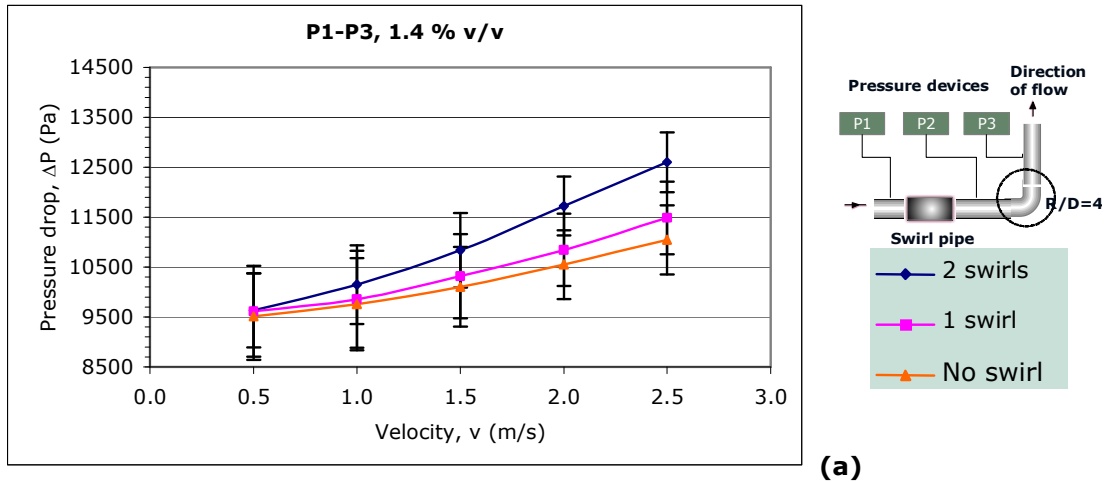


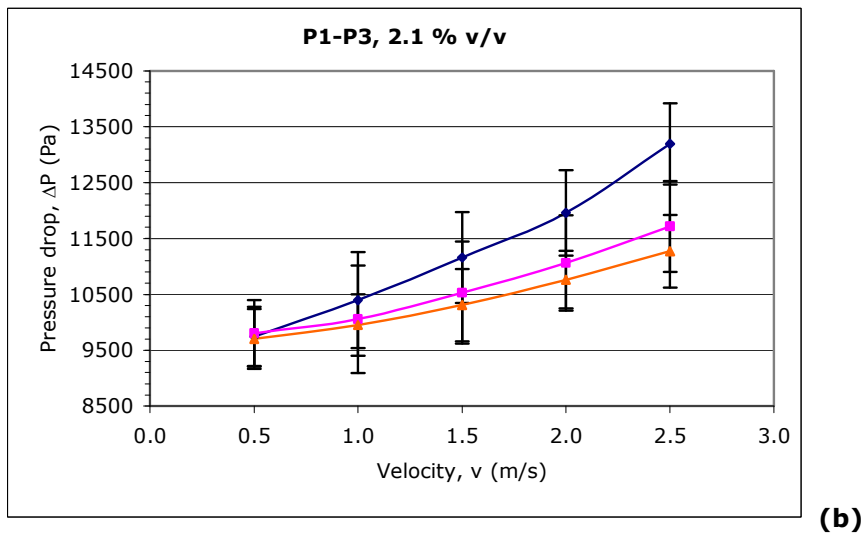
Figure 5.11: Pressure drop, ΔP_{13} (Pa) for water across pipe

Figure 5.11 shows that the pressure drop for water increased with velocity, v (m/s) after preceded with the 4-lobe swirl-inducing pipe. At lowest operating velocity of 0.5m/s, the pressure drops for both conditions, with and without swirl-inducing pipe were not significant. At a high velocity of 2.5 m/s, the pressure drop, ΔP_{12} for 2 swirls and no swirls were 11200 Pa and 9700 Pa respectively. The 2 swirls caused higher pressure

drops compared to 1 swirl applications. The ΔP_{13} for 2 swirls compared to 1 swirl and no swirl, which showed an increase in pressure drop were approximately 800Pa (8.4% increase) and 1350Pa (13.4% increase) respectively.



(a)



(b)

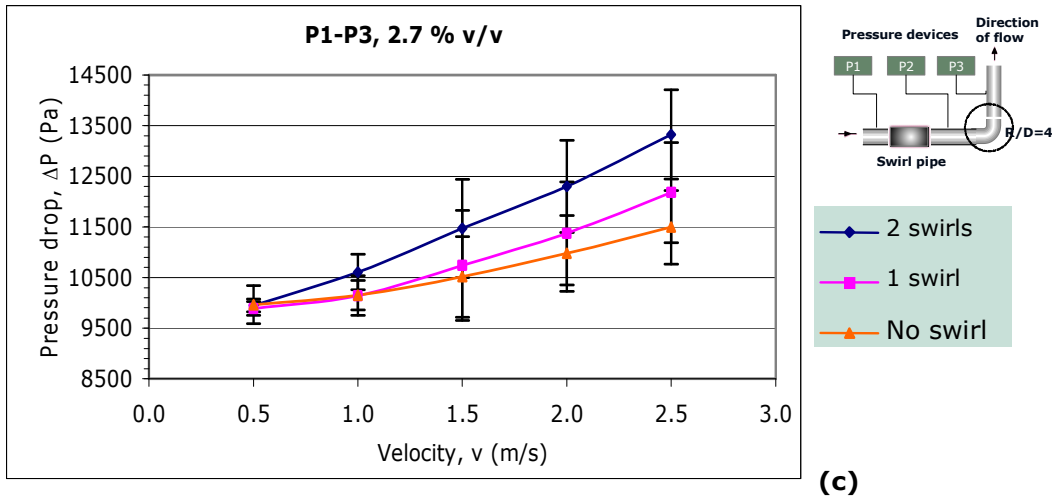


Figure 5.12: Pressure drop, ΔP_{13} (Pa) for slurries at different concentrations across pipe (a) 1.4% v/v; (b) 2.1% v/v; and (c) 2.7% v/v

The effects of swirl-inducing flow on pressure drop for sand-water slurries at different concentrations in Figure 5.12, suggested that the application of swirl pipe increased the pressure drop over a standard pipe. When sand-water slurries were induced with swirl flow, the settling of sand particles decreased as velocity increased. At velocity of 2.5 m/s, the total pressure drops for 2.7% v/v slurry concentration across pipe for no swirl, 1 swirl and 2 swirls were approximately 11,500 Pa, 12200 Pa and 13,300 Pa respectively. The pressure drop, ΔP (Pa) increased approximately 16% when using 2 swirls and this varied with the concentration of slurries.

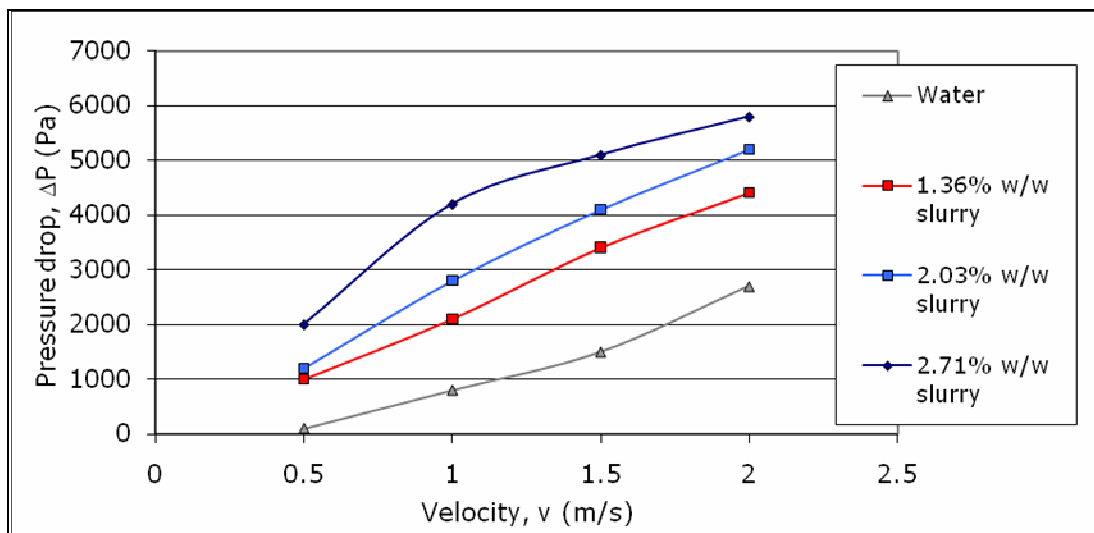
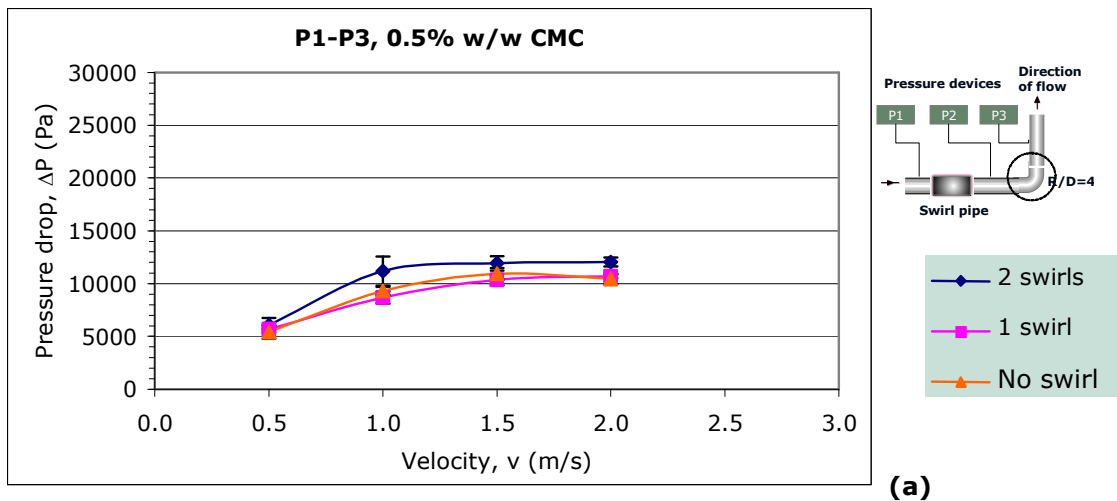
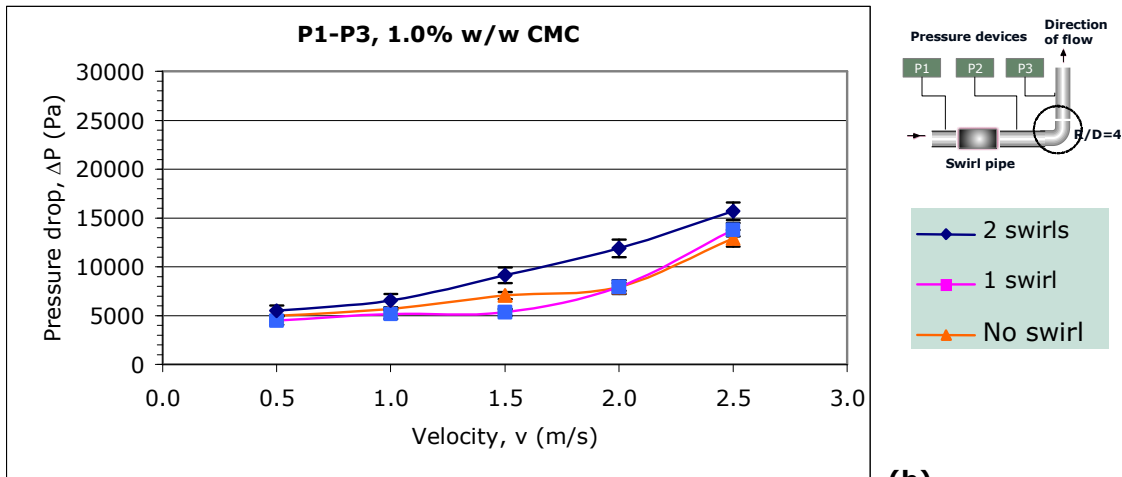


Figure 5.13: Pressure drop, ΔP (Pa) over horizontal pipes for coarse sand slurries (2000 μ m) (taken from Tonkin, 2004)

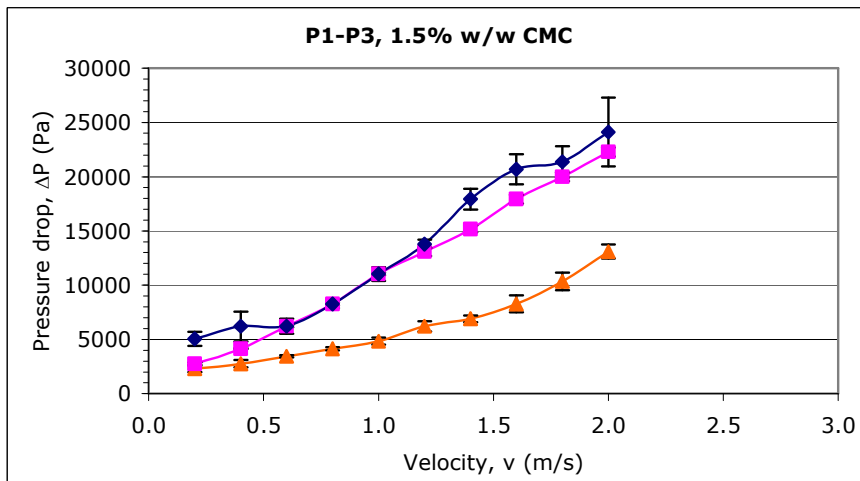
Tonkin (2004) also obtained similar findings on the pressure drops of coarse slurries at different concentrations over horizontal pipe as shown in Figure 5.13. It was obvious that at low velocity (0.5m/s), the pressure difference between water and 2.71% v/v slurry was approximately 2000Pa. At the same condition, the pressure difference between water (figure 5.11) and 2.7% v/v slurry (figures 5.12 (c)) were approximately 2500Pa. This was due to the different 4-lobe swirl-pipe configuration used. Tonkin (2004) showed that when a fluid passes through a non-circular 4-lobe swirl-inducing pipe, it caused some friction which consequently led to a higher pressure drop.

It is interesting to analyse the differences in pressure drop when pumping slurries at different concentrations, compared to water alone. The increases in pressure drop, suggested that swirl-inducing pipe was able to suspend higher solid concentration without creating any blockage, thus decreasing friction factor (reduce wear), which was in agreement with Wood et al. (2001 and 2003). The difference in pressure drop (in this case represented by ΔP_{23}) with and without swirl inducing pipe flow indicated a pressure benefit (pressure cost) (Tonkin, 2004).





(b)



(c)

Figure 5.14: Pressure drop, ΔP_{13} (Pa) against velocity, v (m/s) CMC at different concentrations (a) 0.5% w/w; (b) 1.0% w/w; and (c) 1.5% w/w

Initially, the pressure drop measurements were performed using a simple manometer tube. Due to high concentrations and viscosities of CMC at 1.0 and 1.5 % w/w, the flexible pipes connected to and from de-aerator were disjointed. Therefore, the pressure measurements were measured using a Bourdon gauge. The accuracy of using Bourdon gauge was ± 0.05 bars (5000 Pa), suggesting that a better pressure device was required to estimate the pressure changes when using non-Newtonian fluids at higher concentrations and viscosity.

Figure 5.14 shows the overall pressure drop, ΔP_{13} (Pa) ($P_1 - P_3$) for CMC at different concentrations when preceded with and without swirl inducing pipe flow. The result shows that the pressure drops, ΔP_{13} (Pa) increased with increasing concentrations. In Figure 5.14 (a), the ΔP_{13} (Pa) preceded with two 4-lobe swirl-inducing pipes increased at velocities between 0.5 and 1.0 m/s. However, no significant changes were obtained for ΔP_{13} when performed at velocities between 1.5 and 2.0 m/s.

Figure 5.14 (b) and (c) shows that the ΔP_{13} (Pa) obtained were small between no swirl and with swirl applications. The characteristics at ΔP_{13} between one and two 4-lobe swirl-inducing pipes were not significant for CMC at 1.5% w/w. This was because at 1.0 and 1.5 % w/w, the CMC fluids travelled at laminar regimes ($Re_{cmc} < 2000$). Therefore, the comparison of pressure drops between the applications of 1 swirl and 2 swirls was not able to be determined. In this case, further investigation should be performed at higher velocity profiles using better pressure device to analyse the effect for 1 swirl and 2 swirls with non-Newtonian fluids.

5.6 Summary

The pressure measurements were assessed to evaluate the pressure drops of the incompressible flow of water, slurries and CMC in straight horizontal pipe before and after the bend, when preceded with and without swirl-inducing pipes. The sand particle size used in slurry had a specific gravity of 2.64.

The pressure points for P1, P2 and P3 were located before and after the swirl-induced pipe, and after the bend (R/D=4), respectively. Three pressure drops, ΔP (Pa) were calculated as follows:

1. ΔP_{12} for the effect of 4-lobe swirl-induced pipe on horizontal pipe (lower leg).

$$\Delta P_{12} = P_1 - P_2$$

2. ΔP_{23} for the effect of 4-lobe swirl-induced pipe over the bend (R/D of 4) to indicate the pressure loss due to swirl-inducing flow.

$$\Delta P_{23} = P_2 - P_3$$

3. ΔP_{13} for the effect obtained in ΔP_{12} and ΔP_{23}

$$\Delta P_{13} = \Delta P_{12} + \Delta P_{23} = P_1 - P_3$$

The graphs of pressure drop, ΔP (Pa) against velocity, v (m/s) were plotted to establish data for comparison at different fluid conditions.

The pressure drops, ΔP_{12} (Pa) for water preceded by swirl-inducing pipes were increased compared to application with no swirl. Furthermore, the application of 2 swirls gave higher pressure drops when compared to 1 swirl pipe.

The pressure drops, ΔP_{12} for slurries on horizontal pipe increased with slurry concentrations but no significant changes were obtained at lower velocity of 0.5m/s. The application of 1 and 2 swirl-inducing pipes increased the pressure drops as the velocity of the slurry increase. 1 swirl gave distinctive values of pressure drops when compared to 2 swirls application.

Along the horizontal pipe, the sand particles were observed to be settled at the bottom of pipe due to gravitational force. However, when the sand particles were preceded with swirl-induced pipe, the sand particles behaved homogeneously and distributed well in a pipe-cross section.

The sand particles tend to distribute evenly due to swirl-inducing flow, which lifted the solid-liquid mixture and changed the flow direction in its axial line along the horizontal pipe. This increased the sand particles homogeneity and decreased the pressure drops, ΔP_{23} .

The CMC fluid exhibited non-Newtonian characteristics and travelled within a laminar regime when experimented at nominal velocities ranging from 0.2 to 2.5 m/s. The pressure drops, ΔP_{12} (Pa) for CMC gave higher pressure drops compared to water and slurries because of high apparent viscosity. However, the ΔP_{12} for 1.5% w/w CMC was not significant when preceded by swirl-inducing pipe.

The pressure drops, ΔP_{23} (Pa) over the bend for water and slurries were reduced after proceeded by swirl-inducing pipe flow due to the reacceleration of fluids when travelled over the bend. Secondary generation flows also affected the pressure drop over the bend. However, the pressure drops, ΔP_{23} (Pa) for CMC fluids produced different results as the swirl-induced pipe gave higher pressure drops compared to application with no swirl. The ΔP_{23} (Pa) for CMC exhibited irregular curves. Further investigation is required.

The overall pressure drops, ΔP_{13} (Pa) for water, slurries and CMC were increased due to the swirl-inducing pipe. The pressure drops, ΔP (Pa) across a pipe increased and was summarised as follows:

- a. ΔP (high concentration) \geq ΔP (low concentration)
- b. $\Delta P_{13} \geq \Delta P_{12} \geq \Delta P_{23}$
- c. Increased the flow rates, increasing the ΔP

The application of two swirl pipes showed further increase in ΔP compared to using one 4-lobe swirl-inducing pipe, which depended on the velocity and types of fluids tested:

$$\Delta P (2 \text{ swirls}) \geq \Delta P (1 \text{ swirl}) \geq \Delta P (\text{no swirl})$$

Chapter 6

CONCLUSIONS AND RECOMMENDATIONS

The effect of 4-lobe swirl-inducing pipe on pressure drop, ΔP was investigated at different concentrations and flow rates.

6.1 Effect of 4-Lobe Swirl-Inducing Pipe on Settling Slurries

1. The 4-lobe swirl pipe increased the pressure drop, ΔP on settling slurries across a pipe but reduced the ΔP over the bend.
2. The sand-water slurry exhibited homogeneous flow when preceded with 4-lobe swirl pipe. Swirling flow increased the sand particles homogeneity and subsequently reduced the solid particles friction across the pipe wall.
3. At high velocity, the sand particles were evenly distributed when proceeded with swirl-inducing pipe. This showed that the application of swirl-inducing flow was most effective even at higher slurry concentrations.

6.2 Effect of 4-lobe Swirl-Inducing Pipe on Non-Newtonian Fluid

Carboxymethyl cellulose (CMC) exhibited power-law or shear thinning fluid. At nominal velocity between 0.2 and 2.5 m/s, CMC flowed within a laminar regime.

The pressure drops, ΔP increased when 4-lobe swirl pipe was used compared to without swirl-inducing pipe.

The application of using either one or two 4-lobe swirl pipes on ΔP showed almost similar results. Application at higher velocities needs to be performed and better pressure devices should be used.

The pressure drop over a bend for CMC was higher compared to sand-water slurries and water. The swirl-inducing pipe had no decreasing effect the pressure drops over a bend compared to slurries and water.

6.3 Contribution of Thesis

1. Swirling flow application reduced the pressure drop, ΔP over the bend but increased the ΔP across a pipe. However, these results do not fully apply to CMC as it travelled at laminar regime and had higher viscosity.
2. Swirling flow increased the sand particles distribution in a pipe-cross section.
3. The application of two swirl pipes showed increased in ΔP compared to one 4-lobe swirl-inducing pipe or without swirl-inducing pipe.
4. The effect of 4-lobe swirl-inducing pipe on ΔP over the bend is reduced. The swirl-induced pipe tend to create a swirling flow or orientation of the fluid, which caused less centrifugal forces and shear stress on the boundary layer over the bend and led to low secondary generation.

6.4 Recommendations

The experimental data was performed with a pipe diameter of 0.05m under different conditions. Results indicate that the use of swirl-inducing pipe increased the pressure drop across the horizontal pipe but reduced the pressure drop over the bend (R/D of 4). It is recommended that the swirl-inducing pipe of 4-lobe should be performed at smaller pipe diameter (1cm or less) and thickness as well as on 90° bend.

The modelling on 4-lobe swirl-inducing pipe should be carried out intensively to ensure it gives a better performance on any types of fluid especially when the swirl-inducing pipe is applied before a bend.

The application of 180° bend is very common in the pipeline system, condenser, evaporator etc. It is recommended to investigate the swirl-inducing flow behaviours and effects when using vertical or horizontal 180° bends.

REFERENCES

Agarwal, N., and Chhabra, R.P., (2007) 'Settling velocity of cubes in Newtonian and power law liquids', *Powder Technology*, Vol. 178, pp17-21.

Akpinar E.K., and Bicer, Y., (2005) 'Investigation of heat transfer and exergy loss in a concentric double pipe exchanger equipped with swirl generators', *International Journal of Thermal Sciences*, Vol. 44, Issue 6, pp598-607

Azzi, A., Friedel, L., and Belaadi, S., (2000) 'Two-phase gas/liquid flow pressure loss in bends', *Forschung im Ingenieurwesen*, Vol. 65, pp309-318.

Azzopardi, B.J., (2006), Personal Communication

Azzopardi, B.J., (2007), Personal Communication

Ayukawa, K. (1969) 'Pressure Drop in the Hydraulic Conveyance of Solids Materials Through a Bend in a Vertical Plane', *Bull. JSME* Vol. 12, No.54, pp1388-1396.

Brookfield Engineering Laboratories, Inc. Middleboro, MA, USA, http://www.can-am.net/suppliers/brookfield/dial_new.pdf (last accessed on 3rd February 2007)

Brown, N.I., & Heywood, N.I., (1991) *Slurry Handling: Design of Solid-Liquid Systems*. Elsevier Science Publishers, London.

Cenna, A.A., Page, N.W., Williams, K.C., and Jones, M.G., (2007) 'Wear mechanisms in dense phase pneumatic conveying of alumina', *Wear*.

Chanchala Ariyaratne (2005) *Design and Optimisation of Swirl Pipes and Transition Geometries for Slurry Transport*. PhD Thesis 2005. School of Chemical, Environmental and Mining Engineering, University of Nottingham, United Kingdom.

Charles, M.E., and Charles, R.A., (1971) 'The use of heavy media in the pipeline transport of particulate solids', *In Advances in Solid-Liquid Flow in Pipes and Its Applications*, Ed. I. Zandi, Pergamon Press, Oxford, pp187-197.

Chu, K.C., and A.B. Yu, A.B., (2007) 'Numerical simulation of complex particle–fluid flows' *Powder Technology*.

Cilliers, J.J., Xie, W., Neethling, S.J., Randall, E.W., and Wilkinson, A.J., (2001), 'Electrical resistance tomography using a bi-directional current pulse technique', *Meas. Science Technology*, Vol. 12, pp997-1001.

Clayton T. Crowe (2006) *Multiphase Flow Handbook*.

Daniel D. Joseph (2005) *Potential flow of viscous fluids: Historical notes*; Department of Aerospace Engineering and Mechanics; University of Minnesota.

Darby, R., (2001) *Chemical Engineering Fluid Mechanics: Second Edition, Revised and Expanded*, Texas A & M University, College Station, New York.

Dehbi, A., (2007) 'A CFD model for particle dispersion in turbulent boundary layer flows', *Nuclear Engineering and Design*.

Delgado, M.A., Franco, J.M., Partal, P., and Gallegos, C., (2005) 'Experimental study of grease flow in pipelines: wall slip and air entrainment effects', *Chemical Engineering and Processing*, Vol. 44, Issue 7, pp805-817

Doron, P., and Barnea, D., (1995) 'Pressure drop and limit deposit velocity for solid-liquid flow in pipes', *Pergamon*, Vol. 50, No. 10, pp1595-1640.

Donald S. Miller; *Internal flow: A guide to losses in pipe and duct systems*

Fangary, Y.S., Abdel Ghani, A.S., El Haggag, S.M., and Williams, R.A., (1997), 'The effect of fine particles on slurry transport processes', *Minerals Engineering*, Vol. 10, No.4, pp427 – 439.

Ganeshalingam, J., (2002) *Swirl-Induction for Improved Solid-Liquid Flow in Pipes*. PhD Thesis, 2002. School of Chemical, Environmental and Mining Engineering, University of Nottingham, United Kingdom.

Geldard, R.J.J., Jones, T.F., Miles, N.J., and Rhodes, N.J., (2002) Selection of a suitable non-Newtonian fluid for swirling pipe flow tests. BHR Group, *Hydrotransport*, Vol. 15, pp287–298.

Geldard, R.J.J., Jones, T.F., Miles, N.J., and Ganeshalingam, J. (2001) Upstream swirl-induction for reduction of erosion damage from slurries in pipeline bends. *Wear*, Vol. 250, pp770–778.

Gordon, H.M & Gordon, H.A. (1899), Conduit or Pipe, 630, 605 (patent)

Gospel T, 2007, Personal Communication

Govier, G. W. and Aziz, K. (1972) *The Flow of Complex Mixtures in Pipes*. Van Nostrand Reinhold Co., London.

Haugen, K., Kvernfold, O., Ronold, A., and Sandberg, R., (1995) *Wear* 186/187, pp179-188.

Hemamalini, R.R., Partheeban, R., Sarat Chandrababu, J., and Sundaram, S., (2005) 'The effect on pressure drop across horizontal pipe and control valve for air/palm oil two-phase flow', *International Journal of Heat and Mass Transfer*, Vol. 28, pp2911-2921.

Heywood, N.I., Alderman, N.J., & Cursley, C.J. (1998), *In Plant Slurry Pumping Systems* Unpublished, Copyright AEA Technology PLC.

Heywood, N.I., (2000) 'Online monitoring of slurry flows in the process industries', *Proceedings of the 10th Conference on the Transport and Sedimentation of Solid Particles*, Wroclaw, Poland, pp59-83.

Hou, H.C., (1986) 'On the optimal concentration of fine particles in hydrotransport', *Hydrotransport BHRA Fluid Engineering*, Vol. 11, pp177-183.

Howard, G.W., (1939) 'Transportation of sand gravel in a four-inch pipe', *Trans ACSE*, Vol. 104, pp1334-1380.

Howard, G.W., (1941) 'Effect of Riffing on Four-Inch Pipe Transporting solids', *Trans ACSE*, Vol. 106, pp135-157.

Hussain, E.A.M., and Robinson, M.J., (2007) 'Erosion–corrosion of 2205 duplex stainless steel in flowing seawater containing sand particles', *Corrosion Science*, Vol. 49, Issue 4, pp1737-1754.

Ingham, J., Dunn, I.J., Heinzle, E., Prenosil, E.J., and Snape, J.B., (2007) *Chemical Engineering Dynamics: An Introduction to Modelling and Computer Simulation*, WILEY-VCH Verlag GmbH & Co. KGaA, Weinheim.

Jones, T.F (1997), *Pipe Design for Improved Particle Distribution and Reduced Wear*, ECSC Final Report 7220-EA/841

Käistner, U., Hoffmann, H., Dönges, R., and Hilbig, J., (1997) *Structure and solution properties of sodium carboxymethyl cellulose*; *Colloids Surfaces A: Physicochem. Eng. Asp.* 123-124 (1997) pp307-328.

Kaushal, D.R., Tomita, Y., and Dighade, R.R., (2002) 'Concentration at the pipe bottom at deposition velocity for transportation of commercial slurries through pipeline', *Powder Technology*, Vol. 125, Issue 1, pp89-101

Konrad, K. and Harrison, D., (1980) 'Prediction of pressure drop for horizontal dense phase pneumatic conveying of particles', *Proceedings of Pneumotransport 5*, BHRA Fluid Engineering, London, U.K., pp225-244.

Marin, G.B., (2006) *Advances in Chemical Engineering: Volume 31: Computational Fluid Dynamics*, Ghent University, Ghent, Belgium.

Marn, J., and Ternik, P., (2006) 'Laminar flow of a shear-thickening fluid in a 90° pipe bend', *Fluid Dynamics Research*, Vol. 38, pp295-312.

Matousek, V., (2002) 'Pressure drops and flow patterns in sand-mixture pipes', *Experimental Thermal and Fluid Science*, Volume 26, Issues 6-7, pp693-702

Matoušek, V., (2005) 'Research developments in pipeline transport of settling slurries', *Powder Technology*, Volume 156, Issue 1, pp43-51

Mitsumata, T., Suemitsu, Y., Fujii, K., Fujii, T., Taniguchi, T., and Koyama, K., (2003) 'pH-response of chitosan, κ -carrageenan, carboxymethyl cellulose sodium salt complex hydrogels', *Polymer*, Vol. 44, pp7103-7111.

Mukhtar, A., Singh, S.N., & Seshadri, V., (1995) 'Pressure Drop in A Long Radius 90o Horizontal Bend For The Flow of Multisized Heterogeneous Slurries' *International Journal of Multiphase Flow*, Vol.21, No.2, pp329-334.

Newitt, M.C., Richardson, J.F., Abbott, M., & Turtle, R.B. (1955), 'Hydraulic Conveying of Solids in Horizontal Pipes', *Transactions of the Institution of Chemical Engineers*, Vol.33, No.2, pp92-110.

Oddie, G., Shi, H., Durlofsky, L.J., Aziz, K., Pfeffer, B., and Holmes, J.A., (2003) 'Experimental study of two and three phase flows in large diameter inclined pipes', *International Journal of Multiphase Flow*, Vol. 29, pp527-558.

Peakall, J., Amos, K.J., Keevil, G.M., Bradbury, P.W., and Gupta, S., (2007) 'Flow processes and sedimentation in submarine channel bends', *Marine and Petroleum Geology*, Vol 24, Issues 6-9, pp470-486.

Peixinho, J., Nouar, C., Desaubry, C., and Theron, B., (2005) 'Laminar transitional and turbulent flow of yield stress fluid in a pipe', *Journal of Non-Newtonian Fluid Mechanics*, Vol. 128, pp172-184.

Perry, R.H., and Green, D.W., (1997) *Perry's Chemical Engineers' Handbook*, McGraw-Hill, 7th Edition.

Pinho, F.T. & Whitelaw, J.H. 1990, 'Flow of Non-Newtonian Fluids in Pipe', *Journal of Non-Newtonian Fluid Mechanics*, Vol.34, pp129-144

Poulten Selfe & Lee Ltd: Glass Capillary Viscometers,
<http://www.soctrade.com/pdf/pslglass.pdf> (last accessed 6 July 2007)

Raylor, B. (1998) *Pipe Design for Improved Particle Distribution and Improved Wear*, PhD Thesis, School of Chemical, Environmental and Mining Engineering, University of Nottingham, United Kingdom.

Paavola, A., Yliruusi, J., and Rosenberg, P., (1998) 'Controlled release and dura mater permeability of lidocaine and ibuprofen from injectable poloxamer-based gels', *Journal of Controlled Release*, Vol. 52, Issues 1-2, pp169-178

Richardson, J.F., Coulson, J.M., Backhurst, J.R., and Harker, J.H., (2004) *Chemical Engineering Volume 1*, Sixth Edition.

Sarac, B.A., and Bali, T., (2007) 'An experimental study on heat transfer and pressure drop characteristics of decaying swirl flow through a circular pipe with a vortex generator', *Experimental Thermal and Fluid Science*,

Spedding, P.L., and Benard, E., (2007) 'Gas-liquid two phase flow through a vertical 90° elbow bend', *Experimental Thermal and Fluid Science*, Vol. 31, pp761-769.

Sonja Ryst (8 August 2006); BP's Pipeline Trouble; Business Week Magazine, http://www.businessweek.com/investor/content/aug2006/pi20060808_987974.htm?chan=top_news_top_news (last accessed 12 August 2007)

Stack, M.M., and Abd El-Badia, T.M., (2007) 'Some comments on mapping the combined effects of slurry concentration, impact velocity and electrochemical potential on the erosion-corrosion of WC/Co-Cr coatings', *Wear*.

Stevenson, R., Harrison, S.T.L., Miles, N., and Cilliers, J.J., (2006) 'Examination of swirling flow using electrical resistance tomography', *Powder Technology*, Vol. 162, pp157-165.

Tan, K.S., Wood, R.J.K, and Stokes, K.R., (2003) 'The slurry erosion behaviour of high velocity oxy-fuel (HVOF) sprayed aluminium bronze coatings', *Wear*, Vol. 255, pp195-205.

Tonkin, R., (2004) *Swirling Pipeflow of Non-Newtonian and Particle-Laden Fluids*. PhD Thesis, 2004. School of Chemical, Environmental and Mining Engineering, University of Nottingham, United Kingdom.

Turian, R.M., Ma, T.M., Hsu, F.L., and Sung, D.J., (1997) 'Characterization, settling and rheology of concentrated fine particulate mineral slurries', *Powder Technology*, Vol. 93, pp219-233.

Turian, R.M., Ma, T.M., Hsu, F.L., Sung, D.J., and Packmann, G.W., (1998) 'Flow of concentrated non-Newtonian slurries', *Int. J. Multiphase Flow*, Vol. 24, pp225-242.

Wolfe, S.E. (1967) 'The Transport of Solids in Helically Ribbed Pipes', *The Canadian Mining and Metallurgical Bulletin*, February, pp221-223

Wood, R.J.K, Jones, T.F., Miles, N.J., and Ganeshalingam, J., (2001) 'Upstream swirl-induction for reduction of erosion damage from slurries in pipeline bends', *Wear*, Vol. 250, pp770-778.

Wood, R.J.K, Jones, T.F., Ganeshalingam, J., and Miles, N.J., (2004) 'Comparison of predicted and experimental erosion estimates in slurry ducts', *Wear*, Vol. 256, pp937-947.

Xu, J., Wu, Y., Shi, Z., Lao, L., and Li, D., (2007) 'Studies on two-phase co-current air/non-Newtonian shear-thinning fluid flows in inclined smooth pipes', *International Journal of Multiphase Flow*

Yasar, F., Togrul, H., and Arslan, N., (2007) 'Flow properties of cellulose and carboxymethyl cellulose from orange peel', *Journal of Food Engineering*, Vol. 81, Issue 1, pp187-199




Yaseen, E.I., Herald, T.J., Aramouni, F.M., and Alavi, S., (2005), 'Rheological properties of selected gum solutions', *Food Research International*, Vol. 38, Issue 2, pp 111-119

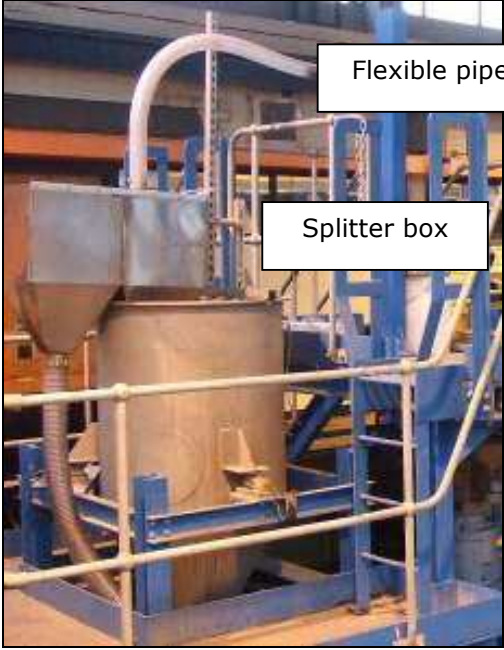


Yuille, N.A. (1928), *Dredger Pipe Line*, 1, 662, 178 (patent)


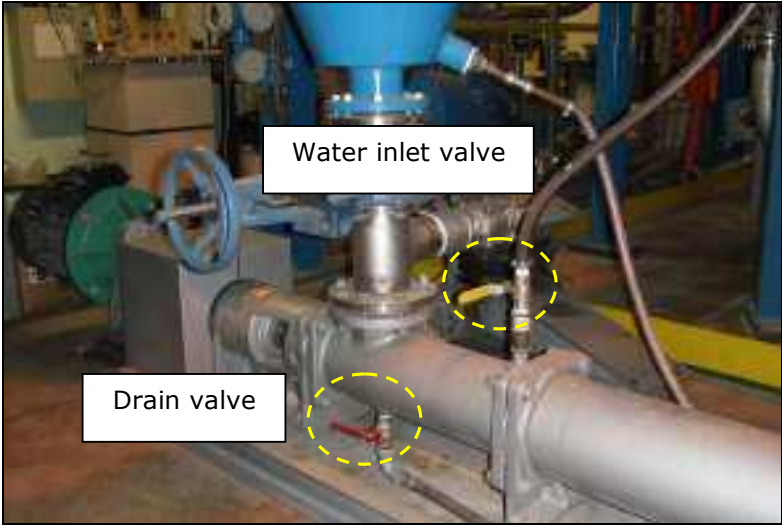

APPENDIX A STEEL PIPE RIG COMPONENTS

Instrumentation and steel pipe rig

Components / Instruments	Descriptions
	A.1 Submersible Pump
	A.2: Lower leg horizontal pipe

Components / Instruments	Descriptions
	A.3: Upper leg horizontal pipe
	A.4: Motor
	A.5: Inverter

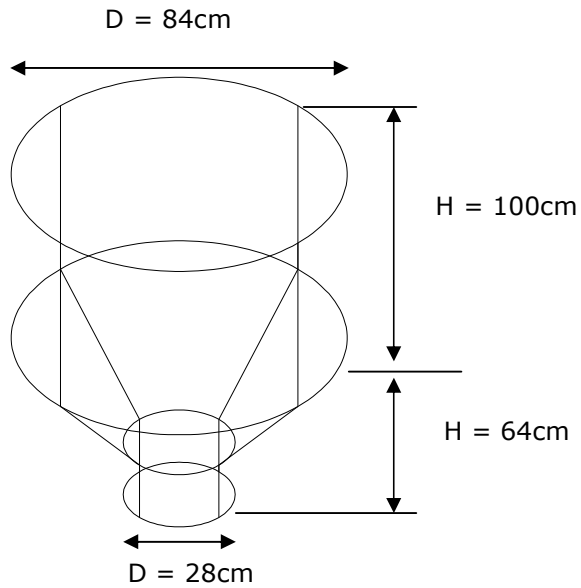
Components / Instruments	Descriptions
	<p>A.6: The position of splitter box attached to weigh tank</p>
	<p>A.7: Flow meter transducer and thermometer K-type</p>
	<p>A.8: Digital flow meter</p>

Components / Instruments	Descriptions
	<p>A.9: Controller box with temperature reader</p>
	<p>A.10: Drain and water inlet valves at Mono Pump</p>
	<p>A.11: Drain valve (located at the bottom of de-aerator)</p>

Steel pipe flow loop calculations

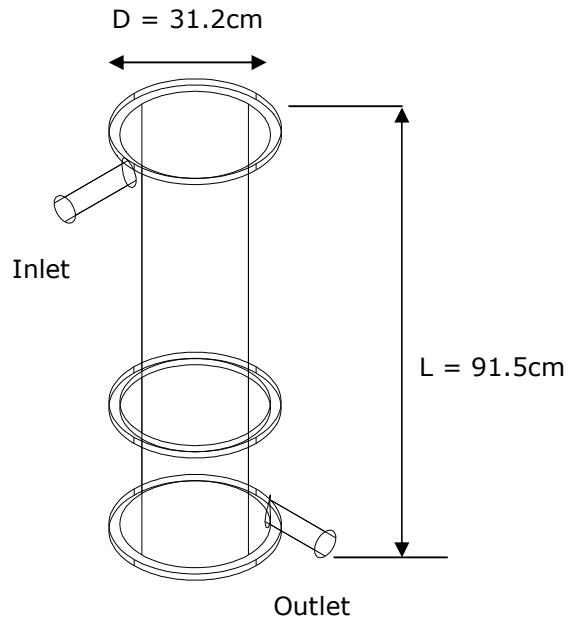
A.12 Weigh tank

Volume, V
 $= 0.725\text{m}^3$



A.13 De-aerator

Volume, V
 $= \frac{\pi \cdot D^2}{4 \cdot H}$
 $= \frac{\pi \times 0.312^2}{4 \times 0.915}$
 $= 0.070\text{ m}^3$



A.14 Volume of pipe loop

Length, $L = 40\text{m}$

Diameter, $D = 0.05\text{m}$

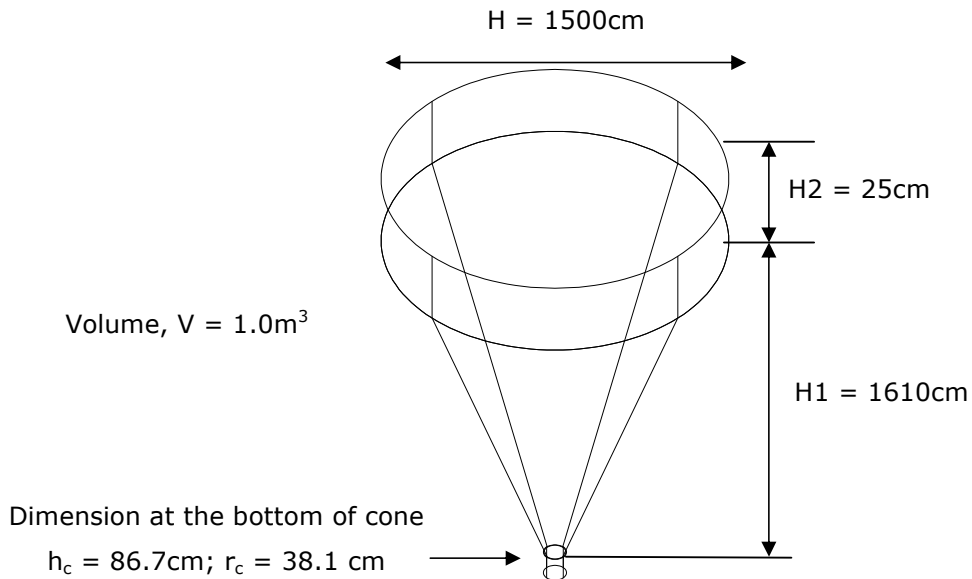
$$\text{Volume, } V = \pi \cdot \left(\frac{D}{2}\right)^2 \cdot L = \pi \times \left(\frac{0.05}{2}\right)^2 \times 40 = 0.0785 \text{ m}^3$$

Total volume, V_T of flow loop require

$$V_T = 0.725 + 0.070 + 0.0785 = 0.8735 \text{ m}^3$$

A.15 Conical tank

The conical tank used in this experiment was designed to hold a volume of entire flow loop. The volume required was the sum of pipe volume, weigh tank and de-aerator with extra adjustment on the volume remaining in the tank.



An extra of cylinder of 0.25m high was installed on the top of the conical tank to prevent the overflow of fluids.

A.16 Net positive suction head (NPSH) calculation

The NPSH calculation was carried out to check the minimum head in the pump is sufficient to avoid the cavitation. Robert et. al (2006) suggested that to avoid the cavitation in the pump, the NPSH available should be less than the NPSH required. When fluid velocity travelled at 4.0m/s, the NPSH required from manufacturer was 2.5m. The NPSH available for water and CMC fluids can be determined as follows:

For water equation (Coulson et al., 2000):

$$NPSH_{available} = h_s - h_v + H_v \quad \text{Eq. A1}$$

For CMC fluids equation (Condron, 2002):

$$NPSH_{available} = H_v - hf + \frac{10.2}{\rho_f(P_t - P_v)} \quad \text{Eq. A2}$$

h_s and h_v is the suction head and liquid vapour head respectively.

H_v (m) is the liquid height at minimum volume, which given by:

$$H_v = r \cdot \tan 66 \quad \text{Eq. A3}$$

and r is given by:

Volume of liquid in + Volume of cone (bottom) = Total volume of cone conical tank

$$0.11 + \left(\frac{\pi r_c^2 h_c}{3} \right) = \left(\frac{\pi r^2 H_v}{3} \right) \quad \text{Eq. A4}$$

Where r_c and h_c is 0.0381m and 0.0867m respectively. R can be determined using quadratic equation:

$$r = \sqrt[3]{\frac{3(0.11 + 1.3 \times 10^{-4})}{\pi \tan 66}} = 0.36 \text{ m} \quad \text{Eq. A5}$$

Substitute r into equation A2,

$$H_v = 0.36 \times \tan 66 = 0.81 \text{ m}$$

Suction head, h_s is given by:

$$h_s = \frac{P_t}{\rho_f g} - h_f \quad \text{Eq. A6}$$

and liquid vapour head, h_v is given by:

$$h_v = \frac{P_v}{\rho_f g} \quad \text{Eq. A7}$$

Where at 18°C,

P_t = Pressure at the tank (atmospheric pressure = 101.3 kPa)

P_v = Liquid vapour pressure (2059 Pa; Joergens, 2002)

ρ_f = Fluid density (kg/m^3) (water = 1000kg/m^3 ; CMC = 1002.8kg/m^3)

h_f = Frictional head losses through t-piece and gate valve

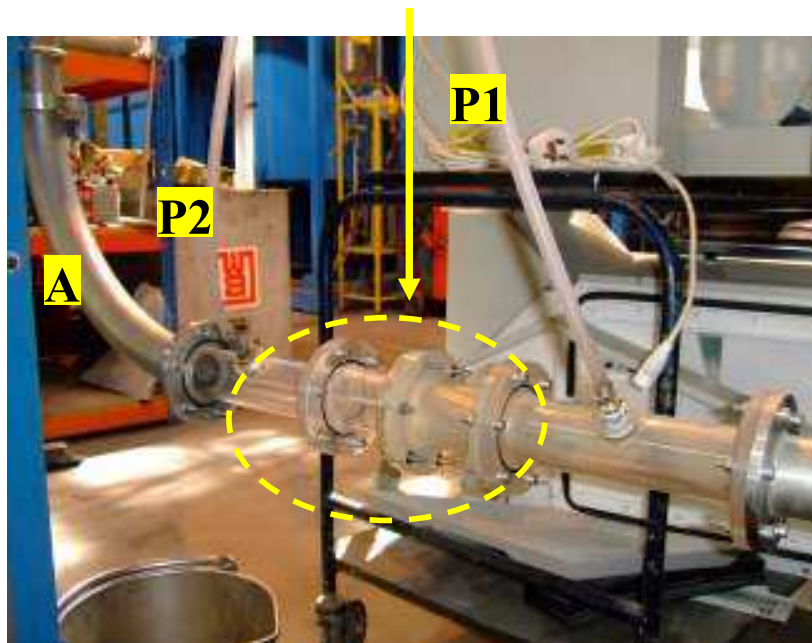
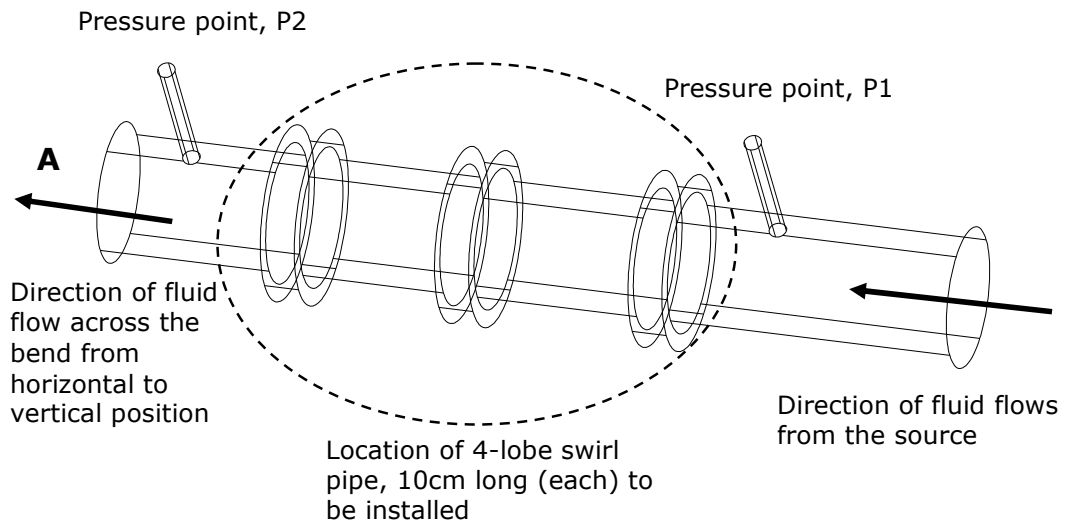
h_f is given by:

$$h_f = \frac{kv^2}{2g} \quad \text{Eq. A8}$$

Nesbitt (2000) determined the k index of water for t-piece and gate valve is 0.1 and 0.2 respectively. For non-Newtonian fluid from Reynolds number using correlations of Kittredge and Rowley (1957), the k index for t-piece and gate valve is 0.6 and 2.0 respectively. Substitute these values in equation A7 gives h_f for water and CMC at 0.24m and 2.12m respectively.

Therefore, the NPSH available for water and CMC fluids from equation A1 and A2, is 10.7m and 8.9m respectively.

A.17 Swirl pipe and pressure locations



- A Radius to diameter (R/D) bend = 4
- P1 Pressure tube 1, measuring the pressure elevation before the swirl pipe
- P2 Pressure tube 2, measuring the pressure elevation after the swirl pipe

A.18 Bend

Radius to diameter (R/D) ratio:

Radius of pipe, R = 0.22m Diameter of steel pipe, D = 0.05m

Therefore,

$$\frac{R}{D} = \frac{0.22}{0.05} = 4$$

A.19 Moody Chart and Pressure Drop

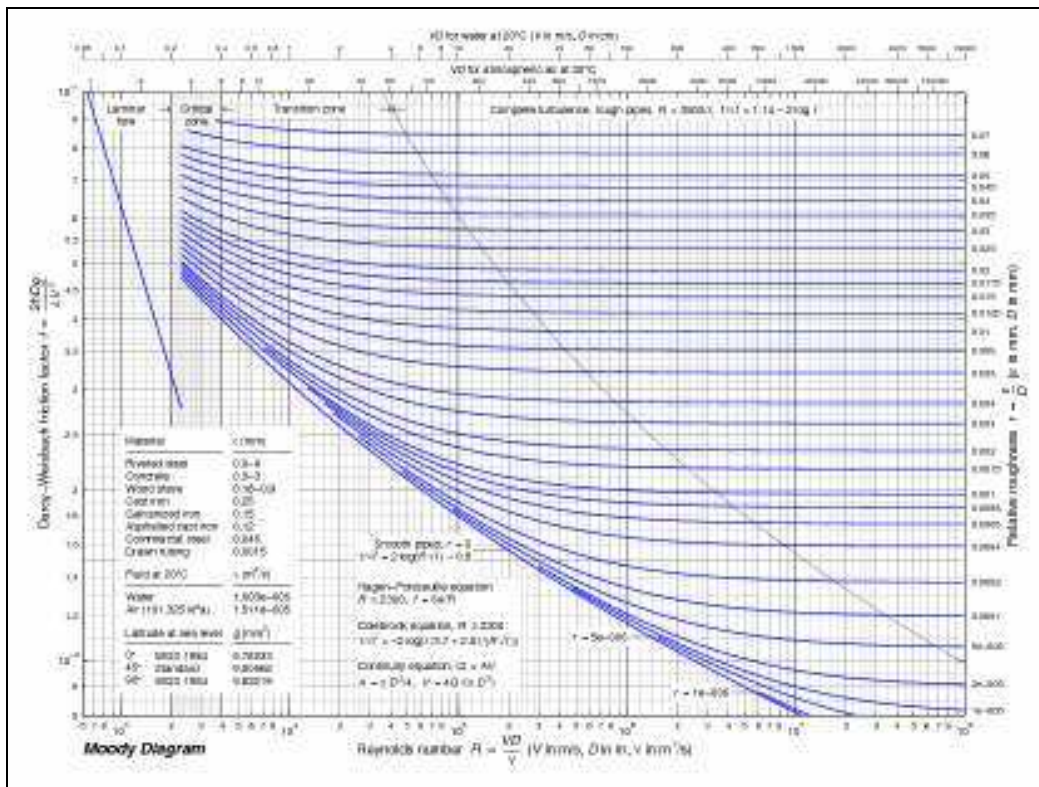


Figure A.1: Moody diagram (adopted from www.softpedia.com)

Table A.1: Values of surface roughness index for various materials (Darby, 2001)

Material	Condition	Roughness range (mm)	Recommended (mm)
Commercial steel	New	0.1 - 0.02	0.045
	Light rust	1.0 - 0.15	0.300
	General rust	3.0 - 1.00	2.000
Concrete	Very smooth	0.18 - 0.025	0.040
	Wood floated	0.8 - 0.20	0.300
	Rough	2.5 - 0.8	2.000
Glass or plastic	Drawn tubing	0.01 - 0.0015	0.002

Appendix B

TEST MATERIALS AND VISCOSITY

Brookfield viscometer



B.1



B.2



B.3

B.1: Brookfield Viscometer Model LV

B.2: Reading dial bar

B.3: Spindles 1, 2 and 3

Table B.1: Brookfield Viscometer Model LV spindle/speed/factor combination (taken from www.can-am.net)

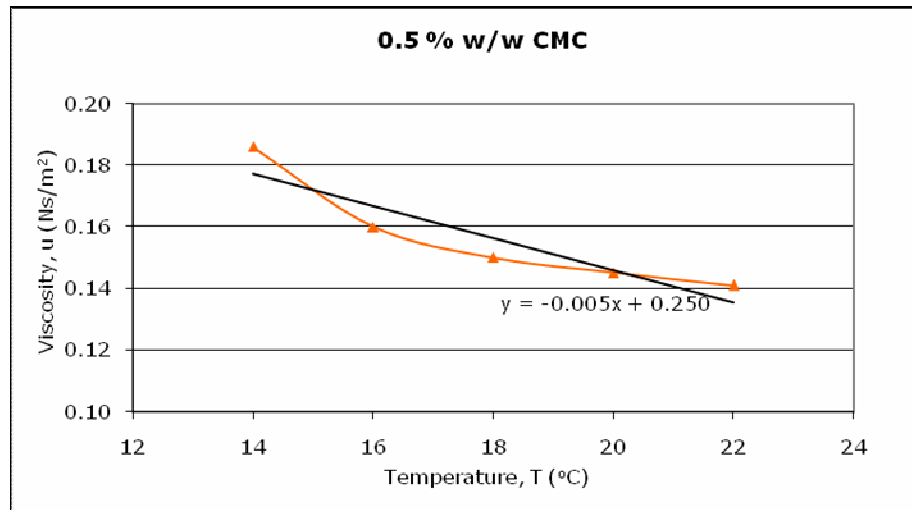
Brookfield Viscometer Model LV							
Spindle 1		Spindle 2		Spindle 3		Spindle 4	
Speed	Factor	Speed	Factor	Speed	Factor	Speed	Factor
0.3	200	0.3	1M	0.3	4M	0.3	20M
0.6	100	0.6	500	0.6	2M	0.6	10M
1.5	40	1.5	200	1.5	800	1.5	4M
3	20	3	100	3	400	3	2M
6	10	6	50	6	200	6	1M
12	5	12	25	12	100	12	500
30	2	30	10	30	40	30	200
60	1	60	5	60	20	60	100

The dynamic viscosity reading using Brookfield Viscometer LV

Dial reading x Factor = Viscosity in cP (mPa.s)

Table B.2: Data results for apparent viscosity of CMC at different concentrations and temperatures, T (°C)

Temperature T (°C)	CMC % w/w at T = 18°C		
	0.5	1.0	1.5
	Apparent viscosity (Ns/m ²)		
14	0.186	0.991	2.093
16	0.160	0.817	1.710
18	0.150	0.712	1.523
20	0.145	0.654	1.445
22	0.141	0.600	1.360

**Figure B.1: Apparent viscosity of 0.5% w/w CMC at different temperatures**

The relationship between shear stress and shear rate using Ostwald-de Waele law:

$$\tau = k \left(\frac{du}{dy} \right)^n$$

Where, τ is the shear stress (Pa.s), k is the apparent viscosity (Ns/m²), $\frac{du}{dy}$ is the velocity profile (m/s) and n is the CMC flow behaviour index (0.47).

Table B.3: Data results for shear rate, τ of CMC at different concentration and velocity gradient, $\frac{du}{dy}$ (m/s)

Velocity v (m/s)	CMC % w/w at T = 18°C			Velocity v (m/s)	CMC % w/w at T = 18°C		
	0.5	1.0	1.5		0.5	1.0	1.5
	Shear stress, (Pa.s)				Shear stress, (Pa.s)		
0.00	0.000	0.000	0.000	1.30	0.170	0.805	1.723
0.10	0.051	0.241	0.516	1.40	0.176	0.834	1.784
0.20	0.070	0.334	0.715	1.50	0.181	0.861	1.843
0.30	0.085	0.404	0.865	1.60	0.187	0.888	1.899
0.40	0.098	0.463	0.990	1.70	0.192	0.914	1.954
0.50	0.108	0.514	1.100	1.80	0.198	0.939	2.008
0.60	0.118	0.560	1.198	1.90	0.203	0.963	2.059
0.70	0.127	0.602	1.288	2.00	0.208	0.986	2.110
0.80	0.135	0.641	1.371	2.10	0.213	1.009	2.158
0.90	0.143	0.678	1.449	2.20	0.217	1.031	2.206
1.00	0.150	0.712	1.523	2.30	0.222	1.053	2.253
1.10	0.157	0.745	1.593	2.40	0.226	1.074	2.298
1.20	0.163	0.776	1.659	2.50	0.231	1.095	2.343

For power law fluid (non-Newtonian and time-independent), Metzner and Reed (1955) developed the Rabonowitsch-Mooney equation to:

$$Re_{RM} = \frac{\rho D^n V^{2-n}}{\gamma} \quad \text{Eq. 8}$$

and

$$\gamma = k^* \cdot 8^{n-1} \quad \text{Eq. 9}$$

$$k^* = k \left(\frac{1+3n}{4n} \right)^n \quad \text{Eq. 10}$$

Where,

k^* = Non-Newtonian fluid consistency index,

n = Non-Newtonian flow behaviour index, 0.47 (Tonkin, 2004)

Equations 8 – 10 for CMC Reynolds number:

$$\text{Re}_{cmc} = \frac{\rho_{cmc} Du}{\eta} \quad \text{Eq. B1}$$

Where, u is the velocity profile (m/s), η is the apparent viscosity of CMC (Ns/m²) at different concentrations, D is the internal diameter of pipe (0.05m), and ρ is the density of CMC (1000 kg/m³).

The data for CMC Reynolds number is shown in Table B.4.

Table B.4: Reynolds number for CMC at different concentrations and shear rates depends on velocity requirements. Average temperatures were 18°C.

Velocity v (m/s)	CMC % w/w at T = 18°C		
	0.5	1.0	1.5
	Shear rate, $\dot{\gamma}$		
	0.150	0.732	1.660
Reynolds number			
0.20	66.67	13.66	6.02
0.40	133.33	27.32	12.05
0.50	166.67	34.15	15.06
0.60	200.00	40.98	18.07
0.80	266.67	54.64	24.10
1.00	333.33	68.31	30.12
1.20	400.00	81.97	36.14
1.40	466.67	95.63	42.17
1.50	500.00	102.46	45.18
1.60	533.33	109.29	48.19
1.80	600.00	122.95	54.22
2.00	666.67	136.61	60.24
2.50	833.33	170.77	75.30

The Reynolds numbers for CMC were exhibited within laminar flow.

Appendix C

EXPERIMENTAL DATA

C.1 Calculation procedures for pressure drop

1. Determine the Reynolds number (Newtonian fluid)

$$\text{Re} = \frac{u \times D}{\nu} = \frac{\rho \times u \times D}{\mu} \quad \text{Eq.15}$$

2. Pipe friction coefficient

For laminar flow, the pipe friction coefficient, f (Hagen-Poiseuille equation):

$$f = \frac{64}{\text{Re}} \quad \text{Re} \leq 2000 \quad \text{Eq.20}$$

For turbulent flow, the pipe friction coefficient, f (Colebrook equation, 1939):

$$\frac{1}{\sqrt{f}} = -4 \log \left[\frac{1.256}{\text{Re} \sqrt{f}} + \frac{\varepsilon}{3.7D} \right] \quad \text{Re} \geq 5000 \quad \text{Eq.21}$$

3. Head loss

The pressure head loss (friction head), P_f is required to overcome the resistance of fluid to flow in pipe and fittings. From equation 11 and 12, the friction head loss, f in a length of pipe is given by:

$$P_f = f \times \frac{L}{D} \times \frac{u^2}{2g} \quad \text{Eq.23}$$

4. Pressure by vertical elevation (pressure-height relation)

$$P = P_f + P_h \quad \text{Eq.24}$$

$$\text{Where, } P_h = \rho \cdot g \cdot H_n \quad \text{Eq.25}$$

5. Pressure drop, ΔP (Pa)

$$\Delta P_{n,n+1} = P_n - P_{n+1} \quad \text{Eq.26}$$

C.2 Pressure drop calculation for water

Condition (ONE 4-lobe swirl pipe):

Density of water, ρ_w (at 18°C)	= 998.36 kg/m ³
Viscosity of water μ_w (at 18°C)	= 1.063x10 ⁻³ Ns/m ²
Relative roughness, ε	= 0.045 mm.
Velocity, v	= 0.5 m/s

Reynolds number (Eq.15):

$$Re_{0.5} = \frac{998 \times 0.05 \times 0.5}{1.063 \times 10^{-3}} = 23471.31 \quad (\text{Turbulent})$$

Friction factor, f and rearrange Eq.21:

$$f = 0.25 \left[\log \left(\frac{\frac{\varepsilon}{D}}{3.7} + \frac{5.74}{Re^{0.9}} \right) \right]^{-2} \quad \text{Eq.27}$$

$$f = 0.25 \left[\log \left(\frac{\left(\frac{0.045 \times 10^{-3}}{0.05} \right)}{3.7} + \frac{5.74}{23471^{0.9}} \right) \right]^{-2} = 0.02705$$

Pressure head loss, P_f to overcome the friction factor, f (Eq.23):

$$P_f = 0.02705 \times \frac{35.8}{0.05} \times \frac{0.5^2}{2g} = 0.247 \text{ Pa}$$

The elevations, H (m) obtained from simple manometer tubes at 0.5m/s:

H1	= 6.740m
H2	= 6.738m
H3	= 5.818m

Pressure, P (Pa) (Eq.25):

P1	= 66010.96 Pa
P2	= 65991.38 Pa
P3	= 56980.98 Pa

Therefore, the pressure drop, ΔP for water without swirl-inducing pipe (Eq.26):

$$\Delta P_{12} = P_1 - P_2 = 66010.96 - 65991.38 = 19.58 \text{ Pa} \quad (\sim 20 \text{ Pa})$$

$$\Delta P_{23} = P_2 - P_3 = 65991.38 - 56980.98 = 9010.40 \text{ Pa} \quad (\sim 9010 \text{ Pa})$$

$$\Delta P_{13} = P_1 - P_3 = 66010.96 - 56980.98 = 9029.98 \text{ Pa} \quad (\sim 9030 \text{ Pa})$$

Table C.3: Flow rate, velocity, height of manometer tube and pressure drop data for water with and without swirl inducing pipe

Data	Flowrate	Velocity	Average Frequency	Average T		Average height, H (m) manometer tube		
	Q (m ³ /hr)	V (m/s)	F (Hz)	°C	K	H1	H2	H3
2 Swirls	3.534	0.5	9.35	18.2	291.2	6.743	6.738	5.818
	7.069	1.0	12.25	18.2	291.2	6.288	6.258	5.333
	10.603	1.5	16.30	18.4	291.4	6.593	6.528	5.593
	14.137	2.0	20.60	18.6	291.6	7.053	6.938	5.988
	17.672	2.5	25.15	18.7	291.7	7.588	7.418	6.463
1 Swirl	3.534	0.5	9.35	18.2	291.2	7.588	7.418	6.463
	7.069	1.0	12.30	18.3	291.3	7.053	6.938	5.988
	10.603	1.5	16.35	18.5	291.5	6.593	6.528	5.593
	14.137	2.0	20.65	18.5	291.5	6.288	6.258	5.333
	17.672	2.5	25.15	18.6	291.6	6.743	6.738	5.818
No swirl	3.534	0.5	9.40	18.3	291.3	6.744	6.738	5.817
	7.069	1.0	12.30	18.4	291.4	6.287	6.257	5.332
	10.603	1.5	16.40	18.6	291.6	6.592	6.525	5.592
	14.137	2.0	20.70	18.7	291.7	7.054	6.939	5.987
	17.672	2.5	25.20	18.9	291.9	7.598	7.419	6.465

Table C.3 (continue):

Data	Flowrate Q (m ³ /hr)	Velocity V (m/s)	(Average) Pressure drop, ΔP (Pa)		
			P1-P2	P2-P3	P1-P3
2 Swirls	3.534	0.5	52.23	9013.41	9065.65
	7.069	1.0	293.81	9059.18	9352.99
	10.603	1.5	643.12	9150.52	9793.63
	14.137	2.0	1126.25	9310.36	10436.61
	17.672	2.5	1694.29	9349.59	11043.88
1 Swirl	3.534	0.5	10.45	9011.84	9015.11
	7.069	1.0	143.67	9060.76	9204.43
	10.603	1.5	346.10	9158.48	9504.58
	14.137	2.0	590.98	9207.52	9798.50
	17.672	2.5	809.73	9383.71	10193.44
No swirl	3.534	0.5	9.13	9010.98	9014.24
	7.069	1.0	9.79	9151.43	9161.22
	10.603	1.5	10.77	9290.71	9301.49
	14.137	2.0	19.59	9435.35	9454.94
	17.672	2.5	22.53	9621.83	9644.36

C.4 Sand-water slurries

The sand-water slurry concentration in terms of percentage volume per volume (% v/v), (Tonkin, 2004):

To obtain a slurry concentration of 1.4% v/v, with 1.0m³ of water, the amount of sand needed (kg):

$$C_v = \frac{V_s}{V_l} \times 100 \quad \text{Eq. 10}$$

$$V_s = \frac{C_v \times V_l}{100\%} = \frac{1.4 \times 1.0}{100} = 0.014 \text{ m}^3$$

So,

$$V_s (\text{m}^3) = \frac{m_s (\text{kg})}{\rho_s (\text{kg/m}^3)} \quad \text{Eq. 9}$$

$$V_s (\text{kg}) = V_s (\text{m}^3) \times \rho_s (\text{kg/m}^3) = 0.014 \times 2640 = 36.96 \text{ kg}$$

The sand needed is approximately 37.0 kg.

At 18°C, the density of water is approximately 998.0 kg/m³. Therefore, the density of sand-water slurry, ρ_m (kg/m³) (Nesbitt, 2000) equation 12:

$$\rho_m = \rho_l + \frac{C_v(\rho_s - \rho_l)}{100} = 998.0 + \frac{1.4(2640.0 - 998.0)}{100} = 1021.0 \text{ kg/m}^3$$

Table C.6: Sand-water slurries concentrations

Concentration of solids C_1 (% v/v)	Volume			Total volume V_T (L)	Density of slurries ρ (kg/m ³)
	Water (L)	Sand			
		L	Kg		
1.4	986.19	13.81	36.45	1000	1022.96
2.1	979.43	20.57	54.30	1000	1034.44
2.7	973.71	26.29	69.41	1000	1044.28

C.7 Pressure drop calculation for sand-water slurry

Condition (ONE 4-lobe swirl pipe):

Concentration of sand-water slurry = 1.4% v/v

Density of mixture, ρ_m (at 18°C) = 1021.0 kg/m³

Viscosity of mixture, μ_m (at 18°C) = 1.063x10⁻³ Ns/m²

Relative roughness, ε = 0.045 mm.

Velocity, v = 0.5 m/s

Assumption:

Viscosity of mixture, μ_m is the same as viscosity of water, μ_w at given temperature condition.

Pressure, P (Pa) values for P1, P2 and P3 when used one 4-lobe swirl-inducing pipe at nominal velocity of 0.5 m/s were calculated as follows:

Reynolds number (Eq.15):

$$Re_{0.5} = \frac{1021.0 \times 0.05 \times 0.5}{1.063 \times 10^{-3}} = 24012.2 \quad (\text{Turbulent})$$

Friction factor, f Eq.27:

$$f = 0.25 \left[\log \left(\frac{\left(\frac{0.045 \times 10^{-3}}{0.05} \right)}{3.7} + \frac{5.74}{24012^{0.9}} \right) \right]^{-2} = 1.175$$

Pressure head loss, P_f to overcome the friction factor, f (Eq.23):

$$P_f = 1.175 \times \frac{35.8}{0.05} \times \frac{0.5^2}{2g} = 10.72 \text{ Pa}$$

The elevations, H (m) from simple manometer tubes at 0.5m/s

$$H_1 = 7.533 \text{ m}$$

$$H_2 = 7.511 \text{ m}$$

$$H_3 = 6.574 \text{ m}$$

Pressure, P (Pa) (Eq.25):

$$P_1 = 75450.60 \text{ Pa}$$

$$P_2 = 75230.18 \text{ Pa}$$

$$P_3 = 65845.18 \text{ Pa}$$

Therefore, the pressure drop, ΔP for water without swirl-inducing pipe (Eq.26):

$$\Delta P_{12} = P_1 - P_2 = 220.42 \text{ Pa} \quad (\sim 220 \text{ Pa})$$

$$\Delta P_{23} = P_2 - P_3 = 9385.00 \text{ Pa} \quad (\sim 9400 \text{ Pa})$$

$$\Delta P_{13} = P_1 - P_3 = 9605.42 \text{ Pa} \quad (\sim 9600 \text{ Pa})$$

Table C.8: Flow rate, velocity, height of manometer tube and pressure drop data for sand-water slurries with and without swirl inducing pipe

Data	Flow rate Q (m ³ /hr)	Velocity V (m/s)	(Average) Frequency, F (Hz)				(Average) Temperature, T	
			Water 800L	Sand-water % v/v			°C	K
				1.4	2.1	2.7		
				30.0 kg	45.3 kg	58.6 kg		
2 Swirl	3.534	0.5	9.35	9.40	9.50	9.60	18.6	291.6
	7.069	1.0	12.25	12.30	12.50	12.50	18.6	291.6
	10.603	1.5	16.30	16.30	16.50	16.70	18.7	291.7
	14.137	2.0	20.60	18.70	21.00	21.40	18.8	291.8
	17.672	2.5	25.15	23.80	25.50	26.10	18.9	291.9
1 Swirl	3.534	0.5	9.35	9.50	9.50	9.60	18.8	291.8
	7.069	1.0	12.30	12.40	12.60	12.70	18.9	291.9
	10.603	1.5	16.35	16.50	16.80	17.00	18.9	291.9
	14.137	2.0	20.65	20.70	21.80	22.10	19.0	292.0
	17.672	2.5	25.15	25.40	26.10	26.80	19.0	292.0
No swirl	3.534	0.5	9.40	9.50	9.60	9.60	18.4	291.4
	7.069	1.0	12.30	12.50	12.70	12.80	18.6	291.6
	10.603	1.5	16.40	16.70	17.00	17.20	18.6	291.6
	14.137	2.0	20.70	20.80	22.00	22.40	18.7	291.7
	17.672	2.5	25.20	25.60	27.30	27.80	18.8	291.8

Table C.8 (continue):

Data	Velocity V (m/s)	Average elevation, H (m) of manometer tube								
		H1	H2	H3	H1	H2	H3	H1	H2	H3
		Sand-water % v/v								
		1.4			2.1			2.7		
2 Swirls	0.5	7.505	7.455	6.541	7.436	7.386	6.471	7.380	7.329	6.405
	1.0	7.038	6.917	6.025	6.985	6.863	5.959	7.003	6.878	5.956
	1.5	7.360	7.198	6.283	7.311	7.148	6.213	7.338	7.172	6.210
	2.0	7.894	7.717	6.718	7.829	7.652	6.643	7.860	7.678	6.639
	2.5	8.488	8.299	7.228	8.452	8.262	7.148	8.461	8.267	7.144
1 Swirl	0.5	7.533	7.511	6.574	7.471	7.449	6.504	7.405	7.383	6.439
	1.0	6.969	6.910	5.985	6.913	6.853	5.920	6.852	6.792	5.860
	1.5	7.263	7.129	6.233	7.203	7.068	6.163	7.149	7.013	6.100
	2.0	7.715	7.585	6.632	7.651	7.520	6.559	7.603	7.471	6.492
	2.5	8.260	8.123	7.114	8.192	8.053	7.035	8.153	8.013	6.963
No swirl	0.5	6.786	6.784	5.837	6.732	6.730	5.775	6.691	6.689	5.717
	1.0	7.010	7.002	6.036	6.954	6.946	5.971	6.905	6.896	5.912
	1.5	7.333	7.319	6.325	7.275	7.261	6.257	7.223	7.208	6.195
	2.0	7.765	7.744	6.712	7.703	7.681	6.640	7.647	7.625	6.574
	2.5	8.282	8.253	7.179	8.215	8.186	7.102	8.155	8.126	7.031

Data	Velocity V (m/s)	Average pressure drop, ΔP (Pa)								
		P1-P2	P2-P3	P1-P3	P1-P2	P2-P3	P1-P3	P1-P2	P2-P3	P1-P3
		Sand-water % v/v								
		1.4			2.1			2.7		
2 Swirl	0.5	500.99	9131.71	9632.71	507.55	9240.75	9748.30	521.13	9426.11	9947.25
	1.0	1234.86	8933.65	10151.85	1238.43	9157.00	10395.42	1267.44	9340.13	10607.57
	1.5	1657.88	9208.60	10836.01	1657.64	9503.74	11161.38	1690.73	9779.32	11470.05
	2.0	1672.41	9964.93	11722.05	1792.35	10165.54	11957.89	1829.54	10469.07	12298.61
	2.5	1859.52	10710.18	12601.02	1926.79	11265.97	13192.77	1966.28	11358.40	13324.68
1 Swirl	0.5	222.43	9390.15	9612.58	226.45	9577.98	9804.43	230.01	9657.48	9887.49
	1.0	589.76	9268.35	9858.11	603.34	9451.78	10055.12	615.37	9529.29	10144.66
	1.5	862.36	8979.21	10321.56	1142.37	9159.34	10528.16	1395.99	9342.43	10738.42
	2.0	1301.35	9544.28	10845.63	1327.50	9734.80	11062.30	1354.02	10017.04	11371.06
	2.5	1377.01	10109.26	11486.27	1405.81	10310.75	11716.56	1434.12	10743.70	12177.82
No swirl	0.5	19.66	9492.18	9511.84	16.20	9682.30	9700.86	19.78	9943.40	9963.18
	1.0	79.73	9678.69	9758.42	80.85	9871.53	9952.38	83.24	10069.06	10152.30
	1.5	141.63	9963.48	10105.11	145.18	10163.52	10308.70	147.19	10365.86	10513.05
	2.0	211.18	10340.78	10551.96	215.34	10547.50	10762.84	219.56	10758.46	10978.02
	2.5	287.77	10760.18	11047.95	295.31	10975.82	11271.13	298.85	11195.10	11493.95

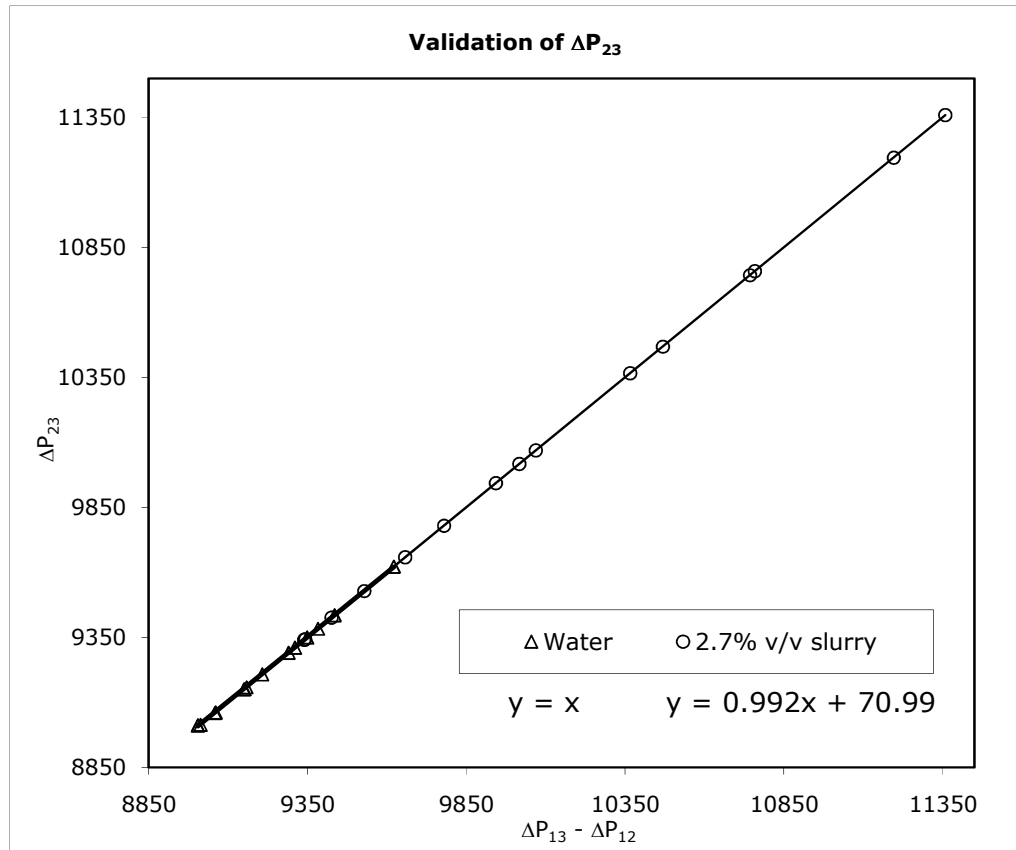


Figure C.9: Graph to show the validation of ΔP_{23} against $\Delta P_{13} - \Delta P_{12}$ for water and sand-water slurry at 2.7% v/v

The swirl-inducing pipe caused lower pressure drops compared to when fluids were preceded without the swirl-inducing pipe. The graph in figure C.9 shows a validation of pressure drops for ΔP_{23} . The overall pressure drop across the pipe rig was obtained from ΔP_{13} , which was equal to $\Delta P_{12} + \Delta P_{23}$. Therefore, the ΔP_{23} should be equal to $\Delta P_{13} - \Delta P_{12}$. The statistical data obtained and plotted for the effect of swirl inducing pipe flow over the bend showed similarity in the gradient (approximately, $m = 1$) when ΔP_{23} was plotted against $\Delta P_{13} - \Delta P_{12}$. The ΔP_{23} data was obtained directly from the results (Table C:3 for water and table C.8 for 2.7% v/v slurry) and plotted against the value of $\Delta P_{13} - \Delta P_{12}$. These results proved that the pressure drops obtained from the bend were acceptable.

C.10 Carboxymethyl cellulose (CMC)

Reynolds number for CMC can be obtained in Appendix B.4. The pressure measurements for 0.5% w/w CMC were obtained using equations 11 – 16. While, the pressure measurements for 1.0 and 1.5% CMC were obtained directly from Bourdon gauge.

Table C.11: 0.5% w/w CMC

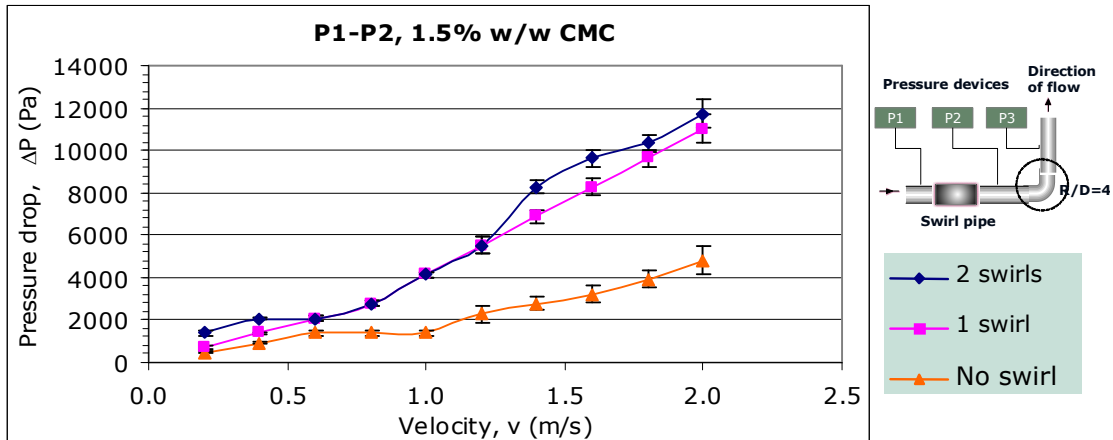
0.5 % w/w	Q (m ³ /hr)	v (m/s)	F (Hz)	T °C	η Ns/m ²	Heigh, H (m)			Pressure different, DP (Pa)		
						H1	H2	H3	$\Delta P1$	$\Delta P2$	$\Delta P3$
2 swirl	3.534	0.5	9.4	18.2	0.149	7.058	7.015	6.440	425.10	5509.95	6065.85
	7.069	1.0	12.3	18.3	0.149	7.438	7.304	6.296	1313.45	8087.80	11199.75
	10.603	1.5	16.4	18.3	0.149	7.298	7.062	6.083	2310.80	8452.95	11919.15
	14.137	2.0	20.7	18.3	0.149	7.738	7.518	6.510	2158.20	9913.55	12049.95
1 swirl	3.534	2.0	9.4	18.3	0.149	7.078	7.050	6.496	272.50	5466.35	5706.15
	7.069	1.5	12.3	18.4	0.149	7.278	7.229	6.392	485.05	8202.25	8688.12
	10.603	1.0	16.4	18.4	0.149	7.438	7.322	6.381	1139.05	9232.30	10371.35
	14.137	0.5	20.7	18.4	0.149	7.688	7.585	6.597	1013.70	9684.65	10698.35
No swirl	3.534	0.5	13.4	18.2	0.149	7.098	7.085	6.547	130.80	5648.93	5403.68
	7.069	1.0	17.7	18.3	0.149	7.238	7.226	6.290	114.45	8976.15	9303.15
	10.603	1.5	21.2	18.3	0.149	7.398	7.373	6.285	245.25	9695.55	10917.71
	14.137	2.0	25.2	18.3	0.149	7.668	7.641	6.604	261.60	10186.05	10441.11

Table C.12: 1.0% w/w CMC

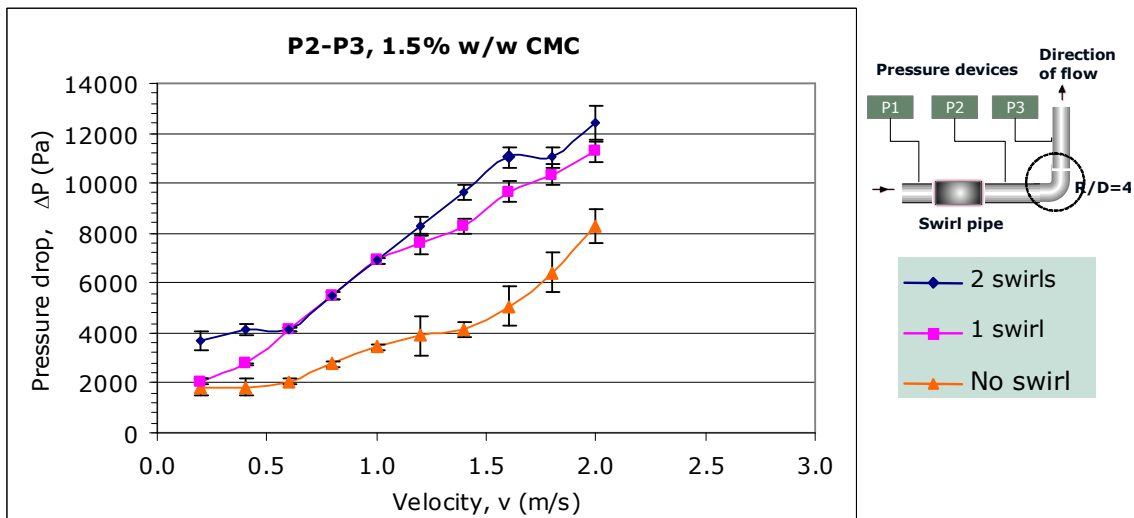
1.0% w/w	Q (m ³ /hr)	v (m/s)	F (Hz)	T °C	η Ns/m ²	Ave pressure (psi)			Pressure different, ΔP (Pa)		
						P1	P2	P3	$\Delta P1$	$\Delta P2$	$\Delta P3$
2 swirl	3.534	0.5	10.6	17.9	0.7199	7.8	7.5	7.0	1896.05	3619.75	5515.80
	7.069	1.0	12.7	18.1	0.7091	8.1	7.6	7.0	2930.27	3619.75	6550.02
	10.603	1.5	16.6	18.4	0.7004	8.4	7.8	7.1	4309.22	4826.33	9135.55
	14.137	2.0	20.9	18.8	0.6903	9.0	8.2	7.3	4688.17	6205.28	11893.45
	17.671	2.5	25.4	19.0	0.6821	10.6	9.6	8.4	6411.86	8273.71	15685.57
1 swirl	3.534	0.5	11.2	17.9	0.7199	8.2	8.0	7.6	1378.94	3102.64	4481.58
	7.069	1.0	15.0	18.1	0.7091	8.6	8.4	8.0	1551.32	3619.75	5171.07
	10.603	1.5	19.5	18.3	0.7033	9.2	8.8	8.4	2757.90	2585.53	5343.43
	14.137	2.0	24.2	18.9	0.6874	9.8	9.3	8.6	3447.38	4481.59	7928.97
	17.671	2.5	28.9	19.2	0.6763	11.0	10.4	9.0	4136.86	9652.66	13789.52
No swirl	3.534	0.5	12.0	17.8	0.7225	9.5	9.4	8.8	689.47	4309.22	4998.70
	7.069	1.0	17.6	18.1	0.7077	10.0	9.8	9.1	1551.32	4136.85	5688.17
	10.603	1.5	22.5	18.4	0.7019	10.5	10.2	9.5	2413.17	4653.96	7067.13
	14.137	2.0	27.3	18.7	0.6917	11.0	10.6	9.8	2585.54	5343.44	7928.97
	17.671	2.5	32.4	19.0	0.6836	12.0	11.5	10.1	3619.74	9307.92	12927.67

Table C.13: 1.5% w/w CMC

1.5 %w/w	Q (m ³ /hr)	v (m/s)	F (Hz)	T °C	η Ns/m ²	Bourdon gauge (Ave. psi)			Pressure different, ΔP (Pa)		
						P1	P2	P3	$\Delta P1$	$\Delta P2$	$\Delta P3$
2 swirl	1.414	0.2	7.5	17.6	1.5664	9.0	8.8	8.2	1378.95	3677.20	5056.15
	2.827	0.4	9.8	17.6	1.5664	9.4	9.1	8.5	2068.43	4136.85	6205.29
	4.241	0.6	12.1	17.7	1.5511	9.8	9.5	8.9	2068.43	4136.85	6205.28
	5.655	0.8	14.4	17.8	1.5417	10.0	9.6	8.8	2757.90	5515.81	8273.71
	7.069	1.0	16.6	17.9	1.5324	10.4	9.8	8.8	4136.85	6894.76	11031.61
	8.482	1.2	18.9	18.1	1.5191	10.8	10.0	8.8	5515.81	8273.71	13789.51
	9.896	1.4	20.7	18.4	1.5074	10.8	9.6	8.2	8273.71	9652.66	17926.37
	11.310	1.6	22.9	18.6	1.4996	10.8	9.4	7.8	9652.66	11031.61	20684.28
	12.723	1.8	25.3	18.7	1.4957	11.4	9.9	8.3	10342.14	11031.61	21373.75
	14.137	2.0	27.4	18.7	1.4957	11.8	10.1	8.3	11721.08	12410.56	24131.65
1 swirl	1.414	0.2	7.8	17.6	1.5664	11.6	11.5	11.2	689.48	2068.43	2757.90
	2.827	0.4	12.0	17.7	1.5511	13.6	13.4	13.0	1378.95	2757.90	4136.85
	4.241	0.6	15.6	17.8	1.5417	15.0	14.7	14.1	2068.43	4136.85	6205.28
	5.655	0.8	18.9	17.9	1.5324	16.0	15.6	14.8	2757.90	5515.81	8273.71
	7.069	1.0	21.9	17.9	1.5324	17.2	16.6	15.6	4136.85	6894.76	11031.61
	8.482	1.2	24.8	18.0	1.5230	18.0	17.2	16.1	5515.81	7584.23	13100.04
	9.896	1.4	27.4	18.1	1.5191	18.8	17.8	16.6	6894.76	8273.71	15168.46
	11.310	1.6	30.0	18.6	1.4996	19.8	18.6	17.2	8273.71	9652.66	17926.37
	12.723	1.8	32.6	18.6	1.4996	20.0	18.6	17.1	9652.66	10342.14	19994.80
	14.137	2.0	35.2	18.6	1.4996	20.4	18.8	17.1	11031.61	11261.44	22293.04
No swirl	1.414	0.2	7.9	18.1	1.5191	12.0	11.9	11.6	459.65	1838.60	2298.25
	2.827	0.4	12.1	18.2	1.5152	14.0	13.9	13.6	919.30	1838.60	2757.90
	4.241	0.6	15.8	18.2	1.5152	15.8	15.6	15.3	1378.95	2068.43	3447.38
	5.655	0.8	19.1	18.2	1.5152	17.0	16.8	16.4	1378.95	2757.90	4136.86
	7.069	1.0	22.1	18.2	1.5152	18.0	17.8	17.3	1378.96	3447.38	4826.33
	8.482	1.2	24.9	18.2	1.5152	19.0	18.7	18.1	2298.25	3907.03	6205.28
	9.896	1.4	27.6	18.3	1.5113	19.8	19.4	18.8	2757.90	4136.85	6894.76
	11.310	1.6	30.2	18.3	1.5113	20.0	19.5	18.8	3217.55	5056.16	8273.71
	12.723	1.8	32.8	18.4	1.5074	20.5	19.9	19.0	3907.03	6435.11	10342.14
	14.137	2.0	35.4	18.4	1.5074	21.0	20.3	19.1	4826.33	8273.71	13100.04

C.14 Pressure drop, ΔP_{12} (Pa) against velocity, v (m/s) for CMC at 1.5% w/w

The pressure drops, ΔP_{12} (Pa) for 1.5% w/w CMC were increased when the velocity, v (m/s) increasing. The swirl-inducing pipe gave higher pressure drops compared to the CMC fluid flows without proceeded swirl-inducing pipe. At 0.2m/s, the pressure drops for 2 swirls, 1 swirl and no swirl were approximately at 1400Pa, 700Pa and 460Pa respectively. At 1.0m/s, the pressure drops were approximately at 4100Pa, 4100Pa and 1400Pa respectively. At 2.0m/s, the pressure drops were approximately at 12000Pa, 11300Pa and 8300Pa respectively.

C.15 Pressure drop, ΔP_{23} (Pa) for CMC at over the bend (R/D of 4)

The pressure drops, ΔP_{23} over the bend for 1.5% w/w CMC proceeded with swirl-inducing pipe were higher compared to a flow without swirl-inducing pipe. Due to its higher apparent viscosity, the ΔP_{23} over the bend has similar graph trends with ΔP_{12} (C.12) and ΔP_{13} (Figure 5.14 c).